# Temperature variations across socioeconomic status and built environment in the state of Illinois and the Netherlands

MSc thesis

September 6, 2021-February 4, 2022

30 ECTS

Robert Lebshier

Student # 9251340

First Supervisor: Dr. Derek Karssenberg

Second Supervisor: Dr. Jon Wang

Faculty of Geosciences, Utrecht University

Earth Surface and Water program

Geohazards and Earth Observation track

Utrecht University

## Abstract

Urban heat islands cause heat stress to urban residents and their severity is increasing due to both climate change and ever-increasing urbanization. Investigation of the issue has a storied past, but the methods used have all shared serious limitations. The goal of this study was to document and analyze correlations between surface air temperature and the average incomes of residents or the population density of areas affected. The study hypothesized that a positive correlation would be found between surface air temperature and population density, while a negative correlation would be found between surface air temperature and average income. The study's literature review gives readers an easily comprehensible primer for this topic, covering both the nature of UHI and its methods of investigation. The issue of environmental justice and vulnerability to heat amongst certain populations is also explored as these ideas heavily informed the study's purpose and hypothesis. This study used crowdsourced point measurements of the surface air temperature taken via NETATMO weather-recording devices in private homes. This data was used to investigate UHI and surface temperatures in general in the state of Illinois, the city of Chicago, the continental Netherlands, and the city of Amsterdam. This data was collected at four different times over the course of August 20, 2021. The point data was then used to create continuous field temperature maps of each study area, extrapolating temperature values between the points for which data was recorded. Average temperatures were then found for each administrative unit (county, municipality, or neighborhood) at each of the four times in each study area, resulting in four air surface temperature maps for each study area that track values throughout the day. Average income per household and population density data were collected for administrative units in all study areas and then compared with the surface air temperature maps to find trends, patterns, and possible correlations. Geographically weighted regression (GWR) and bivariate analysis (BA) were used to analyze the resulting map data in order to better understand how temperature values varied with distance between data points and across all four study areas. The results are strongest and most clear for the Netherlands, where data points are the most robust and widespread. Overall, the GWR results indicate a consistent and moderately strong correlation between surface air temperature and both average income values and population density. The BA results suggest that the correlation is negative for average income values and positive for population density. The majority of the results at each step of the investigative process are shown using maps created in ArcGIS Pro.

## Table of Contents

# 1. Introduction

The 20th century saw the highest rate of urbanization of humanity in the history of planet Earth, and this trend continues in the 21st century. In the year 2009, urban residents outnumbered rural residents globally for the first time in human history (Siu & Hart, 2013). Current estimates project that urban residents will reach 60% of the global population by 2030 and 67% by 2050 (Chapman et al., 2013; Mirzaei & Haghighat, 2010). This means that problems unique to or caused by urbanization will become increasingly pressing and in need of amelioration. One of the more subtle examples of these problems is that of the urban heat island (or UHI). Cities tend to have higher average surface air temperatures than non-urban areas. The reasons for this are still not perfectly understood, but they all are tied to the processes that humans engage in when transforming a non-urban area into an urban area as well as the ongoing processes which occur due to human activities inside urban areas. Some studies suggest that the severity of this phenomenon is increasing over time too (Levermore et al., 2018).

The problem of urban heat islands becomes even more concerning when climate change is considered. The last 100 years has seen a steady increase in average global temperatures around the world, and models have sought to predict how severely this trend might continue depending on the anthropogenic activities that seem to be driving it. For cities, observed temperature increases within urban areas have actually exceeded those predicted by many climate change models (Jeganathan et al., 2016). This means that climate change is exacerbating the effects of urban heat islands, increasing the severity of the problem and its many effects for an ever-increasing share of the human population.

## *1.1 Investigating UHI- Methods and limitations*

Investigating UHI is not a simple or straightforward procedure. Studying the atmospheric system of a city is inherently complicated due to the complexity of the energy exchange occurring there, the range of space and time scales available, and the spatially disordered nature of the sources and sinks therein. This is exacerbated by the significant human factors involved as well as the expense and difficulty of gathering data within an active, populous city. Not only is the city atmosphere subject to huge variability, but investigators are restricted by the physical structure of cities (building blockage) as well as municipal safety laws that restrict how, when, and where data can be gathered using certain kinds of equipment. This requires significant expense, unorthodox methodologies, and/or newer technologies to circumvent (Oke, 1982).

At present, there are two primary ways in which UHI is investigated, but many of the methods used have either come into existence or been greatly improved in the last 20-30 years. The first involves measuring the canopy layer via air temperature detected by either in-

situ fixed location sensors or traverses of vehicle-mounted sensors. The second is to measure surface UHI via land surface temperature derived from airborne or satellite-based remote sensing (Ngie et al., 2014; Sheng et al., 2017; D. R. Streutker, 2002; David R. Streutker, 2003).

*1.1.1- Surface air temperature*

UHI is typically quantified by calculating the surface air or surface temperature differences between an urban area and a nearby non-urban area with similar geographic features simultaneously (Memon et al., 2009). However classifications for what constitutes an "urban" location and a "non-urban" location are often vague or ill-defined. Particularly when applied to metropolitan areas that exhibit urban sprawl or extensive surrounding suburbs, the line between the two classifications becomes increasingly blurry (Ngie et al., 2014; Siu & Hart, 2013). Many of these classification decisions are made implicitly by the investigating scientists and/or are not comparable with other investigators' delineations. Many UHI studies also use outdated urban extent maps that often fail to account for more recent urban boundary expansion. This may introduce significant bias into the data collection that later results in UHI being underestimated by as much as 50% (Zhao et al., 2016).

The study of UHI has also struggled with a lack of standardization in terms of land use and land cover mapping for urban areas where UHI is present. There has long been an absence of coherent, consistent databases with information on urban form and function for even cities with extensive investigation histories. This includes information on land cover, materials, building dimensions, and occupation patterns (Hidalgo et al., 2019). This information is vital for finding correlations between UHI and urban form in order to better understand what causes variations in UHI and to inform mitigation efforts. Several classification systems have been put forward to address this issue, but most have been unique to each study and city, limiting the ability to compare

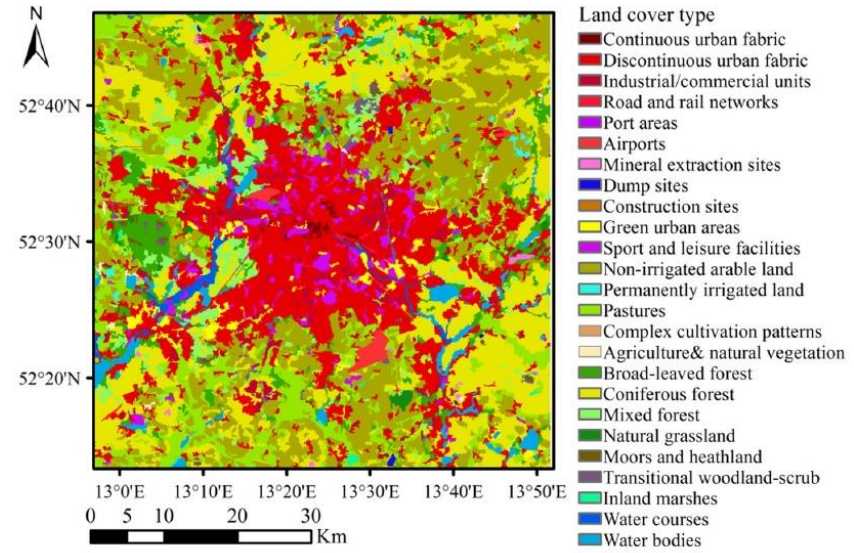


Figure 1-1: A land cover classification system used to study Berlin. It is non-standardized and unique to the city. (H. Li et al., 2018)

findings between different studies of UHI and land use (B. Bechtel et al., 2016). Figure 1-1 shows one such example of this sort of classification scheme.

Using air temperature to derive UHI is the older of the two primary methods and typically involves fieldwork investigation. The in situ air temperature approach is a direct measurement that often requires less in terms of correction/ adjustment. It also has the benefit of measuring the living environment and recording what urban residents are actually experiencing in the city, although this is less true when such measurements are taken from building roofs or higher elevations in the cityscape. When these issues are properly accounted for, direct measurement of urban temperature can prove useful for trying to investigate the effects of heat on human health and/or measuring thermal comfort since this is what people actually "feel" as they go about their day (Hu & Brunsell, 2015; Sheng et al., 2017). Because field work is costly in terms of time and equipment, this approach has inherent limits. Crowdsourcing the data collection process may address this limitation but the quality of the data collected becomes questionable (Benjamin Bechtel et al., 2017).

Air temperatures taken in-situ often rely on meteorological stations for their data. These stations are typically located outside their respective cities where buildings and smog will not interfere with their ability to gather data. The advantage of these in-situ observations, is that they have strong temporal resolution. But because only so many such stations can be built or deployed in the field, they lack spatial resolution. The result is that much of the data for areas in between the data collection points must be interpolated in order to produce spatially continuous field data. Using vehicles to measure air temperature helps deal with the spatial limitations of taking in-situ data. Cars or trucks are most often used for such field measurements. In these cases, a vehicle-mounted sensor must be attached which will position the sensor to avoid the engine and exhaust heat. Such sensors are typically housed in solar radiation shields to protect from direct solar radiation as well (Yadav & Sharma, 2018). One study conducted in Amsterdam, however, used sensors attached to bicycles- a distinctly Dutch approach to data collection (Steeneveld et al., 2011). As for fixed locations, this method generates a series of point data which then requires interpolation to fill in between and around the traversal paths. Such processes can be completed using inverse distance weighting (IDW) or Kriging for example (Yadav & Sharma, 2018).

*1.1.2- Land surface temperate (remote sensing)*

The alternative to measuring air temperature in-situ is to measure land surface temperature (LST) via remote sensing. Remote sensing can be defined as "the science and art of obtaining information about an object, area, or phenomenon through the analysis of data acquired by a device that is not in contact with the [thing] under investigation." Remote sensing may be conducted by air or by satellite. Either one requires a keen understanding of the sensor's limitations and what/ how it "sees" the surface it is sensing. LST is typically derived via measurement of the thermal infrared spectrum of light at 8-15 μm, but microwave is also sometimes used (Charlie J. Tomlinson et al., 2011). The sensor indirectly estimates the apparent surface temperature based on the radiance received from the area of the surface that lies within the instrument's field of view (FOV) (Voogt & Oke, 1997). A

given FOV includes both sunlit and shaded surfaces, which will require some correction to account for. The sensor itself is sensitive to its assigned location, orientation, FOV, and the structure of the observed surface, requiring further corrections before temperature data can be derived (Soux et al., 2004).

Once the radiance data is collected, several corrections must be applied. These include applying for atmospheric effects, angular effects, and the spectral emissivity of the surface being sensed (Ngie et al., 2014). All of these steps results in so much correction that it may completely overshadow the differences caused by UHI if incorrectly estimated or applied (Voogt & Oke, 2003). Because of the topography of the urban landscape, the same sensor viewing an area from different points above may see a different mix of surface elements because different parts may be obscured from view (Soux et al., 2004). In addition, many definitions of the "surface" and measurements taken there either refer to ground level or rooftop level and neglect the canopy between the two (Voogt & Oke, 1997). All of these caveats conspire to muddy the data and obscure the actual surface temperature being sought.

Using remote sensing to track UHI comes with a more fundamental problem as well. Air temperature cannot be remotely sensed; this is why LST is used as a substitute. The aim is to use LST to estimate air temperatures at/or near the surface. However, the relationship between air temperature and LST is still only partly understood and seems to vary depending on many factors (Benjamin Bechtel et al., 2017; Hu & Brunsell, 2015; Liang et al., 2020). Studies of the same area over the same time have compared LST and air temperature and found significant differences between the two values. Three different studies that all used MODIS data to derive LST discovered that their values differed from air temperature values on the ground by 3-7 ℃, 5-9 ℃, and 6-10 ℃ respectively (Hu & Brunsell, 2015; Lai et al., 2018; Voogt & Oke, 1997). The data shows that air temperature values are consistently higher than LST values, whether derived from aerial or satellite-based sensors. Sensors consistently undersample the surfaces they are measuring for reasons that will be explored shortly (Schwarz et al., 2012; Voogt & Oke, 1997).

Much of the difficulty in using remotely sensed LST as a stand-in for air temperature is due to the topography and verticality of urban areas. As mentioned above, street canyons of various heights dominate significant portions of the urban landscape. Just as these areas drastically change the way solar radiation is absorbed, reflected, and re-emitted, so do they also complicate the ability of sensors to measure LST. This is because the sensor can only estimate LST based on the solar radiation that reaches the sensor. Research has shown that observed surface temperature can be significantly different from ambient air temperature inside street canyons (Mirzaei & Haghighat, 2010). This is due to the high "roughness" of urban topography. With its many height variations between different buildings, different neighborhoods, and the much lower streets between them, urban areas provide a very rough overall surface for remote sensing. This leads to radiance measurements that require innumerable small-scale adjustments to account for. Instead, models are typically used to make a global adjustment to the data or large-scale adjustments for certain types of neighborhoods/ land use. The result is a loss of data and precision (Voogt & Oke, 2003).

A similar problem is that of surface heterogeneity and emissivity. Because different materials have different emissivity values, adjusting remotely sensed data to account for these many small differences is difficult. The typical solution is to use an average emissivity for the entire surface, resulting in a loss of precision here as well (Charlie J. Tomlinson et al., 2011). A final issue is anisotropy. This is the tendency of objects to exhibit different values when measured along different axes. For example, the LST derived for a building may depend on whether the radiation strikes its roof on the horizontal plane or on its side in the vertical place. This adds an additional complication to remotely sensed data because aerial vehicles and satellites housing sensors are always in motion and cannot sense in a perfectly vertical way. Modelers are attempting to address this issue, but it has not been fully resolved (Lai et al., 2018; Voogt & Oke, 2003).

*1.1.3- Variables which affect UHI*

The ultimate goal of the various methods of UHI investigation are to determine what factors cause or exacerbate UHI. Direct measurement of surface air temperature or remotely sensed LST are determined, then an effort is to made to work backwards to derive what factors may have affected the temperature data recorded. As will be addressed in detail in section **2. Literature review**, many different studies have made progress toward elucidating which factors may contribute to UHI and to what extent they do so. The key factors seem to be dependent on urban fabric and patterns of build-up. Because these factors are tied to residents' financial situation, this suggests that UHI may be experienced disproportionately by residents of various means. Residents' socioeconomic status may also determine the type of neighborhood they dwell in and what that physically looks like in terms of building types, contiguity of urban fabric, presence of green space, and how much room/ space each resident can enjoy. With these things in mind, average income per household and population density may act as suitable, quantifiable indicators of these factors. By measuring these variables, UHI's dependency upon them may be derived to some extent.

### *1.2- The present study (MSc thesis)*

This MSc thesis was undertaken in order to contribute to the investigation of UHI as well as how temperature variations correlate with the average incomes values of affected residents and the population densities of the communities in which they live. This thesis includes a broad literature review that looked at previous studies, their insights, their successes, and their shortcomings. Given the many limitations of using remote sensing to investigate surface air temperatures via LST, using in-situ surface air temperature data was preferred for this thesis. The intention was to find ties between the UHI phenomenon and the lives of those affected by it. The main research question was: How are surface temperatures in urban areas tied to factors which may increase or decrease the intensity of UHI for urban residents? Sub-questions included the following: (1) could in-situ surface air temperature data from crowdsourcing provide reliable, accurate results, (2) in the absence of derived UHI data, could surface air temperature alone be sufficient for highlighting where UHI occurred, (3) could average income per household be used as a risk factor for an urban resident's vulnerability to UHI, (4) could population density be used to represent the extent of urban

build-up, (5) could the previously mentioned variables be found to have a statistically significant relationship to each other, (6) if so, what relationship would each have and to what extent, (7) how might all of the aforementioned results and relationships vary between different cities, different continents, and different scales? To answer these questions, this MSc thesis used crowdsourced in-situ surface air temperature data, average income per household data, and population density data for the state of Illinois, the city of Chicago, the continental portion of the Netherlands, and the city of Amsterdam. For this investigation, heavy use was made of ArcGIS Pro and Microsoft Excel to organize, process, produce, and visualize the data and results.

# 2. Literature review

## *2.1 Defining UHI- Components and variability*

The urban heat island effect, often shortened to "UHI", refers to excess warmth in an urban atmosphere compared to its non-urbanized surroundings. The phenomenon was first discovered and subsequently investigated by Luke Howard as he carried out observations on the weather of London in the 1810s, 1820s, and 1830s. It is fundamentally a thermal anomaly with horizontal, vertical, and temporal dimensions (Oke, 1982; Voogt & Oke, 2003). It is typically derived by finding the difference between a temperature taken inside the urban area and one taken outside the urban area. This is typically near the urban point value's location but outside a carefully chosen urban buffer. Alternatively a similar operation can be done using average temperatures inside the urban area versus average temperatures just outside the buffer (Debbage & Shepherd, 2015). This temperature difference may be as small as .1 ℃ or as large as 10 ℃, depending on several factors (Azevedo et al., 2016).

The anomaly itself is made up of multiple layers with their division based on elevation and city structure. The topmost layer is the urban boundary layer (UBL), which begins at the level of the rooftops and extends upwards into the lower atmosphere to end at the atmospheric boundary layer. Whereas the other layers are largely the result of local conditions and microclimate, the UBL represents the integration of these other layers with the surrounding macro- and mesoscale climate (Flores R. et al., 2016; Hu & Brunsell, 2015). Below the UBL lies the urban canopy layer (UCL), which extends from the rooftops to just above the surface or street level. The urban surface layer (USL) encompasses the surface/ street layer and the air resting directly atop it. It is important to note that USL can be measured in the form of air temperature or land surface temperature. One is a measurement of air at the surface while the other is a measurement of the surface itself. Each of these layers exhibits the UHI

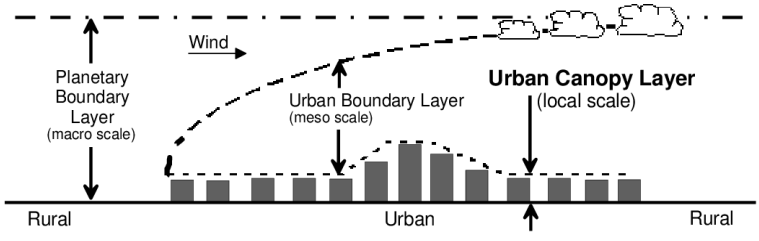


Figure 2-1: A simple diagram of the atmospheric layers that make up the urban heat island (Stewart, 2011)

effect differently and their interactions help to create the UHI (H. Kim et al., 2018; Voogt & Oke, 2003; Yuan & Bauer, 2007). These layers are illustrated in Figure 2-1.

Although UHI has been studied for nearly two centuries, much of that study focused on identifying and isolating the observable effects of UHI. True understanding of this phenomenon began in the 1970s. At that time, scientific inquiry into urban effects on weather and environmental factors had progressed to the point where the underlying causes behind the UHI phenomenon could finally be elucidated (Oke, 1982). Since that time, studies have found that UHI intensity for both air temperature and land surface temperature varies depending on the time of day and the season of the year (Chen et al., 2006; Doick et al., 2014). Furthermore, it seems that these fluctuations even vary depending on where in the world the city in question is located (Mirzaei & Haghighat, 2010). For most of the cities studied in the Upper Hemisphere in North America and Europe, UHI is most intense in the summer (Cheval & Dumitrescu, 2015). However many cities in China experience an equally intense UHI in winter, while cities in tropical or subtropical areas experience the most intense UHI during winter alone (Flores R. et al., 2016; Lai et al., 2018; Yadav & Sharma, 2018). This suggests that the behavior and nature of UHIs depends heavily on regional climate patterns.

When it comes to daily or diurnal temporal patterns, UHI also varies from city to city but shows some consistent regional tendencies. Many studies in mid-latitude cities have shown that UHI intensity is up to three times higher at night than during the daytime. The highest recorded UHIs often occur between midnight and 3:00 AM. Similarly, UHIs are often negative (urban temperatures are lower than non-urban) during early morning hours and cities may experience a relative “urban cooling” between 10:00 AM and noon (Ketterer & Matzarakis, 2015; Memon et al., 2009). To understand some of these variations, it is vital to understand the fundamental causes of the UHI effect.

### *2.2 Causes of UHI*

*2.2.1- Impervious surfaces and street canyons*

Figure 2-2 gives a brief visual overview of the causes of UHI, will be discussed in more detail below. It is important to first note that UHI has been detected in cities with populations of less than 10,000 people (Mathew et al., 2018). This is because many of the primary causes of UHI are due to how humans alter the land when they urbanize an area, regardless of the area's size. The most notable of these is the replacement of vegetated areas with impervious surfaces, fundamentally altering the area's land use and land cover (Azevedo et al., 2016; Chen et al., 2006; Huang et al., 2011; H. Li et al., 2018). Examples of the impervious surfaces ubiquitous in urban areas include concrete, tiles, bricks, and roof sheeting for buildings as well as concrete, bitumen, and asphalt for roads and parking lots (Mathew et al., 2018). Pavements cover about 40% of cities on average, while man-made materials in general cover about 60% of city surfaces. This is problematic because these materials all have significantly lower albedos and greater heat storage capacities than the vegetation they replace. For example, asphalt concrete has an albedo of 5 – 15% depending on its age (Mohajerani et al., 2017). This means that a huge amount of light is being absorbed and converted into heat at the surface rather than being reflected back up into the atmosphere.

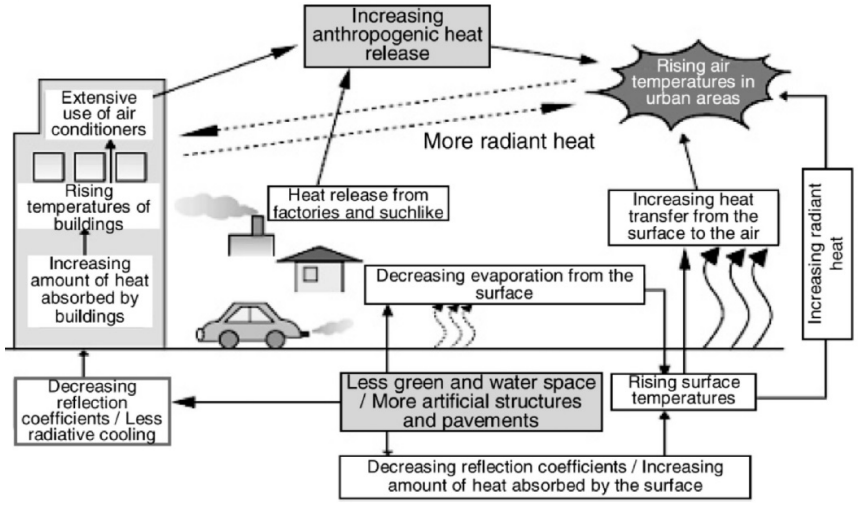


Figure 2-2: A simple diagram of the many causes of UHI and how they interact. (Mohajerani et al., 2017)

These man-made materials also have higher thermal admittance that can capture, store, and then release higher quantities of heat compared to natural surfaces. (Memon et al., 2009) This is problematic because those same materials will re-emit this stored energy later, especially at night, resulting in slower cooling rates for urban areas and higher UHI at night. (Yadav & Sharma, 2018) In terms of physics, cities receive just as much shortwave radiation as their non-urban surroundings but have higher longwave radiation inputs and outputs because of these man-made materials (Oke, 1982). This same effect occurs to a lesser extent when land is cleared of vegetation and left bare. Bare land and land undergoing construction make the greatest contributions to UHI after fully developed urban areas due to increased albedo and lack of vegetation (W. Li et al., 2017).

An additional cause of UHI is the physical structure of cities, particularly the phenomenon of "street canyons." A street canyon consists of a sharp, vertically inclined space surrounded by two or more tall buildings, often along a street (Debbage & Shepherd, 2015; Oke, 1982). These street canyons are more common in more built-up areas with taller buildings, where they suffer from reduced sky view factor. This factor is proportional to the area of overlying hemisphere that is open to the sky (Oke, 1982). Unfortunately reduced sky view factor causes urban surfaces within street canyons to emit less of the long-wave radiation that they have stored over the course of the day, resulting in more stored heat. The severity of this depends on the height to width ratio of the buildings forming the street canyon (Hart & Sailor, 2009). Figure 2-3 gives a glimpse of how SVF varies across a densely populated city.

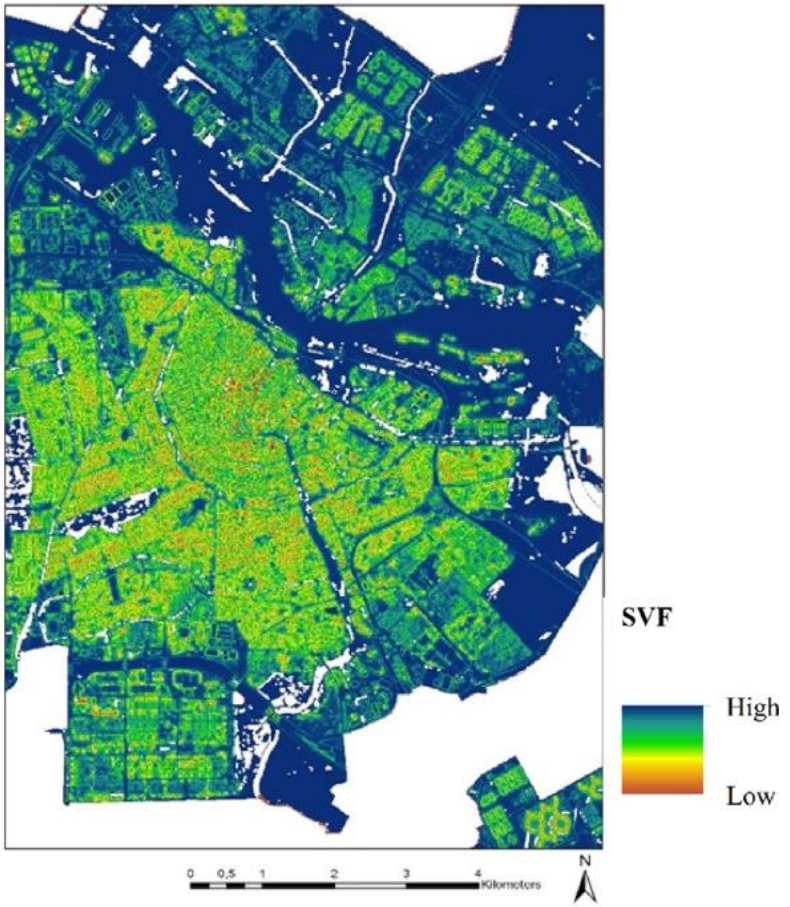

Figure 2-3: A map of the sky view factor (SVF) across the city of Amsterdam. (Rafiee et al., 2016)

Even the radiation that is emitted from man-made surfaces may never reach the atmosphere because of the geometry of the street canyon, which ensures that the surfaces of the structures forming the canyon will endure extensive reflections as the radiation bounces back and forth between them during emission, absorption, and re-emission (Mohajerani et al., 2017). Considering that many of these surfaces have emissivities of .87 to .97, this repeating cycle can form an extensive form of radiative flux in urban areas (Huang et al., 2011; Voogt & Oke, 2003). The end result is that the heat loss rate in a street canyon can be up to four times slower than it would be in a more open setting given the same materials (Rafiee et al., 2016).

*2.2.2- Anthropogenic heating, clouds and wind, and urban geometry*

Anthropogenic heating, or heat produced by man-made activities, is another contributor to UHI. This includes heat released from the engines and exhaust of vehicles,

waste heat produced by heating, ventilation, and air-conditioning of buildings, and heat produced by human metabolic processes (Huang et al., 2011; Mirzaei & Haghighat, 2010). The high population density of many cities ensures that this last value is not negligible within urban areas. Because most cities are high traffic areas due to commuting, and because large buildings dominate the setting, total anthropogenic heating in a given city can really add up (Oke, 1982).

Meteorological conditions can also contribute to UHI. Cloud coverage and wind speed, which act as indicators of atmospheric stability, can have an adverse effect on UHI intensity (Oke, 1982). These two factors are negatively correlated with maximum UHI, meaning that ideal conditions for the highest UHI intensity are a clear sky and still winds (Azevedo et al., 2016; Y. H. Kim & Baik, 2002). Conversely, UHI intensity will steadily diminish as cloud cover and wind speed increase. This is because higher wind speeds lead to more turbulent mixing, which reduces the temperature differences in the near surface air (Yadav et al., 2017). Relative humidity also plays a role in boosting UHI, though this relationship is less linear than for cloud cover and wind speed (Lai et al., 2021).

The shape and layout of urban spaces also contributes heavily to UHI. These are often referred to as urban form indicators (UFIs) and include factors like land use, density of build-up/ urban density, area of the city, city population, population density, and contiguity (connectedness) of built-up areas. There are well-established positive relationships between UHI intensity and both city size and urban density. The heat diffusion rates of high-density urban buildings is lower than for low-density buildings, which results in more heat storage and slower release. (Liang et al., 2020) This would suggest that less dense, more spaced out urban areas would be less prone to UHI. However, cities exhibiting this urban form, often referred to as “urban sprawl”, have been found to exhibit high UHI as well (Debbage & Shepherd, 2015; Kamruzzaman et al., 2018). Instead, contiguity (the degree of connectedness and lack of gaps in said connectivity) of built-up areas may be the dominant factor that determines intensity of UHI. Some studies have indicated that increasing the spatial contiguity of urban development enhances UHI regardless of its urban density (Debbage & Shepherd, 2015; Liang et al., 2020).

Studies also show that population density correlates more strongly with UHI than population alone, which is likely tied to both density of build-up and building type (Debbage & Shepherd, 2015; Steeneveld et al., 2011). Other studies support the theory that building type has a strong effect on UHI. Buildings that are both compact and mid-rise exhibit the highest UHI when compared with low-rise and high-rise buildings as well as open or spare plan buildings (Yang et al., 2020). Perhaps because cities that grow rapidly often do so with less planning, they often exhibit higher urban density and therefore higher UHI. Rapidly industrializing cities in China and India, as well as rapidly growing cities in South Korea have been shown to exhibit some of the most marked increases in UHI over multiple years (Liang et al., 2020; Zhao et al., 2016). Figure 2-4 shows how UHI varies over the summer season in a densely populated European city.

*2.2.3- Vegetation and the role of evaporative cooling*

One of the most significant causes of UHI is the loss of vegetation in urban areas. Studies have repeatedly shown that areas with higher vegetation cover have lower temperatures and lower seasonal thermal amplitudes (Flores R. et al., 2016). One study in New York City found that air temperatures were highest in the most densely urbanized areas of the city while the lowest temperatures were found in the most highly vegetated areas (Susca et al., 2011). By their nature, such vegetated areas are more open than street canyons, allowing for more efficient ventilation and cooling via changes to the local heat flux (Hart & Sailor, 2009; Liang et al., 2020). But the primary reason they are so much cooler is due to evaporative cooling.

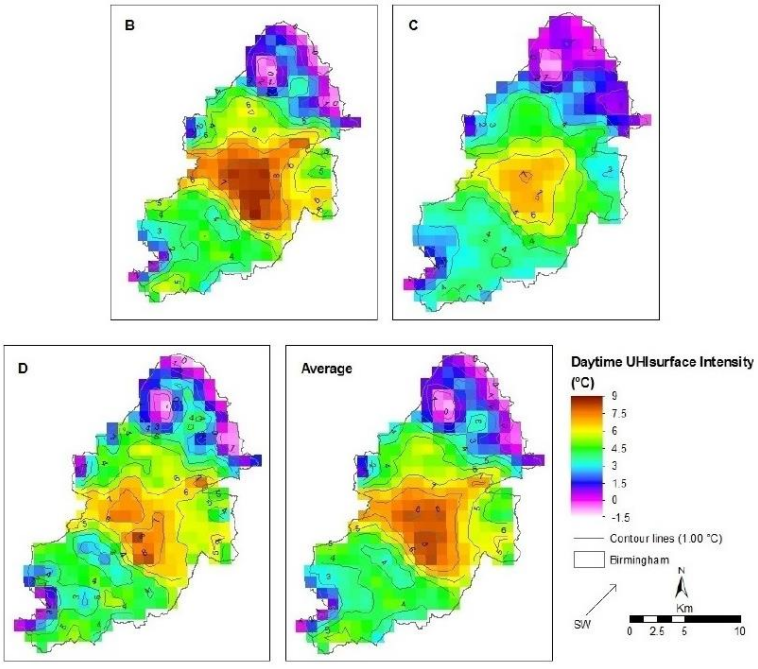


Figure 2-4: A map illustrating the daytime UHI intensity of the city of Birmingham over the months of June, July, and August. (Azevedo et al., 2016)

Evaporative cooling occurs when water is converted from liquid to vapor state using thermal energy in the surrounding area. This reduces the temperature of the air in that area, effectively cooling it. A key component for this to take place is the ability of a surface to retain water, which can then be converted to vapor (Oke, 1982). Bare soil retains water much more effectively than the impervious surfaces that dominate most cities, of course. But the vegetation atop this soil strongly reinforces the effect. Plants and trees transpire water in steady volumes throughout the day, making more water available to drive evaporative cooling, promoting an ongoing cycle (Doick et al., 2014).

This cooling effect is really just an instance of less warming occurring since solar energy is intercepted and used to convert the state of water instead of warming the urban fabric. In the absence of additional warming, the surface is cooler than it would otherwise be (Doick et al., 2014). This further illustrates why land use changes due to urbanization are the underlying cause of many other factors which combine to create the UHI effect (H. Li et al., 2018).

## *2.3 Effects of UHI*

*2.3.1- Climate change and energy infrastructure*

UHI has consequences that go far beyond simply a higher local temperature. Higher temperatures directly contribute to global climate change as well as exacerbating other urban environmental problems (Kamruzzaman et al., 2018; Lowe, 2016). For example, higher temperatures enable the basic chemical reactions that create ground level ozone while emissions from automobiles and motorcycles supply the oxides of nitrogen and volatile organic compounds needed to fuel the reactions. The result is that higher temperatures throughout the day generate more ozone at ground level which then absorbs pollutants and lingers over cities as smog which further concentrates the pollutants (Mirzaei & Haghighat, 2010; Yadav et al., 2017). Unfortunately higher temperatures also encourage people living in cities to use more energy to cool their homes and businesses via fans and air conditioning. The American EPA has recognized that this leads to increased energy consumption, which further augments climate change since producing more energy results in the release of more greenhouse gases. At the same time, air conditioners release excess heat into the outdoor portions of the city, reinforcing the original problem of higher exterior temperatures (Kamruzzaman et al., 2018; Lowe, 2016; Mohajerani et al., 2017).

The higher temperatures caused by UHI also affect vital urban infrastructure, especially the energy grid. Transformers can generally cope with internal temperatures of up to 98 ℃ without affecting their life expectancy and day-to-day operation. However, going above this internal temperature by as little as 6 ℃ can reduce a typical transformer's life expectancy by 50%. During several recent heat waves in Europe, this soft limit has been surpassed for urban transformers in the affected cities over multiple days (Chapman et al., 2013; C. J. Tomlinson et al., 2013). Unfortunately higher temperatures put more pressure on the energy grid even as the transformers it depends on are themselves taxed ever more intensely, leading to an increasingly precarious and costly situation.

UHI affects the environment in and around a city beyond simply increasing the temperature too. UHI has been shown to increase the frequency of storms and precipitation events in many cities (Kamruzzaman et al., 2018). In Bangkok, research showed that UHI led to many other more subtle ecological problems. This included a decrease in groundwater levels, widespread subsidence, and changes to local wind and rainfall patterns (Pakarnseree et al., 2018). In addition to harming the environment, these examples provide further evidence of how UHI, which is caused by man-made activities, makes urban life increasingly difficult for the people whose activities are causing UHI.

*2.3.2- Effects on extreme temperatures and excess heat on health*

The most obvious and noticeable effect UHI has on regular denizens of cities is in the way it augments heat waves. A heat wave can be defined as a prolonged period of hot weather with temperature substantially higher than the seasonal average value for several days (Zinzi et al., 2020). Several studies have shown that UHI increases both the frequency and longevity of heat waves around the world (Lowe, 2016). Considering that heat/ drought is amongst the top 10 fatal natural hazards in the U.S., the danger of heat waves augmented by UHI becomes more clear (Huang et al., 2011). North American cities are not alone in their

suffering, however. The 2003 European heat wave led to thousands of deaths or lasting injuries- somewhere between 35,000 and 50,000 in total. Most of them were in cities, due to augmentation by UHI (Chapman et al., 2013; Cheval & Dumitrescu, 2015). On top of the cost in lives, one study showed that UHI increased the average temperature of a heat wave by 4.3 ℃, which resulted in a 39% increase in energy costs to cope (Zinzi et al., 2020).

Even outside of heat waves, high temperatures pose grave health risks. One study of several cities on different continents found that UHI was amplified for all cities by 2.6 ℃ on average, while this jumped to 4.7 ℃ for cities with areas greater than 500 $km^2$. This is significant because heat stress can be initiated by an increase in body temperature of only 1 ℃ from a baseline of 37 ℃ (Sabrin et al., 2020). Studies investigating the human impact of urban heat have found that thermal discomfort from excess heat is experienced more frequently and/or more intensely in urban areas due to UHI. Research shows that skin temperature and deep body temperature equally contribute to thermal comfort, while air velocity seems to have a significant effect on skin and body temperatures (Guéritée & Tipton, 2015). This means that, even as street canyons trap and hold heat around urban denizens, the wind retarding or blocking effect of large buildings further reduces thermal comfort. Because UHI is most intense when the wind is still, people will experience even more discomfort due to lack of wind velocity against their skin. It is estimated that, at present, 30% of the global population is exposed to climate conditions exceeding established mortality thresholds (Jenerette, 2018). This impairs health in general, but may be even more problematic at night. Because UHI is often most severe at night, urban residents' quality of sleep will be adversely affected. It is well-established that getting less sleep and/or a lower quality of sleep affects overall health and the ability to concentrate, so nighttime UHI has a doubly negative effect on the health of urban residents (Krüger, 2015). Figure 2-5 shows how health risk from heat varies throughout a densely populated city.

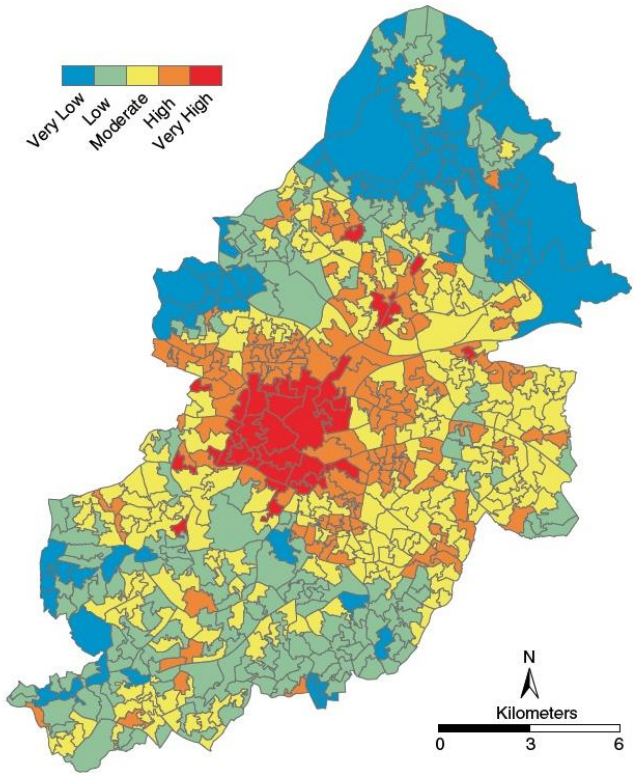


Figure 2-5: A spatially assessed heat-health risk map for the city of Birmingham. (Charlie J. Tomlinson et al., 2011)

Extreme temperatures negatively affect human health in less subtle ways as well. They are directly responsible for heat stroke, heat syncope, heat cramps, and death. Excess heat is responsible for more deaths than all other weather-related hazards combined (Mallen et al., 2019). Additionally, exposure to extreme heat has been shown to exacerbate existing chronic illnesses in human residents (Loughnan et al., 2012). Several different studies have shown how mortality increases with extremely high temperatures; some example results vary from 9% to 17%, but the correlation is clear and consistent- increased temperature means increased mortality (Loughnan et al., 2012; Madrigano et al., 2015).

*2.3.3- Demographic factors and heat vulnerability*

As might be expected, the degree to which urban residents share the burden of thermal discomfort due to UHI varies greatly. Research has shown that income is a powerful determinant of heat exposure, with lower income residents experiencing more heat exposure, particularly because they cannot afford to cool their residences or lack health insurance. There is also an established association between heat-related morbidity and mortality (Hondula et al., 2021; Jaganmohan et al., 2016). Certain other factors increase the risk of heat-related health problems. These factors include being an ethnic minority, lacking a social network, being elderly, and being homeless (Huang et al., 2011). Considering that 77% of the homeless population in the U.S. lives in urban areas, this is especially bad news for them (Lowe, 2016). Other studies have found that additional factors increase vulnerability to heat, including educational level, economic status, population density of residence, dwelling type, and poverty (Loughnan et al., 2012; Madrigano et al., 2015; Méndez-Lázaro et al., 2018; Sabrin et al., 2020). When considering how heat vulnerability varies spatially across a city, one study found that unemployment and lack of access to health insurance accounted for 35% of the observed variation. The same study found that the warmest areas of the city investigated were populated by an increased number of residents who lacked jobs and access to health insurance (Méndez-Lázaro et al., 2018).

Though many consider it common knowledge, ample evidence shows that urbanized areas around the world, but especially in the U.S., are residentially segregated along socioeconomic as well as racial/ ethnic lines (Jenerette et al., 2007). This is borne out by studies that show strong correlations between both median household income and percentage of non-white ethnic residents with both mean vegetation level and population density for a neighborhood (Jenerette et al., 2007). Studies have shown that access to green spaces (which show reduced UHI) is frequently restricted in low-income and minority-dominated neighborhoods (Jenerette, 2018). Strong correlations have also been found between higher incomes and increased mean vegetation by urban neighborhood. Similarly, higher population density is correlated with lower mean vegetation by neighborhood. Finally, higher population density correlates with lower diversity of neighborhood configuration. This is because higher population density leads to fewer possible build-up configurations (Jenerette et al., 2007). This results in neighborhoods with fewer resources exhibiting denser urban build-up and greater contiguity of build-up, so that they experience UHI disproportionately more severely than those with more resources. This is known as the “luxury effect” hypothesis (Jenerette et al., 2007). Because of ethnic and socioeconomic equalities, the neighborhoods most affected

by UHI are typically those inhabited by poorer, underemployed, non-white residents. By the same token, those with the fewest resources often reside in the warmest parts of a city (Huang et al., 2011). All of this is supported by the fact that heat-related mortality varies on the neighborhood scale and the extent and severity of UHI is highly localized (Sabrin et al., 2020).

## 3. Methods

### *3.1- Study areas*

The areas of study chosen for this research were the state of Illinois in the United States and the continental portion of the nation of the Netherlands. Additionally, a metropolis was chosen within each study area in order to analyze the data at a higher resolution. For Illinois, this was the city of Chicago; for the Netherlands, it was the city of Amsterdam. These areas were chosen due to the author's experience living in each one, with the hope being that familiarity with these areas would lead to greater insights when interpreting the results of this study. Additionally, Chicago is known for its dangerously hot conditions in the summer while Amsterdam is known for its mild, rainy climate ("Amsterdam Climate and Weather | Amsterdam.info," n.d.; "City of Chicago :: Weather Extremes - Extreme Temperatures," n.d.). So these study areas were chosen because of their great differences as well. Illinois lies in the Midwest of the United States in North America while the Netherlands lies in Western


Figure 3-1: The state of Illinois. Green areas indicate slightly hilly terrain. ("Illinois Maps & Facts - World Atlas," n.d.)

Europe along the North Sea. They are very different climactically as a result, despite their topographic similarities (both are very flat). Illinois has about 3.5 times as much land area as the Netherlands but only 75% as many residents. Chicago and Amsterdam bear similar contrasts. Chicago has about 2.5 times as much land area as Amsterdam and about 3.5 times as many residents. Despite being so much larger, Chicago's population density is 2-4 times higher than Amsterdam depending on the neighborhood. Below is a brief analysis of each of the four study areas. Detailed information regarding each one's average income and population density are found in the Results chapter where it is presented as maps and briefly described.

The state of Illinois has a total land area of about 55,500 square miles or 143,750 square kilometers. It has a population of 12.8 million people as of July 2021. Of this number, 88% dwell in urban areas, while urban counties only make up around 20% of the state's total area as of 2010 ("U.S. Census Bureau QuickFacts: Illinois," n.d.). Illinois's climate is continental type with cold winters, warm summers, and many aspects of its weather subject to rapid and frequent changes over the course of a day, a week, or a month. Temperatures can range from as high as 35 ℃ in the summer to as low as -20 ℃ in the winter. The state typically experiences 105 days of precipitation each year and its thunderstorms can be quite severe ("Climate of Illinois - Narrative, Illinois State Climatologist Office, Illinois State Water Survey, U of I," n.d.). Topographically, the state is very flat with hilly terrain only found in the northernmost portion of the state. Its western border is made up of the wide Mississippi River, while its northeastern corner abuts Lake Michigan (one of the Great Lakes). Figure 3-1 shows the state and its neighboring states. Illinois's 102 counties were used as the primary spatial units for Illinois mapping processes.


Figure 3-2: The city of Chicago ("File:Chicago community areas map.svg - Wikipedia," n.d.)

The city of Chicago is located in the northeastern corner of Illinois. It has a total land area of about 225 square miles or 580 square

kilometers. It has a population of 2.7 million people as of the 2020 U.S. census ("U.S. Census Bureau QuickFacts: Chicago city, Illinois; Illinois," n.d.). Chicago's climate largely parallels that of Illinois, but winters tend to be cooler on average due to its location at the northern end of the state. Lake effect weather also results in more frequent precipitation and cloudy conditions as well as higher humidity since Chicago's eastern border lies along Lake Michigan. Like most of Illinois, the city is very flat. Figure 3-2 shows the city and its major sectors/ regions. Chicago's 97 neighborhoods were used as the primary spatial units for Chicago mapping processes.

The nation of the Netherlands has a total land area of about 33,700 square kilometers. It has a population of 17.1 million people as of end-of-year 2021. Of this number, 92% dwell in urban areas, while urban municipalities only make up around 37% of the country's total area as of 2010 ("Netherlands Population 2021 (Demographics, Maps, Graphs)," n.d.). The climate of the continental Netherlands is oceanic type with mild summers, cool winters, and significant precipitation throughout the year. Temperatures can range from as high 30 ℃ in the summer to as low as 0 ℃ in the winter. Rainfall is a frequent occurrence, with the country experiencing 139 days of precipitation each year, though storms are typically mild. Much of the country is located at or below sea level and is topographically very flat except for the southern portion near Maastricht. The North Sea forms most of the western and northern border of the country, while the Ijsselmeer dominates the north-central portion of the country. Additionally, much of the center of the country hosts the Rhine, its distributaries, and their large, shared delta that dumps into the North Sea ("Netherlands - Climate data and average monthly weather | Weather Atlas," n.d.). Figure 3-3 shows the Netherlands and its provinces. The Netherlands' 437 municipalities were used as the primary spatial units for Netherlands mapping processes.


Figure 3-3: The continental Netherlands ("Netherlands Maps | Maps of Netherlands," n.d.)

The city of Amsterdam is located just northwest of the center of the Netherlands in the province of Noord-Holland. It has a total land area of about 219 square kilometers. It has a population of 741 thousand people as of end-of-year 2021. Amsterdam's climate is similar to much of the rest of the nation, although it trends a bit more rainy and cloudy on average. This is because the city is cut through by the IJ, which connects to the larger IJsselmeer, influencing the city's weather. Like much of the Netherlands, it is very flat and features several canals that divide the city along their lengths ("Netherlands - Climate data and average monthly weather | Weather Atlas," n.d.; "Netherlands Population 2021 (Demographics, Maps, Graphs)," n.d.). Figure 3-4 shows the city of Amsterdam and its major sectors. Amsterdam's 454 official neighborhoods were used as the primary spatial units for Amsterdam mapping processes.

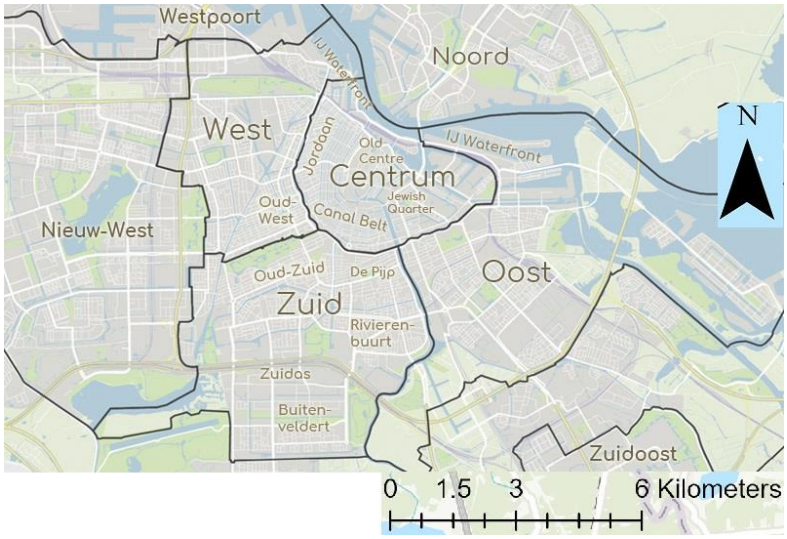


Figure 3-4: The city of Amsterdam ("Amsterdam Districts and Neighborhoods," n.d.)

### *3.2- Overview of methodology*

Figure 3-5 illustrates the overall workflow of the thesis. The first step of the process was data collection. Average income and population density data were collected from several different websites with demographic information for each study area. This information was then added to a shapefile containing the administrative units for each study area in ArcGIS. This resulted in the creation of maps for both variables across the four study areas (the mapping processes stage). Surface air temperature data was then collected for as many points as possible and practical in each study area and then added to ArcGIS as point data. Because temperature values were taken for four different times in a single day, this resulted in four

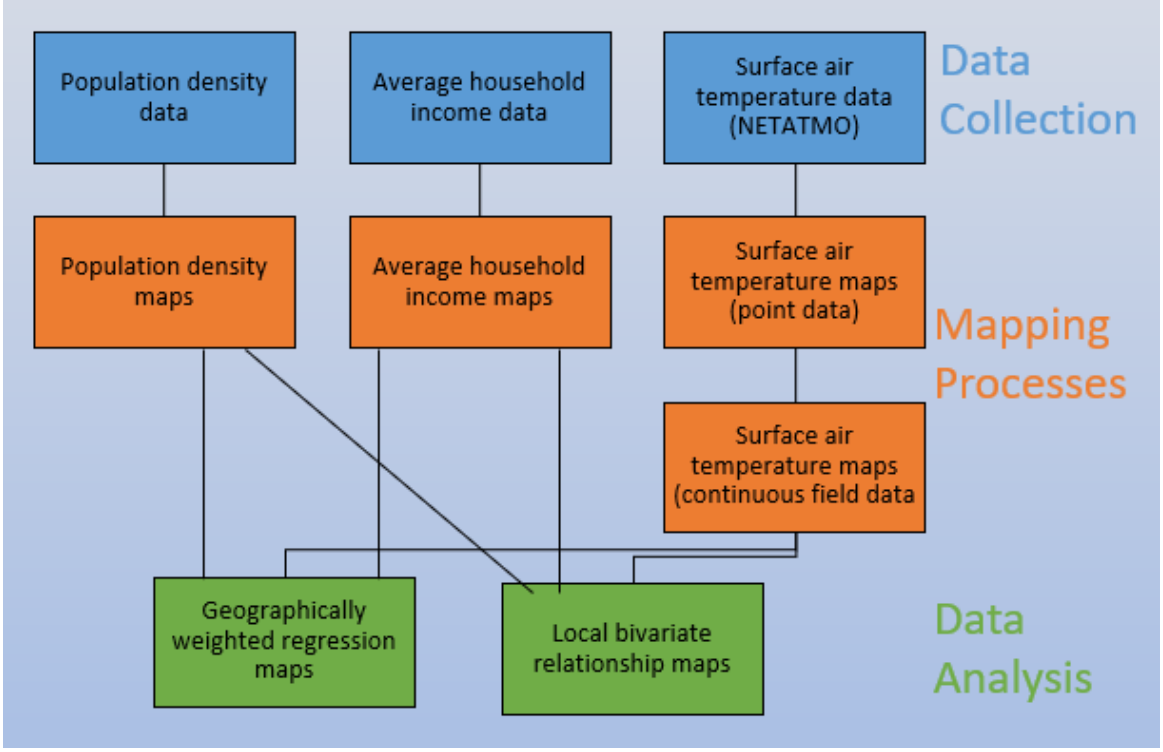


Figure 3-5: A workflow chart of the data collected and processes undertaken to create the maps presented in this study

surface air temperature maps for each study area, giving a total of 16 overall. This part of the mapping processes stage was a bit more time-consuming. Interpolation was then performed on these point data maps in order to create surface air temperature maps with continuous field data across the entirety of each study area. Finally, the data analysis was intended to find correlations between each of the three variables. This was accomplished via geoprocessing tools in ArcGIS using geographically weighted regression and local bivariate relationships. Essentially the surface air temperature maps for each study area were compared with the average income and population density maps for each study area in order to find patterns and correlations across the geographic space of each study area at each of the four times analyzed. The various steps of this methodology are explained in more detail below.

### *3.3- Data collection*

#### *3.3.1- Average income and population density data*

In order to compare how UHI intensity correlated with the vulnerability of urban residents, average household income was chosen as the indicating value. In order to compare how UHI intensity correlated with urbanity and extent of build-up, population density was chosen as the indicating value. For the state of Illinois, average household income values and population density values were collected for each county as of the end of 2018 ("Illinois Median household income (in 2018 dollars), 2014-2018 by County," n.d.). For the city of Chicago, values were collected for each neighborhood; average household income values are as of 2016 while population density values are as of 2019 ("Chicago, IL Neighborhood Map - Income, House Prices, Occupations - list of neighborhoods," n.d.; "Per Capita Income | City of Chicago | Data Portal," n.d.). For Illinois and Chicago, household income values are in U.S. dollars for their respective years, while population density values are in persons per square mile. For the continental portion of the nation of the Netherlands, values were collected for each municipality; average standardized income per household values are as of 2019 while population density values are as of 2020 ("CBS Open data StatLine," n.d.). For the city of Amsterdam, values were collected for each neighborhood; average standardized income per household values are as of 2018 while population density values are as of 2020 ("CBS Open data StatLine," n.d.). For the Netherlands and Amsterdam, income per household values are in Euros for their respective years, while population density values are in persons per square kilometer. The average income per household and population density data gathered were then organized into MS Excel worksheets and recorded there.

#### *3.3.2- Surface air temperature data*

True, accurate measurements of surface air temperature were critical to the success of this study. Therefore surface air temperature values for each study area were collected directly via NETATMO without need for additional correction. NETATMO is a smart home device that, once installed at a person's home, measures and monitors weather conditions nearby via an outdoor module. The values recorded include air temperature, humidity, and wind speed. This data is crowdsourced and freely available online ("Smart Weather Station Indoor Outdoor | Netatmo," n.d.). The website also allows users to filter out sites that its analysis algorithms suspect are inaccurate due to the module having been exposed directly to sunlight or the elements. This would cast doubt on the accuracy of the data, so all sites used for this study were those considered trustworthy according to this filtering process.

Gathering the NETATMO site data was a time-consuming process due, in part, to the way that NETATMO limits the user's access to other users' data. The first step was to select sites for each study area that allowed for the greatest spread/ evenly spaced grid of values across each study area. This was done visually and required much back-and-forth alteration of zoom in order to see all the available sites on the NETATMO weather map webpage. Measurements for all sites were restricted to a single day- August 20, 2021. This day saw relatively mild weather with high temperatures for both Illinois and the Netherlands, so it was considered the best candidate for studying temperature variations and UHI intensity.

Temperature measurements were recorded for 3:00 AM, 9:00 AM, 3:00 PM, and 9:00 PM on this day. These values were organized into and recorded in MS Excel worksheets using the name of the site. During this process, it was discovered that some sites did not have data for the chosen date. In this case, the site was discarded and a near neighbor was used when possible. The nearest town or city to each site was also recorded for increased ease of reference. Latitude and longitude coordinates for each site were then gathered via GoogleMaps by visually comparing the site location on the NETATMO weather map to its counterpart in GoogleMaps. This data was added to the Excel sheet ("Netatmo Weathermap," n.d.). All sites chosen and their respective spatial spreads are illustrated in Appendix A.

### *3.4- Map processes*

#### *3.4.1- Average income and population density maps*

The first step of map creation was to acquire shapefiles for each of the four study areas that contained their administrative boundaries. Therefore a shapefile with these boundaries was collected for each study area from their respective state, national, or municipal government website. These shapefiles were imported into ArcGIS Pro to visually indicate the geographic boundaries of the study. For the Netherlands, these units were municipalities. For the city of Amsterdam, the units were neighborhoods as recognized by the national statistical office (CBS) that belong to the city proper. For Illinois, the administrative units were counties. For the city of Chicago, it was a mix of neighborhoods (fuzzily defined by history and popular convention) and the nearby counties outside the city proper. This is because Chicagoland or Greater Chicago sprawls far beyond Cook County and the official city limits. Although the sizes of these administrative units vary greatly, finding location-specific demographic information for these units is the most straightforward method. This is, of course, since municipal, state/ provincial, and national governments organize and track such information by the administrative units they themselves have created and administered historically.

The average income per household and population density data previously gathered in MS Excel worksheets was then added as tables to ArcGIS. Some adjustments had to be made where neighborhood names for Chicago's demographic data and its shapefile didn't exactly match up, but the process was otherwise smooth. The data in these tables was then attached to each shapefile using the matching administrative units. This was accomplishing using joins, and then the choice was made to represent the range of data visually as graduated coloration with divisions based on the range of values for each data set. This resulted in six classes for average income values and six classes for population density for Illinois, five of each class for Chicago, six of each class for the Netherlands, and six of each class for Amsterdam.

#### *3.4.2- Surface air temperature maps*

The NETATMO surface air temperature data for each site recorded in MS Excel worksheets was then added to ArcGIS as tables for each study area. The temperature data for each site was then added as point data to its respective study area map in ArcGIS, which each of the four times comprising a single layer. This resulted in four maps per study area that

each showed temperatures at the sites chosen for that study area, but with vast swaths of unknown temperatures between sites.

Inverse distance weighting (IDW) is a simple but straightforward method for interpolation when continuous field data is not available. Therefore IDW was used to interpolate the areas between the point data in order to create a raster image of continuous field data for each of the four times in each of the four study areas. For this process, the output cell size used was determined by ArcGIS Pro based on the size and number of the units being mapped and varied by study area. The weighting power used was 2, the search radius was variable, and the number of points to sample was left at 12. These are the default settings for the tool in ArcGIS and experimentation with other settings suggested these were optimal for use in each map. The resulting continuous field temperature data was visualized as a map with color gradations along the range of temperatures found across each study area at each of the four times recorded. Each study area ended up with nine different temperature classes, regardless of the time chosen.

Because this study's demographic data was tied to administrative units, temperature needed to be as well. Using the continuous temperature maps to find the average temperature of each administrative unit was deemed the simplest way to derive temperature data for comparison to the demographic data. This was computed using the Zonal Statistics as Table tool, which created a table with the average temperature information for each administrative unit at each of the four times for each of the four study areas. These values were then mapped by joining the average temperature data from the table to the original shapefile for each study area's administrative units. This produced a map with these same values represented visually across each study area. This map data was then exported as Excel tables for use in the data analysis.

### *3.5- Data analysis*

One of the primary goals of this study was to determine if there was statistical significance between the air surface temperature data and the factors which are believed to be tied to temperature and UHI intensity. Geographically weighted regression (GWR) and local bivariate relationships/ bivariate analysis (BA) were used to explore and characterize these relationships. As a first step, surface air temperature averages for each administrative unit were combined into a single Excel document along with average income per household and population density for each study area. This file acted as a sort of omnibus of all the data gathered. This data held in this file was then joined onto each study area's respective shapefile with administrative boundaries. This correlation map file was then used to process the GWR and BA for each of the four times in each of the four study areas for each of the two relationships being explored. Both forms of data analysis were performed in ArcGIS Pro using the Geographically Weighted Regression and Local Bivariate Relationships geoprocessing tools.

*3.5.1- Geographically weighted regression*

The intention of GWR is to analyze the relationship between two variables across a given space by fitting a regression equation to every feature in the dataset. The tool predicts a value for the dependent variable based on the standard deviation between the two variables chosen. It then compares the actual recorded value to the predicted value and compares the difference between the two across the geographic space being analyzed. The GWR used for this project created a map of each study area color coded into seven classes to illustrate the local R-squared value for each administrative unit. The R-squared values show how closely the predicted values match the recorded values in order to illustrate where other factors may be significantly affecting the relationship between the two variables. R-squared values range from 1 to .01, with 1 indicating a perfect fit between the observed values and those predicted by the model ("How Geographically Weighted Regression (GWR) works—ArcGIS Pro | Documentation," n.d.). The dependent variable for the first GWR run was average household income while the explanatory variable was population density. For all other runs, average surface air temperature acted as the dependent variable while the explanatory/ exploratory variable was either average household income or population density.

Because temperature values formed a normal distribution, a continuous (Gaussian) model type was used. Bandwidth is another consideration for GWR and may be based on distance or number of neighbors. The number of neighbors was chosen for this parameter, and the specific value chosen was arrived at after using the "golden search" option to find the result with the lowest Akaike Information Criterion (AICc) value. This is because a smaller AICc value is used as an estimator of prediction error and thereby relative quality of statistical models for a given set of data. The lower the value, the lower the prediction error and the higher the relative quality of the statistical model ("How Geographically Weighted Regression (GWR) works—ArcGIS Pro | Documentation," n.d.). The optimal number of neighbors considered varied for each study area as follows: two for Chicago, five for Illinois, and ten for Amsterdam and the Netherlands. GWR also requires a weighting scheme to determine the extent to which features further away from a regression point are given less weight. For this aspect of the process, a Gaussian scheme was preferred since a Bisquare scheme causes neighbors outside the number chosen to have zero effect on the area under analysis. Because temperature values, average income values, and population distribution values may have small but real effects on each other over distances (especially within a metropolitan area), the bisquare option seemed less realistic.

*3.5.2- Local bivariate analysis*

BA works similarly to GWR, but goes a step further. It does so by calculating an entropy statistic in each zone that quantifies the amount of shared information between the two variables. This entropy statistic can capture any structural relationships between the two variables, such as exponential, quadratic, sinusoidal, or even complex relationships that cannot adequately be represented by typical mathematical functions. Entropy is a mathematical property used to quantify the amount of uncertainty in a random variable. In general, higher entropy is found where a variable is less predictable. The results of this analysis classify the relationship between the two variables for each zone into one of six

possible results: Not Significant, Positive Linear, Negative Linear, Concave, Convex, or Undefined Complex. A result of Not Significant indicates that the relationship is not statistically significant. A result of Positive Linear indicates that the dependent variable increases linearly as the explanatory variable does the same. The opposite holds true for a result Negative Linear, where the dependent variable decreases linearly as the explanatory variable increases. A result of Concave or Convex indicates how the shape of the curve of the dependent variable changes as the explanatory variable increases. Concave curves tend to bend downwards while convex curves tend to bend upwards. A result of Undefined Complex indicates that the variables are significantly related but the type of relationship cannot be satisfactorily described in a linear manner ("How Local Bivariate Relationships works—ArcGIS Pro | Documentation," n.d.).The BA used for this project created maps with each zone color coded into one of the six classes depending on the statistically significant relationship perceived by the tool. The number of neighbors considered was roughly 50% of the total zones analyzed for each study area since this seemed to give the most balanced results. Additionally, the number of permutations was 199 and the level of confidence was 90%. False Discovery Rate Correction was also applied along with a scaling factor of 0.5 (the default).

## 4. Results and Discussion of Mapping Processes

The results of the mapping processes of the study are presented below. Each section presents the maps and interpretation for one study area. This includes the average income data and population density for each study area presented as a color-coded map. This is then followed by the interpolated surface air temperature data for each study area as a map. These temperature maps have color gradations across the range of temperatures for each of the four times recorded. Finally, the surface air temperature changes across the four times recorded are discussed and interpreted. For measurements of distance, miles were used for Illinois and Chicago, while kilometers were used for the Netherlands and Amsterdam.

### *4.1- Illinois maps*

*4.1.1- Average income and population density*

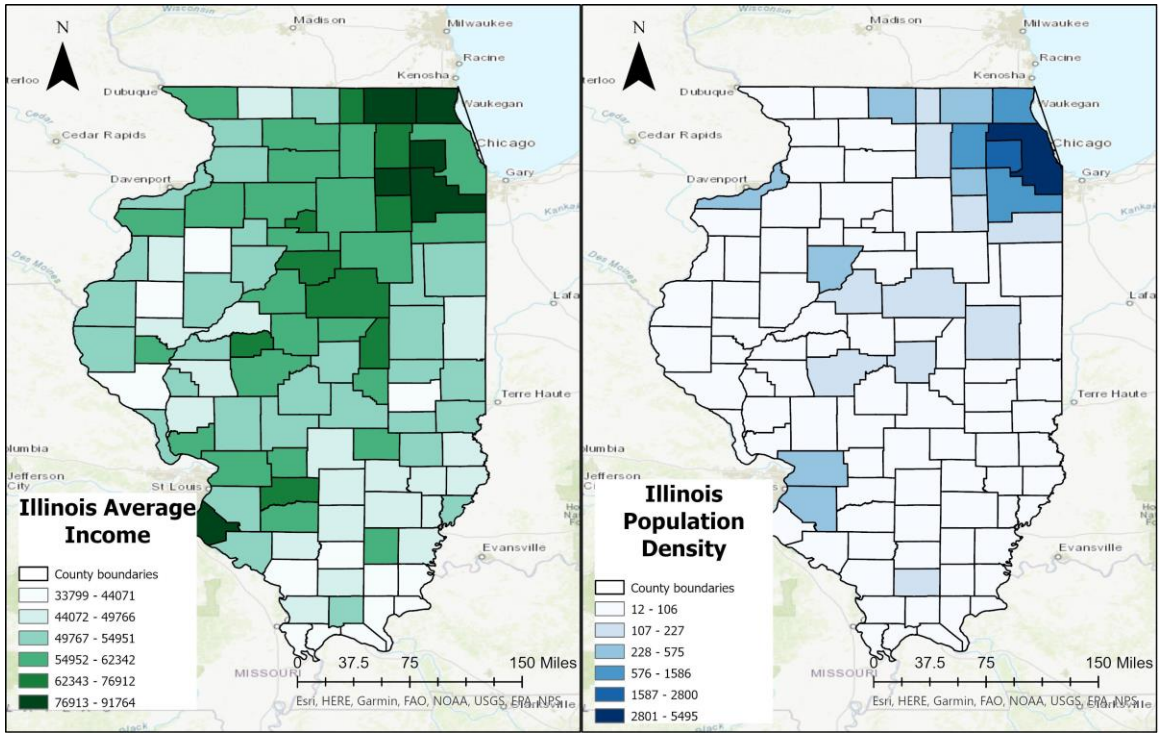


Figure 4-1: Illinois counties by average income (in U.S. dollars) and population density (in persons per square mile)

Figure 4-1 shows the average income values and population density values for Illinois by county. Average incomes for Illinois counties range from $33,799 to $91,764. Although they vary across the state, they tend to be highest near the large cities of Chicago in the northeast, St. Louis in the southwest, and Bloomington in the center-north portions of the state. The southern half of the state also tends to have lower average income compared to the rest of the state, with a similar trend in the western counties.

Population density for Illinois counties ranges from 12 persons to 5,495 persons per square mile- a vast range that illustrates the rural and urban extremes of the state. The majority of the state has relatively low population density aside from the counties that make up the Chicagoland area. This is also true to a lesser extent for the counties near Peoria, the Quad Cities, and St. Louis.

*4.1.2- Surface air temperature values*

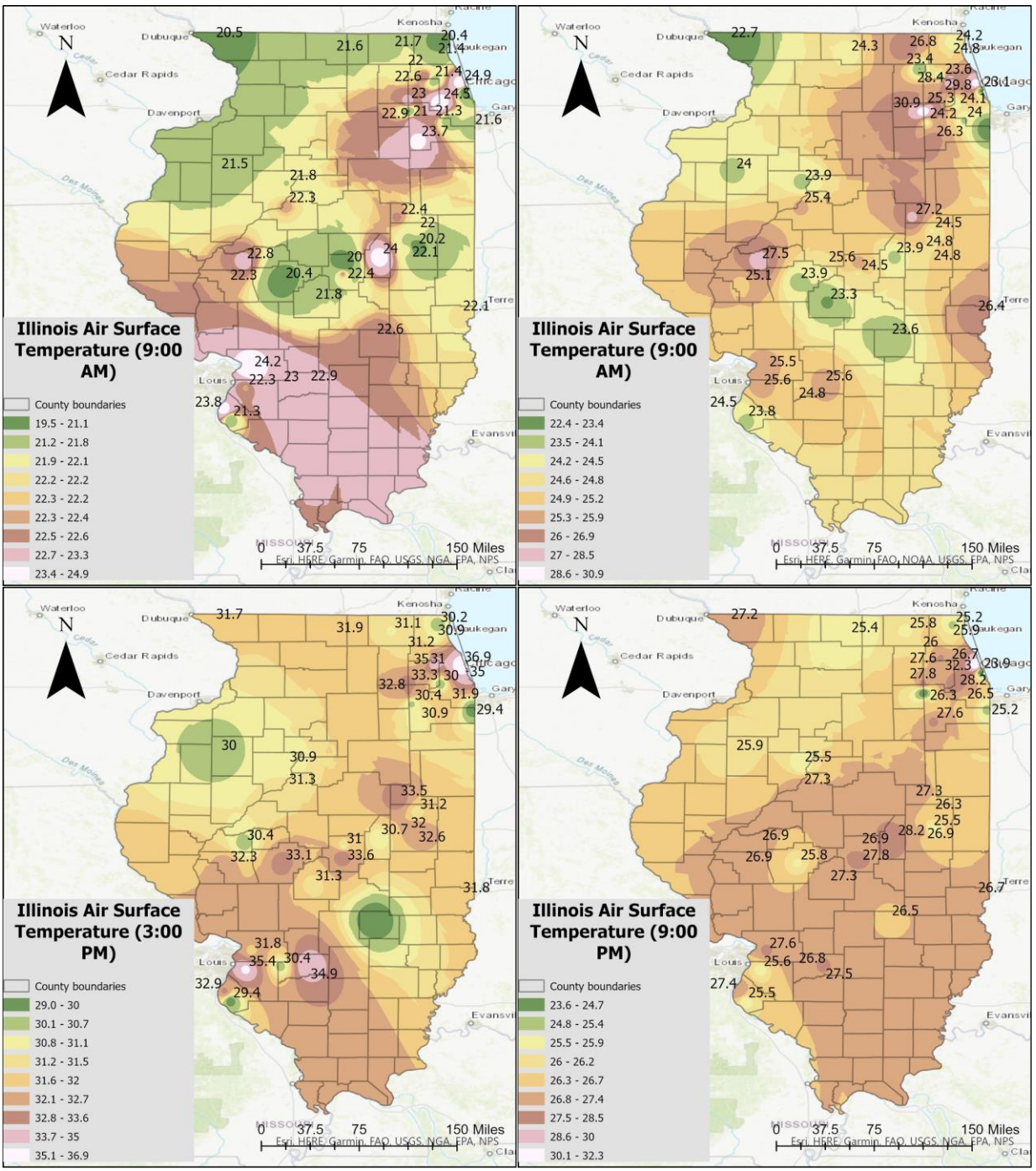


Figure 4-2: NETATMO site temperature data is overlain by interpolated air surface temperature values (in degrees Celsius) for Illinois counties on August 20, 2021.

Figure 4-2 shows the recorded and interpolated temperature data for the state of Illinois. The total range of Illinois temperatures across the day (all four times) includes 19.5

℃ as the lowest temperature and 36.9 ℃ as the highest temperature. The range of highest and lowest temperatures at each of the four times recorded is 19.5-24.9 ℃ at 3:00 AM, 22.4-30.9 ℃ at 9:00 AM, 29.0-36.9 ℃ at 3:00 PM, and 23.6-32.3 ℃ at 9:00 PM. Taken as a whole, temperatures vary across the state but are lowest at 3:00 AM and rise until peaking at 3:00 PM before descending once again. For all times, Chicago is at the highest range of values.

Figure 4-2 shows the largest amount of area dedicated to white (the top end of each time's temperature range) at 3:00 AM, as the day begins. Because UHI is expected to be highest at this time, this is consistent with such an expectation. The areas near Chicago, St. Louis, and Champaign-Urbana (just east of the state's center) are hot spots consistent with the largest urban areas in or near the state (St. Louis lies just across the border with Missouri). However the fact that Springfield, the state's capital and seventh most populous city at the center of the map, is so relatively cool at this time is unexpected. By 9:00 AM, the map is dominated by temperatures in the middle classes with the hottest and coolest temperature ranges noticeably reduced in size, while Champaign-Urbana and Springfield now show small cook spots. By 3:00 PM, as UHI is increasing once again, areas exhibiting temperatures in the bottom two or three classes are fewer and more isolated, with a swath of warmer temperatures in the south that includes the St. Louis hot spot. By 9:00 PM, as UHI is rising once again, the map is dominated by temperature classes in the middle and upper-middle classes of the range.

*4.1.3- Discussion of values*

Figure 4.2 shows how surface air temperature changed throughout the day on August 20, 2021 for the state of Illinois. Although it was a given that the range of temperatures would change throughout the day, the large variation in terms of what parts of the state are hotter or cooler than each other at various times was an unexpected result. For example, the northernmost portion of the state outside Chicago is at the lowest temperature range for 3:00 AM but transitions into the lower-middle range later in the day. This is difficult to interpret and may be a result of regional climate. While showing significant variance, the overall results suggest a consistent transition throughout the day, especially when transitioning from 3:00 PM to 9:00 PM. Aside from a few cool spots, it is feasible that results for 3:00 AM on August 21 would closely resemble those seen at 3:00 AM on August 20. This lends weight to the data's accuracy. However, Figure 7-1 illustrates the poor spread of the data for Illinois, which reduces confidence in the interpolation based on these points.

### *4.2- Chicago maps*

*4.2.1- Average income and population density*

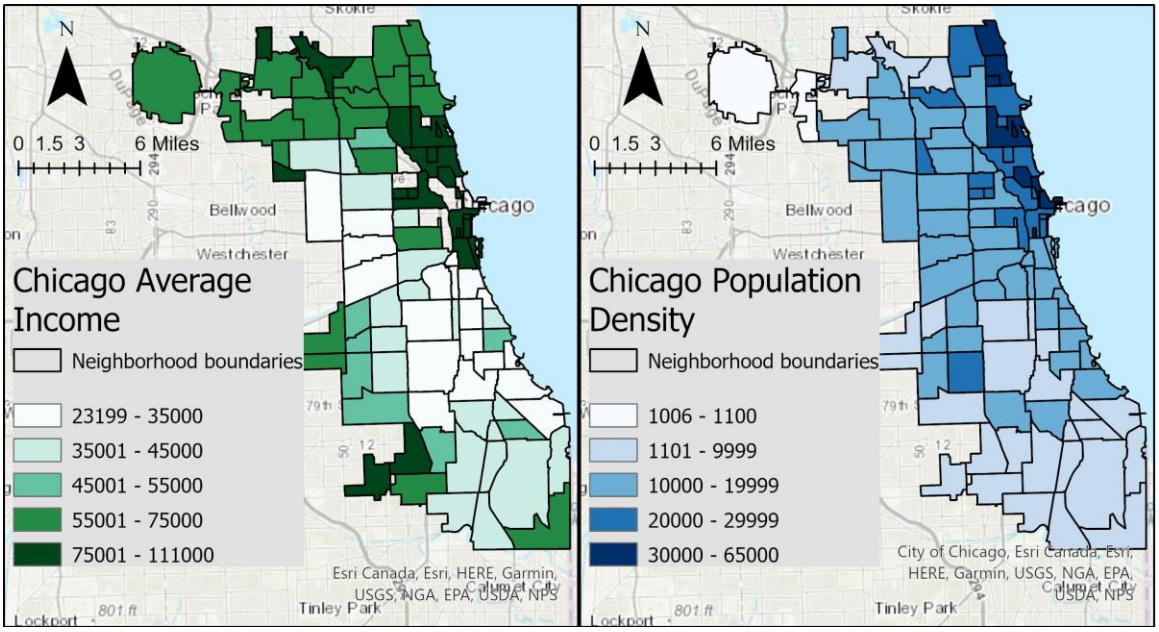


Figure 4-3: Chicago neighborhoods by average income (in U.S. dollars) and population density (in persons per square mile)

Figure 4-3 shows average income values and population density values for the city of Chicago by neighborhood. Average incomes for Chicago neighborhoods range from $23,199 to $111,000. These averages vary wildly across the city, but the near south and near west side neighborhoods have the lowest average income values. This trend reverses for the southern portion as one moves west and nearer to the suburbs. Otherwise the far north and the northern neighborhoods along the lakeshore have the highest average income values.

Population density for Chicago neighborhoods ranges from 1,006 persons to 65,000 persons per square mile. Patterns in this data are more a bit more difficult to discern but the northern lakeshore neighborhoods are the most dense while the neighborhoods near O'Hare Airport are the least dense. In general, the southern and northern periphery of the city become less dense as their nearness to the suburbs increases.

*4.2.2- Surface air temperature values*

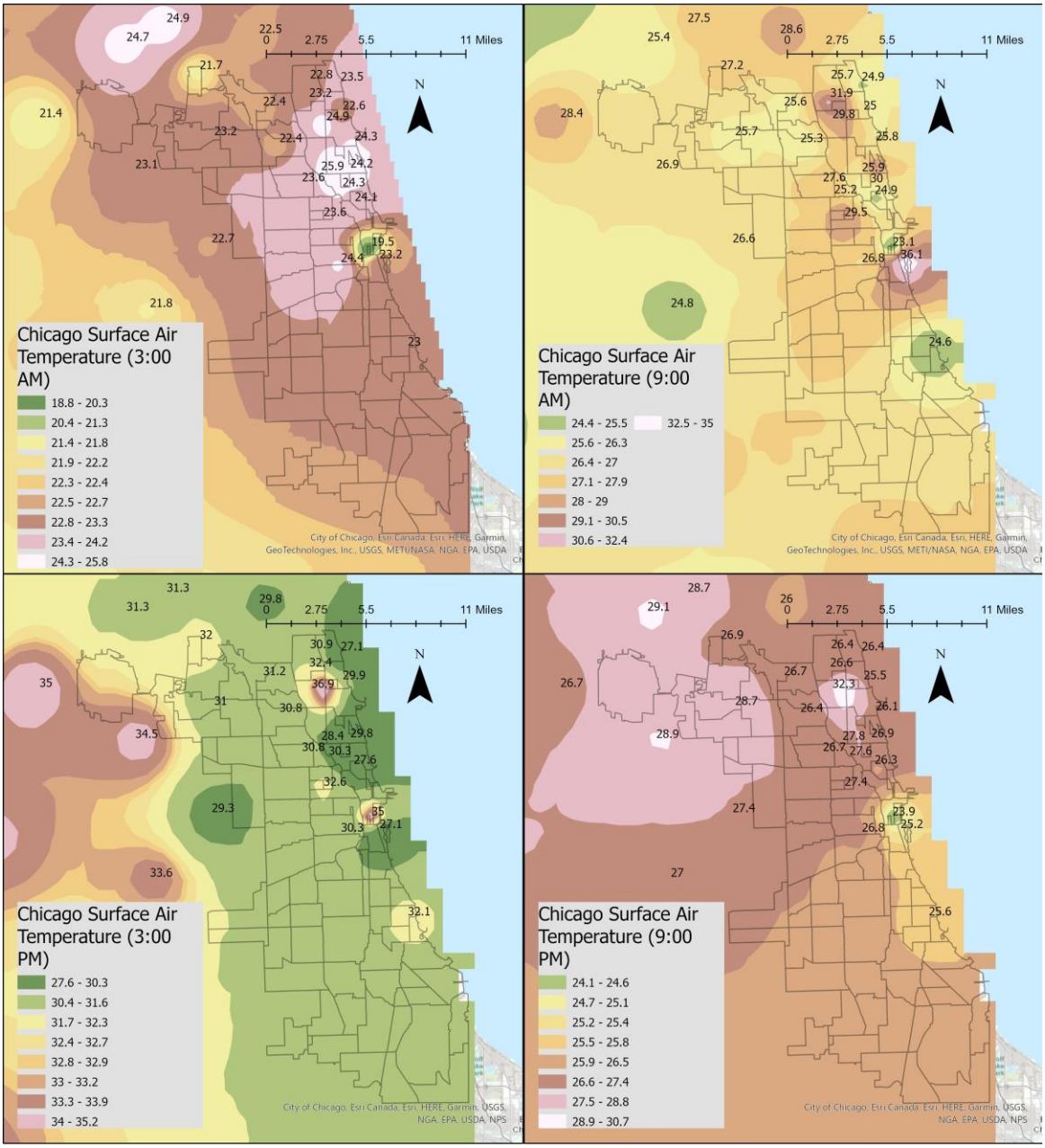


Figure 4-4: NETATMO site temperature data is overlain by interpolated air surface temperature values (in degrees Celsius) for Chicago neighborhoods on August 20, 2021

Figure 4-4 shows the recorded and interpolated temperature data for the city of Chicago. The total range of Chicago temperatures across all four times includes 18.8 ℃ as the lowest temperature and 37.8 ℃ as the highest temperature. The range of temperatures at each of the four times recorded is 18.8-25.8 ℃ at 3:00 AM, 22.8-35.0 ℃ at 9:00 AM, 27.6-37.8 ℃ at 3:00 PM, and 23.0-30.7 ℃ at 9:00 PM. Temperatures across Chicago vary considerably throughout the day with the only constant being a hot spot in the northernmost neighborhoods.

Figure 4-4 shows that at 3:00 AM, all neighborhoods are warmer than the suburbs to the south and west, with a large hot spot on the north side. A small cool spot can be seen near the center of the city that corresponds to the sprawling Millennium Park, a large green space. By 9:00 AM, temperatures have increased but more of those classified in the lower-middle range dominate the map aside from hot spots at the center, near north side, and north side of the city. By 3:00 PM, this trend has amplified with what can be described as "urban cooling" being evident. The vast majority of neighborhoods show temperatures in the coolest two classes while the suburbs in the west and area near O'Hare Airport (the northwesternmost neighborhood shown) exhibit temperatures on the higher end of the range. Finally, at 9:00 PM, we see the city once again dominated by temperatures in the middle and upper-middle temperature classes along with the return of the cool spot near Millennium Park. The hot spot near O'Hare Airport has expanded and the overall map shows a transition back toward what we saw at 3:00 AM.

*4.2.3- Discussion of values*

Figure 4-4 shows how surface air temperatures changed across Chicago throughout the day. The urban cooling trend that begins at 9:00 AM and ramps up by 3:00 PM is consistent with some UHI findings in other studies, such as those mentioned in Chapter 2.1 above, but is often seen a bit earlier in the day. The temperature transition from 3:00 PM to 9:00 PM and the 9:00 PM map's similarity to the 3:00 AM map is striking. Both of these observations suggest a consistent transition of temperature and UHI throughout the day, which increases confidence in the point data and the interpolation. One obvious anomaly is the hot spot over Millennium Park at 3:00 PM, which is difficult to explain. Another is the hot spot at the very center of the city along the lakeshore at 9:00 AM, in neighborhoods of moderate to high population density and very high average income.

### *4.3- Netherlands maps*

#### *4.3.1- Average income and population density*

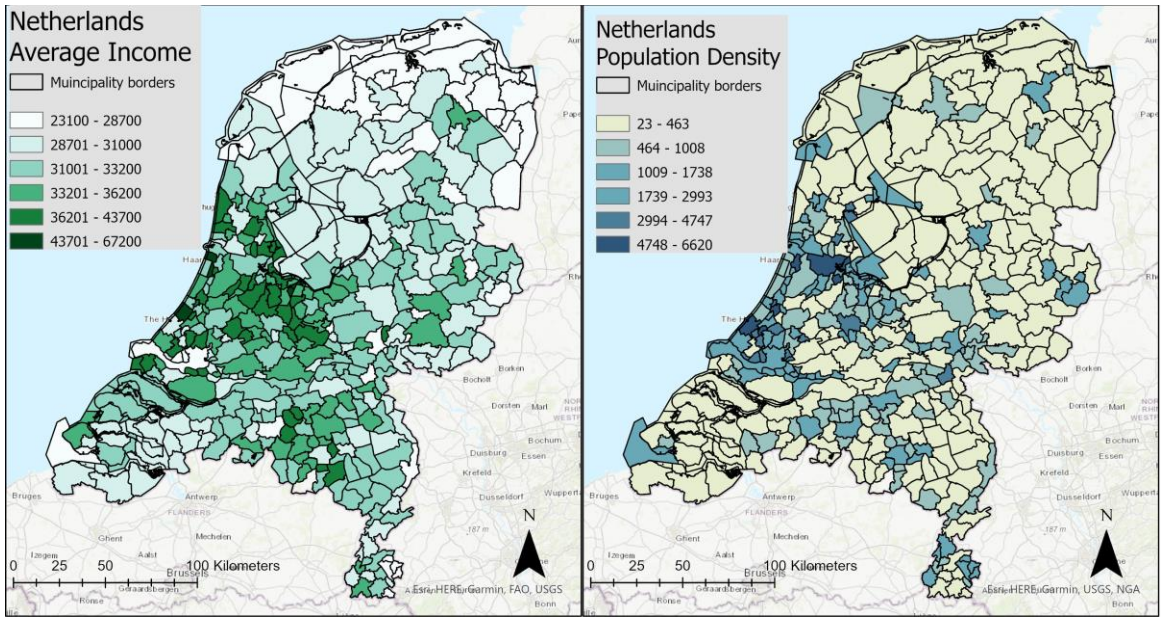


Figure 4-5: Netherlands municipalities by average income (in Euros) and population density (in persons per square kilometer)

Figure 4-5 shows average income values and population density values for the continental Netherlands by municipality. Average incomes for municipalities across the Netherlands range from €23,100 to €67,200. These values vary across the Netherlands but trend higher near the cities of Amsterdam and Utrecht in the center, the Hague along the coast, and Rotterdam in the south. Much of the more rural municipalities of the northeastern portion of the country have comparatively lower average income values.

Population density for the Netherlands ranges from 23 persons to 6,620 persons per square kilometer. The population density of the nation largely parallels the income trends with high points being a bit more isolated and showing more abrupt decreases outside of urban areas.

*4.3.2- Surface air temperature values*

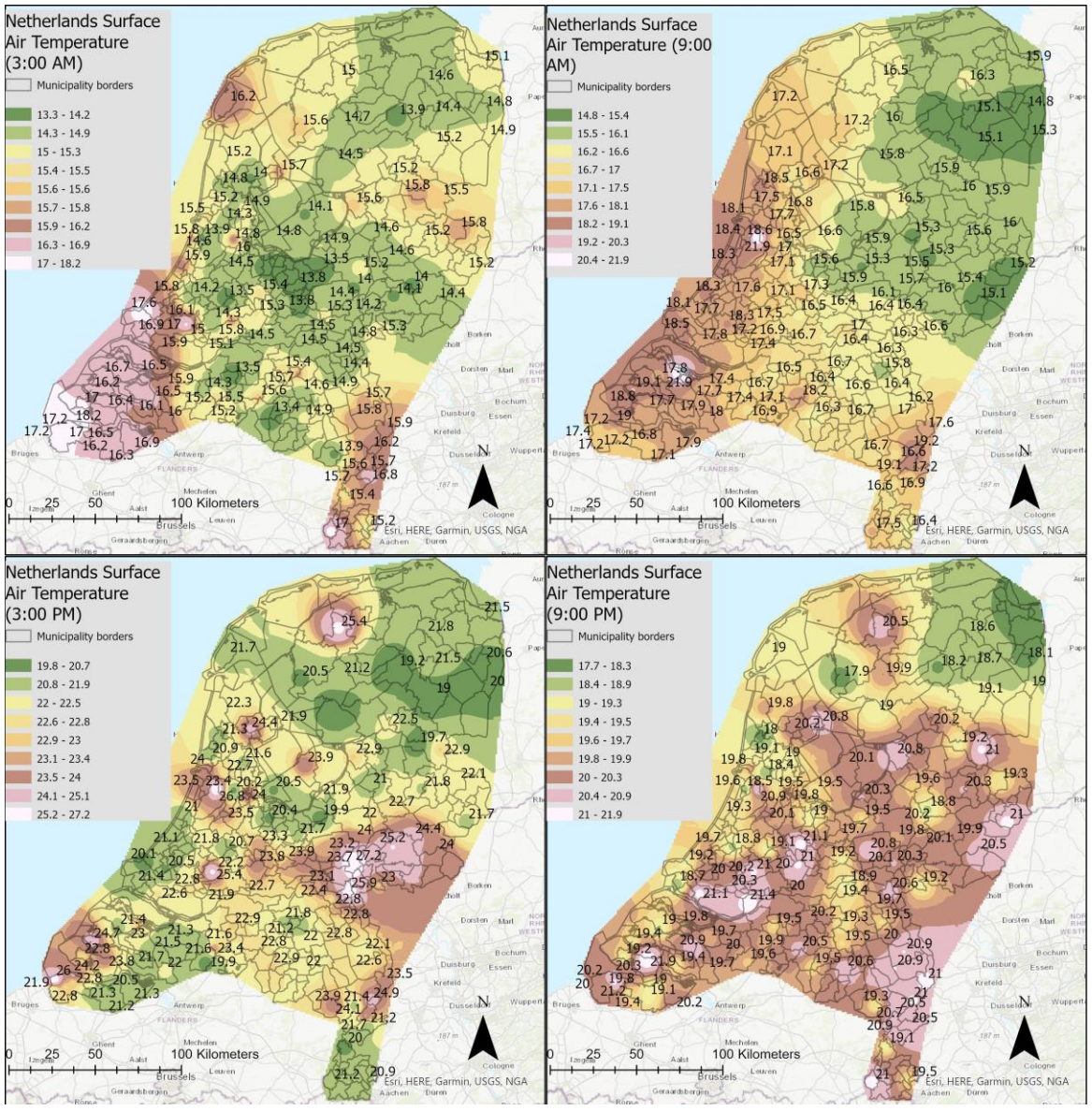


Figure 4-6: NETATMO site temperature data is overlain by interpolated air surface temperature values (in degrees Celsius) for Netherlands municipalities on August 20, 2021

Figure 4-6 shows the recorded and interpolated temperature data for the continental Netherlands. The total range of Netherlands temperatures across all four times includes 13.3 ℃ as the lowest temperature and 27.2 ℃ as the highest temperature. The range of temperatures at each of the four times recorded is 13.3-18.2 ℃ at 3:00 AM, 14.8-21.9 ℃ at

9:00 AM, 19.8-27.2 ℃ at 3:00 PM, and 17.7-21.9 ℃ at 9:00 PM. The Netherlands shows considerable temperature variance throughout the day with few consistencies. The southwestern and northwestern corners of the nation tend be on the warmer end of the range for all times, while the northeastern corner of the nation tends be on the cooler end of the range.

Figure 4-6 shows that at 3:00 AM, when UHI should be highest, the map shows the center of the country at the lowest end of the temperature range with temperatures increasing as distance increases from the center in all directions. This central, cool spot is the fairly built-up area that lies between the cities of Amsterdam and Utrecht. Additionally the hot spots at the four extreme ends of the map all line up with municipalities of higher population density, especially the cities of Maastricht in the southwest and Middelburg in the southeast, as seen in Figure 4-5. By 9:00 AM, temperatures have begun to rise and there is a clear gradation between the cooler regions of the northeast with the warmest regions along the west coast.

Figure 4-6 shows that at 3:00 PM, when UHI should still be fairly low, the picture is far less clear than at 9:00 AM. The northeast continues to be cooler, while cooler swaths have appeared in the southeast, southwest, and along the coast. The warmest areas, surrounded by gradually cooler zones with distance, are found in the far north, the east-central border, the southwestern tip of the country, and the area between Amsterdam and Haarlem. When 9:00 PM arrives, temperatures have begun to fall but the highest and middle-high temperature classes dominate the map in terms of area. The hottest spots are sprinkled throughout much of the lower three-quarters of the country, joined by areas of gradually reducing temperatures in between them. Only the northeasternmost municipalities show the cooler temperature classes.

*4.3.3- Discussion of values*

Figure 4-6 shows surface air temperatures for the Netherlands over the course of the day for August 20, 2021. The zoning and gradations here are markedly smoother and more detailed than the other study areas thanks to a plethora of data points with good spread/ coverage, as shown in Figure 7-3. The warmer bands along the coast at 9:00 AM are difficult to interpret since nearness to the North Sea should allow for more evaporative cooling, which should help keep temperatures down. On the other hand, Figure 4-5 shows that these municipalities all exhibit higher range values for average income and population density, so UHI should be higher here if this study's hypothesis holds true. The more isolated nature of the temperature zoning at 3:00 PM may suggest a lack of wind, leading to more localized climate zones over a larger overall regional one at this time of day. The large cool region in the northeast at 9:00 PM stands out as the rest of the country is dominated by middle and high temperature classes. However, because this region tends to have both lower average income and lower population density, this is consistent with an expectation of lower UHI compared to other parts of the country at this time.

### *4.4- Amsterdam maps*

*4.4.1- Average income and population density*

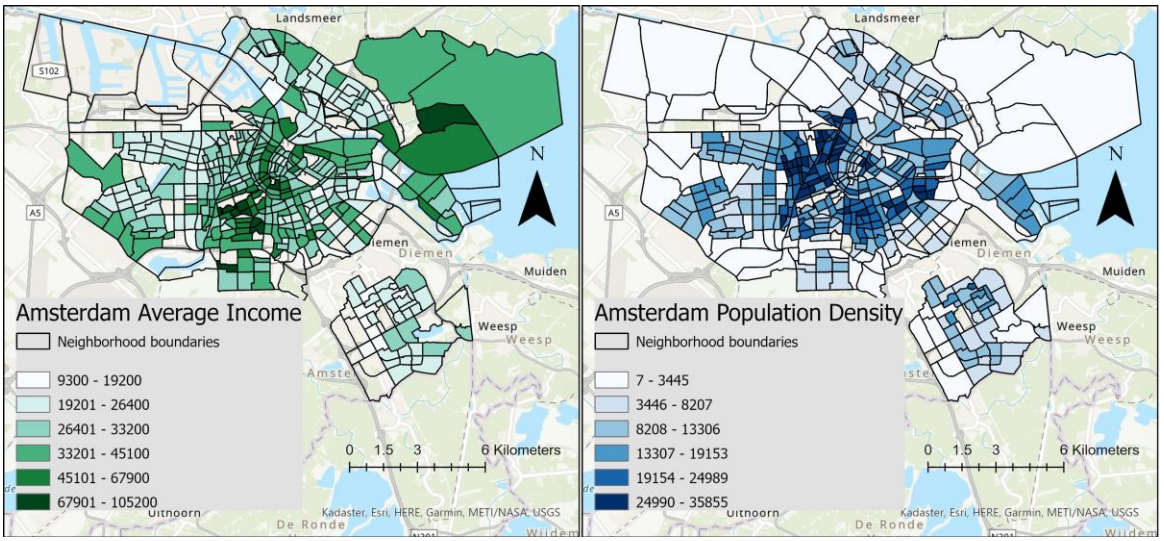


Figure 4-7: Amsterdam neighborhoods by average income (in Euros) and population density (in persons per square kilometer)

Figure 4-7 shows average income values and population density values for the city of Amsterdam by neighborhood. Average incomes for neighborhoods across Amsterdam range from €9,300 to €105,200. Data is missing for several neighborhoods where industry is dominant and residential areas are functionally non-existent. However, the highest income values are found in the central column of the city that runs north to south, the westernmost edge of the city, and the neighborhoods of the Noord sector.

Population density for Amsterdam ranges from 7 persons to 35,855 persons per square kilometer. The distribution of this density is fairly uniform with the center of the city being most dense and decreasing with distance from the center. The industrial Westpoort sector has virtually no residents.

*4.4.2- Surface air temperature values*

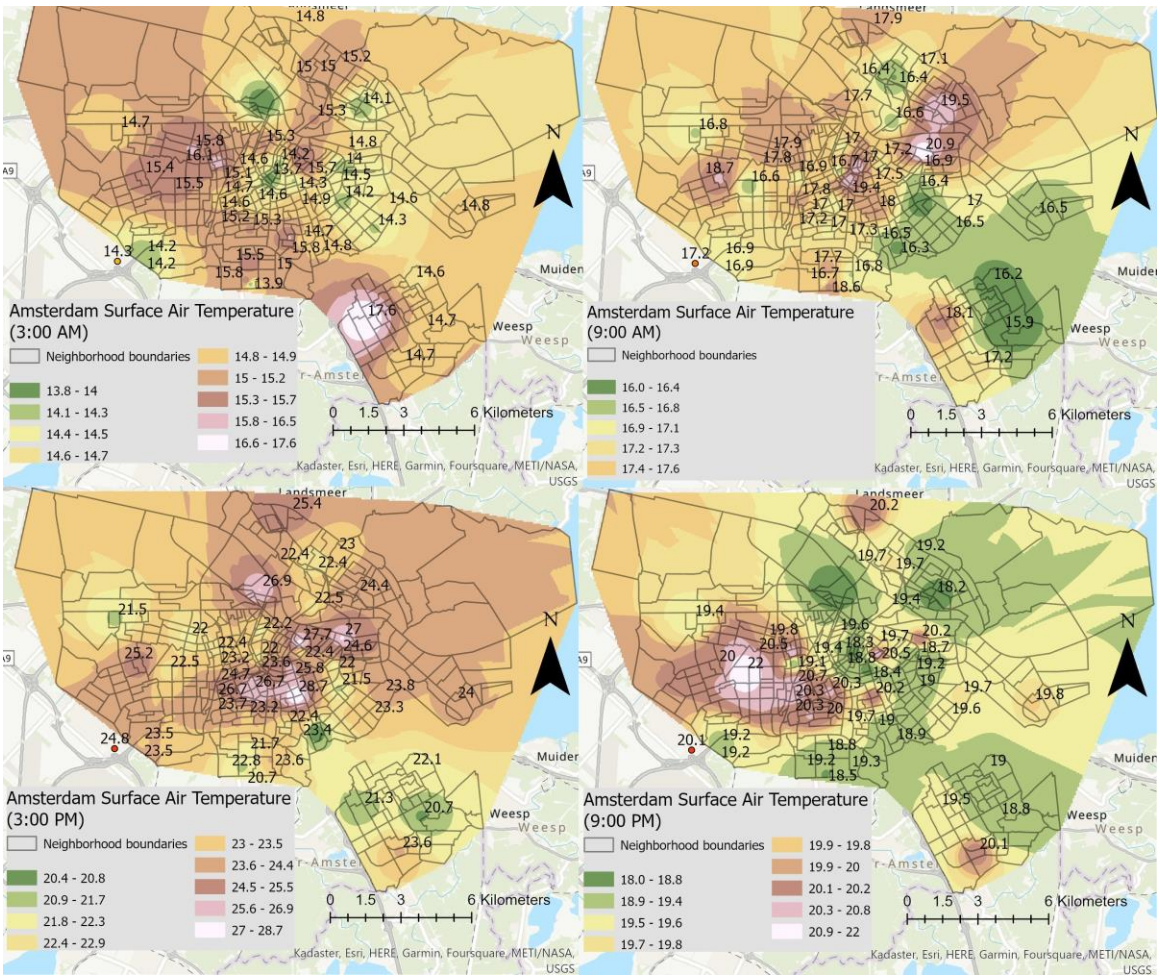


Figure 4-8: NETATMO site temperature data is overlain by interpolated air surface temperature values (in degrees Celsius) for Amsterdam neighborhoods on August 20, 2021

Figure 4-8 shows the recorded and interpolated temperature data for the city of Amsterdam. The total range of Amsterdam temperatures across all four times includes 13.8 ℃ as the lowest temperature and 28.7 ℃ as the highest temperature. The range of temperatures at each of the four times recorded is 13.8-17.6 ℃ at 3:00 AM, 16.0-209 ℃ at 9:00 AM, 20.4-28.7 ℃ at 3:00 PM, and 18.0-22.0 ℃ at 9:00 PM. Amsterdam temperatures

show considerable variation throughout the day with fer readily discernible patterns or consistencies.

Figure 4-8 shows that as the day begins at 3:00 AM, much of the city's neighborhoods show temperatures in the middle to higher classes with cool spots located at the city's largest green spaces- the Westerpark, Vondelpark, and Oosterpark. A very large hot spot dominates the Zuidoost region in the southeast. By 9:00 AM, temperatures across the city have increased. However, the middle classes of temperatures are much more dominant on the map, with the coolest ranges found in the southeast, immediately adjacent to the 3:00 AM hot spot. The more population dense parts of the city, near the center, all show middle-high to high temperature classes. The highest temperatures are found in the higher average income and more population dense neighborhoods near the IJ-waterfront (on the border between Centrum and Oost as seen in Figure 3-4). By 3:00 PM, more hot spots have appeared surrounding the city center while the area taken up by the upper-middle temperature classes has increased while that of the lowest temperature classes has noticeably reduced. This is taking place even as temperatures increase toward their maximums for the day. Finally at 9:00 PM, as UHI should be increasing, the coolest three classes of the temperature range now dominate the eastern half of the map. At the same time, the higher temperatures surround a large hot spot in the west that lies along the border of the Zuid and Nieuw-West regions of the city. This area tends toward lower average income and lower population density, similar to the hot spot seen at 3:00 AM.

*4.4.3- Discussion of values*

Figure 4-8 shows air surface temperatures for Amsterdam as the day of August 20, 2021 progressed. The 3:00 AM hot spot in Zuidoost is anomalous since the range of temperatures in this detached portion of the city would not be expected to be so high. Figure 4-7 shows that this area has both low average income and low population density, further increasing the difficulty of interpreting this result. The 9:00 AM hot spot just northeast of the city center along the IJ is also unexpected. Considering the proximity to the IJ (a large body of water), and the increased evaporative cooling expected, there must be factors at work that this study has not accounted for. The temperature trends at 3:00 PM tend to show warmer areas where population density is higher, but the warmer temperatures in the less dense northeasternmost neighborhoods defy this trend. When comparing the 9:00 PM map to the 3:00 AM, the natural inference is that temperatures in the lowest classes decrease in number as UHI increased overnight. This fails to account for why the largest hot spot seems to migrate from the west to the southeast over that timeframe. This may also suggest that the UHI increase happens later or more slowly for Amsterdam than for the other study areas.

## 5. Results and Discussion of Data Analysis

Several subquestions posed by this study involved the question of whether there were statistically significant relationships between surface air temperature and both average household income and population density within each administrative unit. The ultimate goal of the study was to draw out these otherwise murky relationships in order to elucidate them. The results of geographically weighted regression below illustrate where these relationships

varied from the predicted values enough that they might be considered statistically significant. GWR results are presented and discussed for each area, using a similar format and order as that used for section **4. Results and Discussion of Mapping Processes**

In order to bolster the insights gained from GWR, bivariate analysis was undertake on all study areas at the same times and using the same administrative units. Except for directly comparing average income and population density, the same variables were compared but using a very different methodology. Unlike the GWR results, the BA results varied considerably between the four study areas. Because of this, results for Chicago and Illinois are discussed only briefly while those for Amsterdam and the Netherlands are looked at in more detail.

### *5.1- Geographically weighted regression*

The GWR used for this project began by comparing the average income values with the population densities for each administrative unit. The average surface air temperature for each administrative unit was then compared with that of both average income and population density for each administrative unit. All three iterations of the GWR process created a map of each study area color coded into seven classes to represent the local R-squared value for the dependent and explanatory/ exploratory variables being compared across each study area. The closer the value to 1, the more significant the relationship between the two variables, while lower values indicate either less significance to the relationship or interference by factors unaccounted for in the model. For more detailed information regarding this process and its set-up, please see section ***3.5- Data analysis***.

#### *5.1.1- GWR for Illinois*

The GWR for Illinois begins by comparing average income with population density, as shown in Figure 5-1. The overall R-squared value was .64, indicating a moderate goodness of fit. The mapped results show no trend in terms of which classes are more or less populated, but do show a clear trend toward a best fit in the northeastern portion of the state in counties just outside greater Chicagoland. This

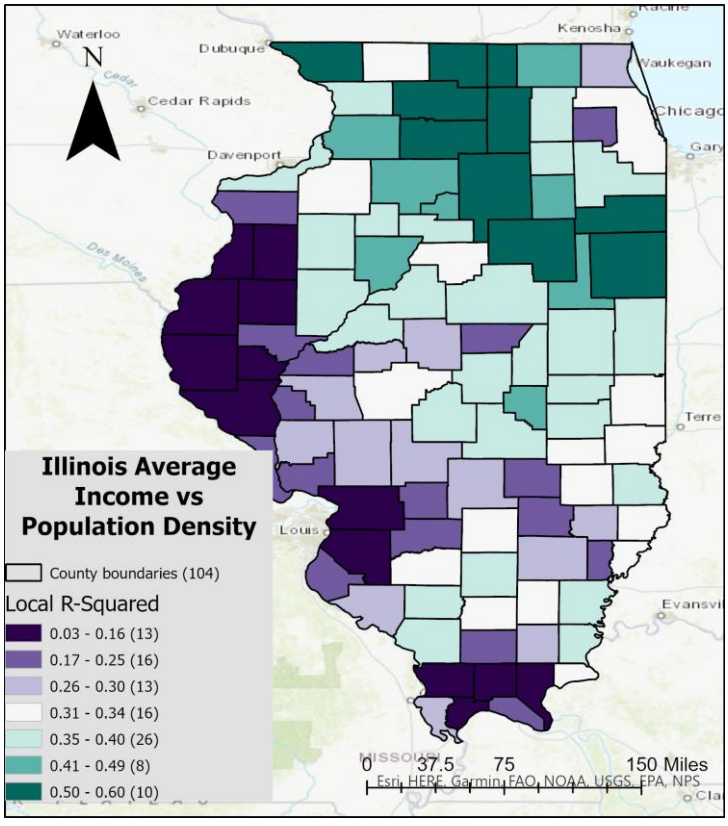


Figure 5-1: Geographically weighted regression of average income vs. population density for Illinois

decreases moving south and west with the lowest R-squared values at the southern and western borders of the state. With the exception of the west-central counties near St. Louis,

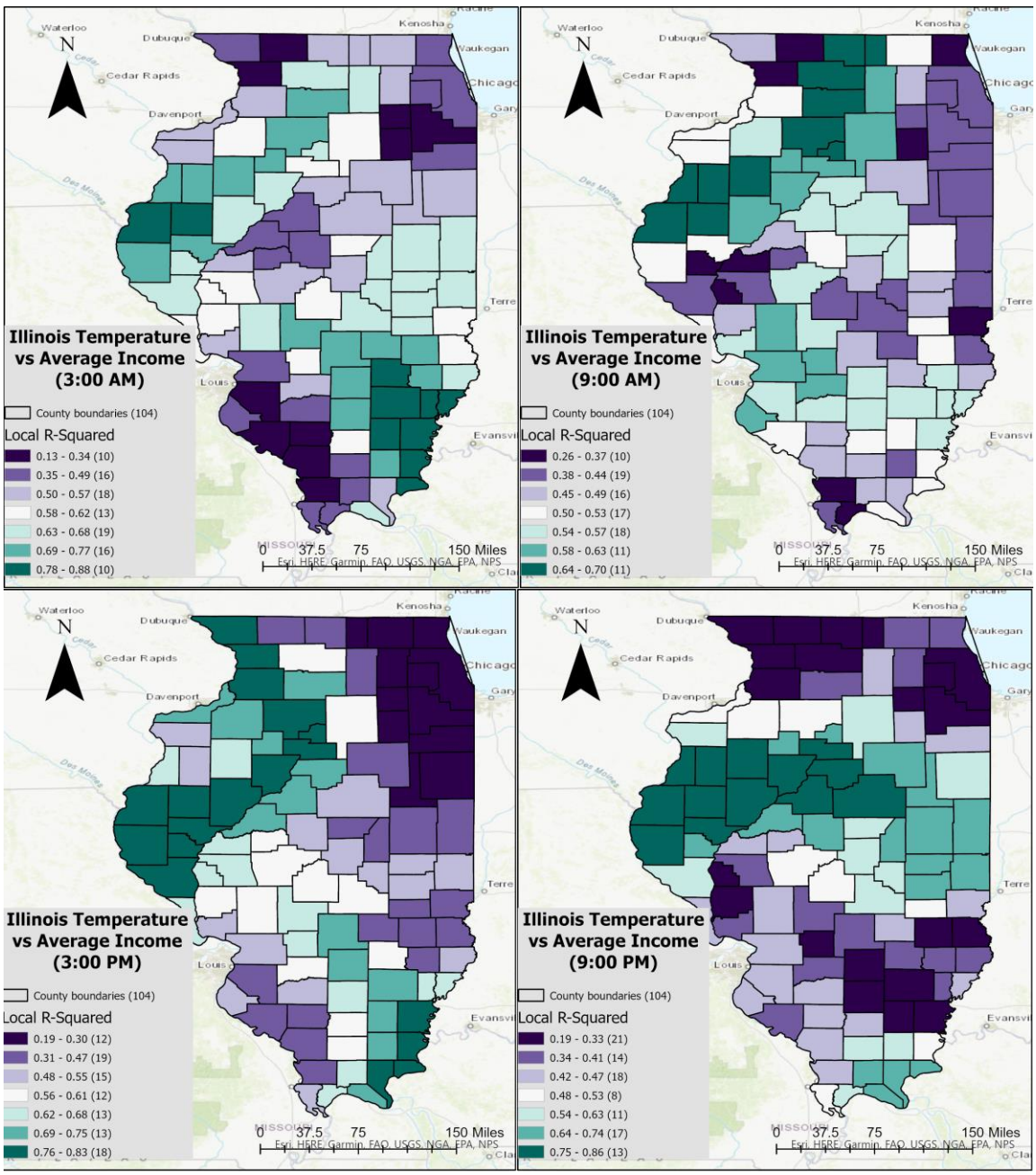


Figure 5-2: Geographically weighted regression of temperature vs. average income for Illinois

all of counties with R-squared values of .03 to .16 have very low population densities and low to moderate average income values.

Figure 5-2 illustrates the GWR results for temperature values and average income across the four times chosen. The average overall R-squared value for all four maps was .72,

indicating a fairly strong goodness of fit. The population of each class varies throughout the day with no clear pattern aside from an upswing in values of .19 to .33 and a marked decrease in values of .48 to .47 at 9:00 PM. The overall trend on the map is for the highest R-squared values to appear in a long strip across the northwestern portion of the state along with a cluster in the southeastern portion. This is most evident at 3:00 AM and 9:00 PM. Conversely, the lowest R-squared values tend to be found in the northeastern portion of the state but a large cluster also appears in the southern end of the state at 3:00 AM and 9:00 PM. Most of the clustering found on the map shows clear gradations of increases and decreases, though some of the moderate values in between skip one or two classes when one cluster abuts another of an opposing trend. Although the clusters shift and move a bit across the four times, there is no clear increase or decrease in the R-squared values as the day goes on. For example, the population of the highest three classes shifts across each time but the total for the three classes always stays between 40 and 45, making deeper interpretations difficult. UHI should be highest at 3:00 AM, and yet this time shows the lowest number of values in both the lowest class (.13 to .34) and the highest class (.78 to .88).

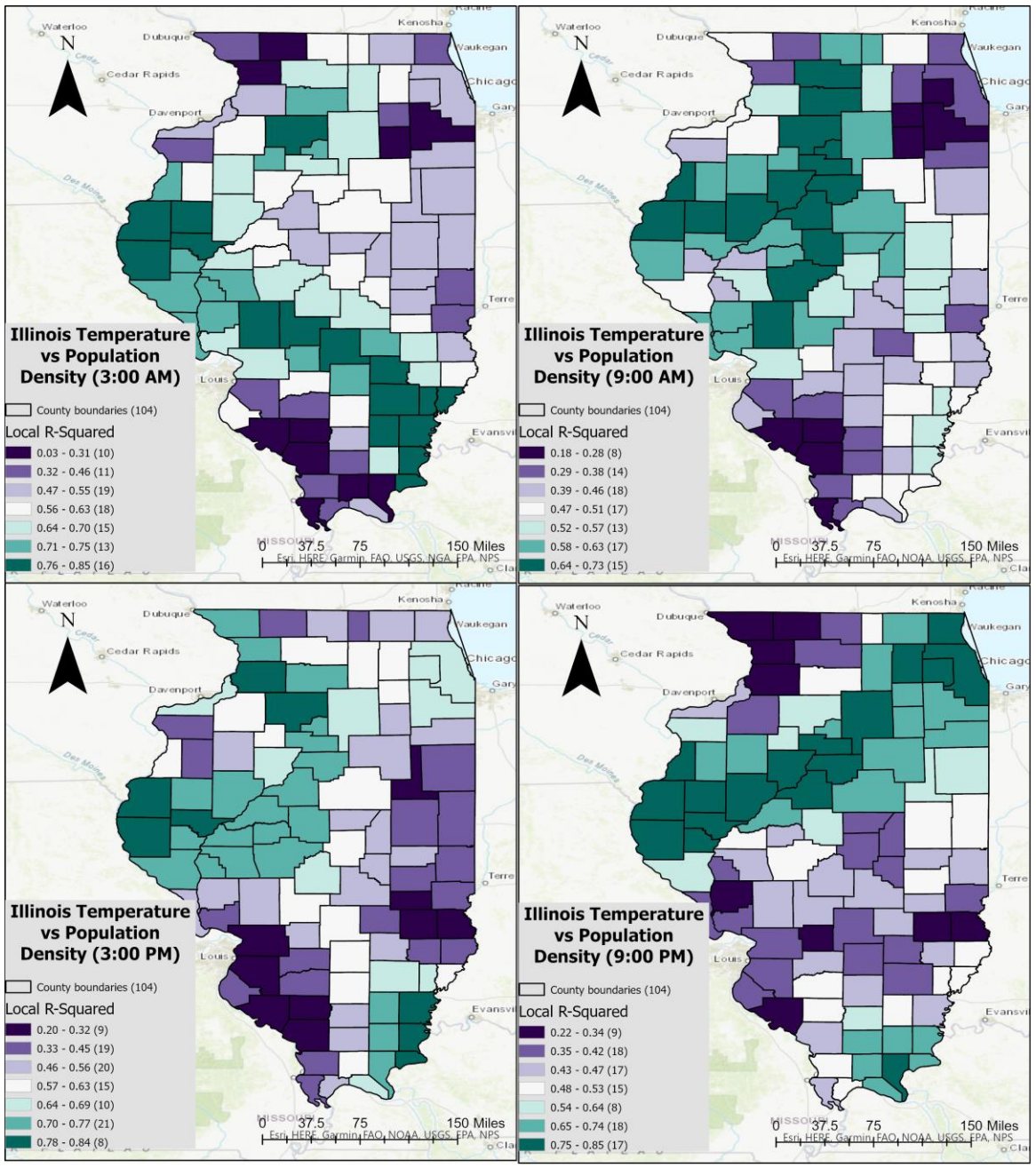


Figure 5-3: Geographically weighted regression of temperature vs. population density for Illinois

Figure 5-3 illustrates the GWR results for temperature values and population density. The average overall R-squared value for all four maps was .73, indicating a fairly strong goodness of fit. The mapped results are very similar to those seen in Figure 5-2, with 3:00 AM and 9:00 AM nearly identical between the two figures. Results for 3:00 PM and 9:00 PM are noticeably different, however. At 9:00 PM, the band of high R-squared values that begins in the west continues northeast to the state's border instead of reversing in trend as it does in Figure 5-2. The R-squared values in the southwest are also a bit higher in general when

compared to the other figure. The greatest difference can be seen at 3:00 PM, where R-squared values are considerably higher in the northeast when compared to Figure 5-2. Values in the southwest a bit higher as well, while values along the western border are slightly lower in general.

Figure 5-3 also shows no discernible trend in terms of the populations of each class. Once again the distribution is seemingly random and uneven aside from a hollowing out of the middle classes at 3:00 PM. One noticeable trend as the day goes on is how the moderately high R-squared values along the northeast-southwest running band increase at 9:00 AM, decrease at 3:00 PM, then increase once more at 9:00 PM. Another change can be seen where the cluster in the south-central portion of the state exhibits values of .71 to .85 at 3:00 AM, drops to .29 to .46 at 9:00 AM, then slightly increases at 3:00 PM only to return to lower values at 9:00 PM.

*5.1.2- GWR for Chicago*

Comparing average income with population density is the first GWR processed for Chicago, as shown in Figure 5-4. The overall R-squared value was .89, indicating a strong goodness of fit. The mapped results show a semi-even distribution across the seven classes with the highest R-squared values present in the center of the city aside from two outliers in the extreme northeast. The lowest R-squared values appear in the southern half of the city, where data points were the most scarce and both population density and average income values tend to be lower. This trend is defied by higher values in the southwestern and west-central portions of the city.

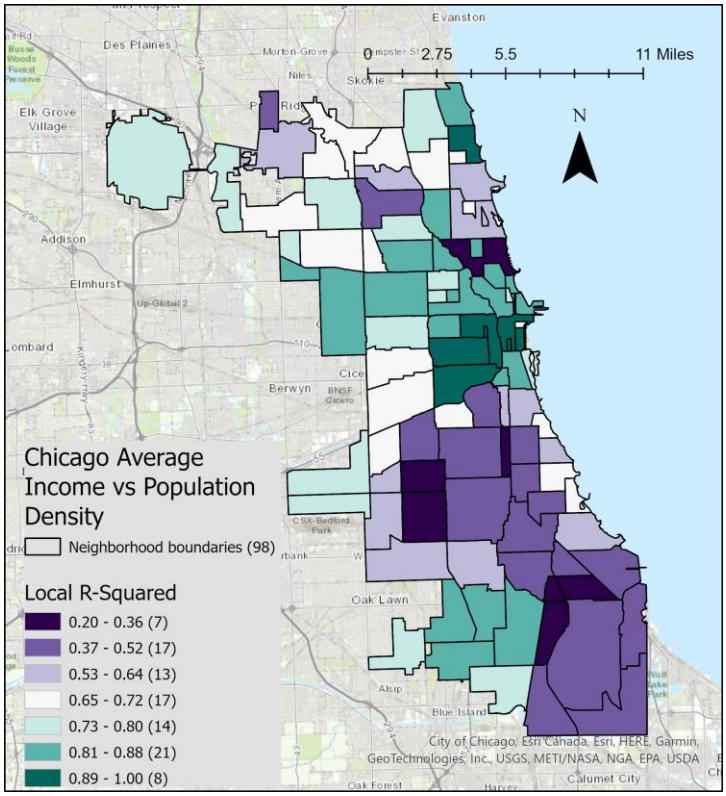


Figure 5-4: Geographically weighted regression of average income vs. population density for Chicago

Figure 5-5 illustrates the GWR results for temperature values and average income across the four times chosen. The average overall R-squared value for all four maps was .81, indicating a strong goodness of fit. The population of the seven classes here is a bit more normally distributed with smaller populations on the extreme ends of the class divisions for most of the four times. The R-squared values exhibit considerable changes throughout the

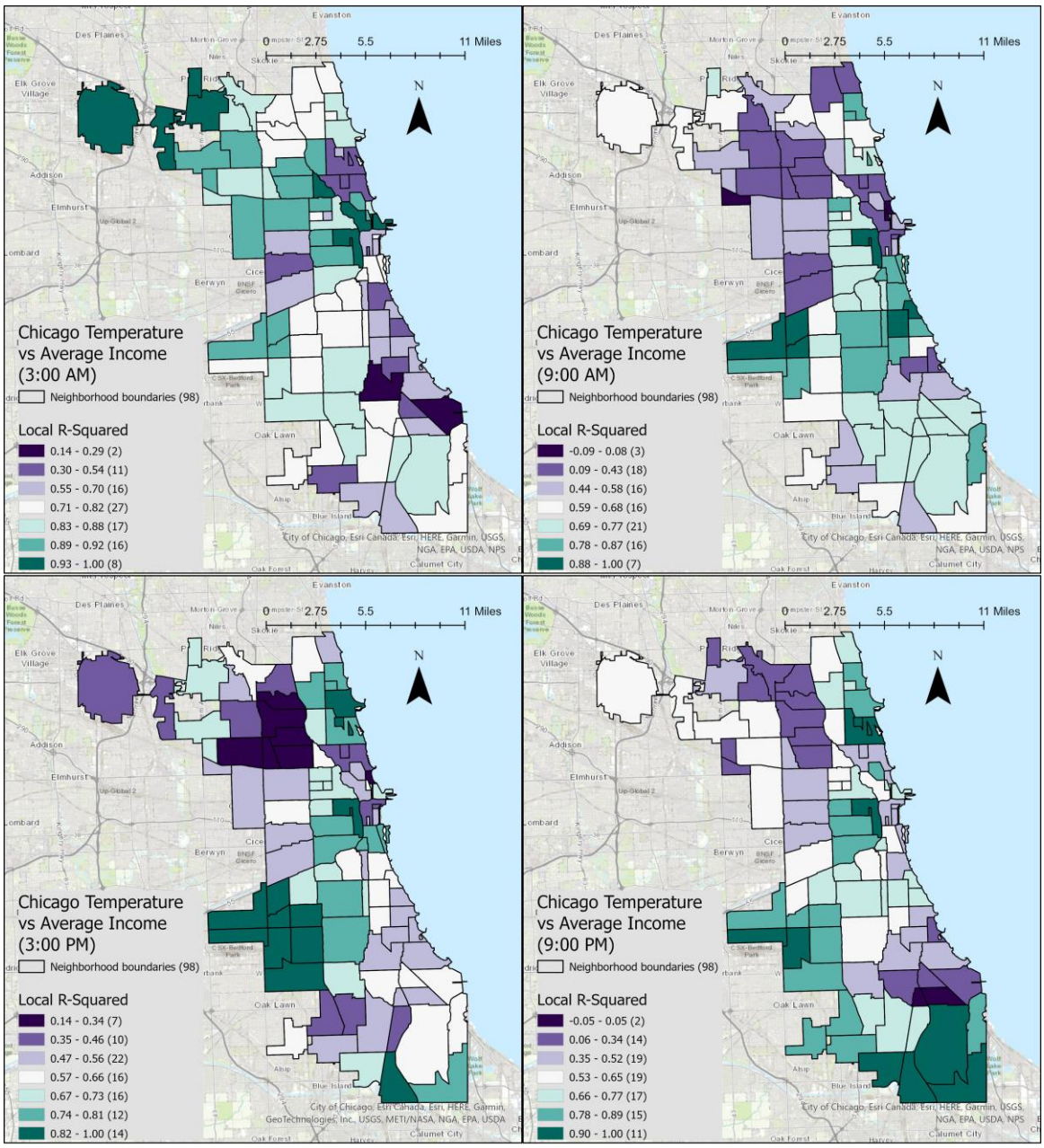


Figure 5-5: Geographically weighted regression of temperature vs. average income for Chicago

day but values in the near South Side, particularly in west, remain above .81. In the northwest, values begin high at .89 or above at 3:00 AM, drop precipitously at 9:00 AM, continue this trend at 3:00 PM, then bounce back a bit by 9:00 PM. In the southeastern corner of the city, values at 3:00 AM range from .30 to .88, move up to a minimum of .44 by 9:00 AM, and then reach minimum values of .66 by 9:00 PM; this shows a clear and steady increase over the day. In addition, many of the gradations around clusters are steady and consistent but there several examples of opposing trends abutting each other with gaps

between transition classes appearing in the far southern, central, and northeastern portions of the city.

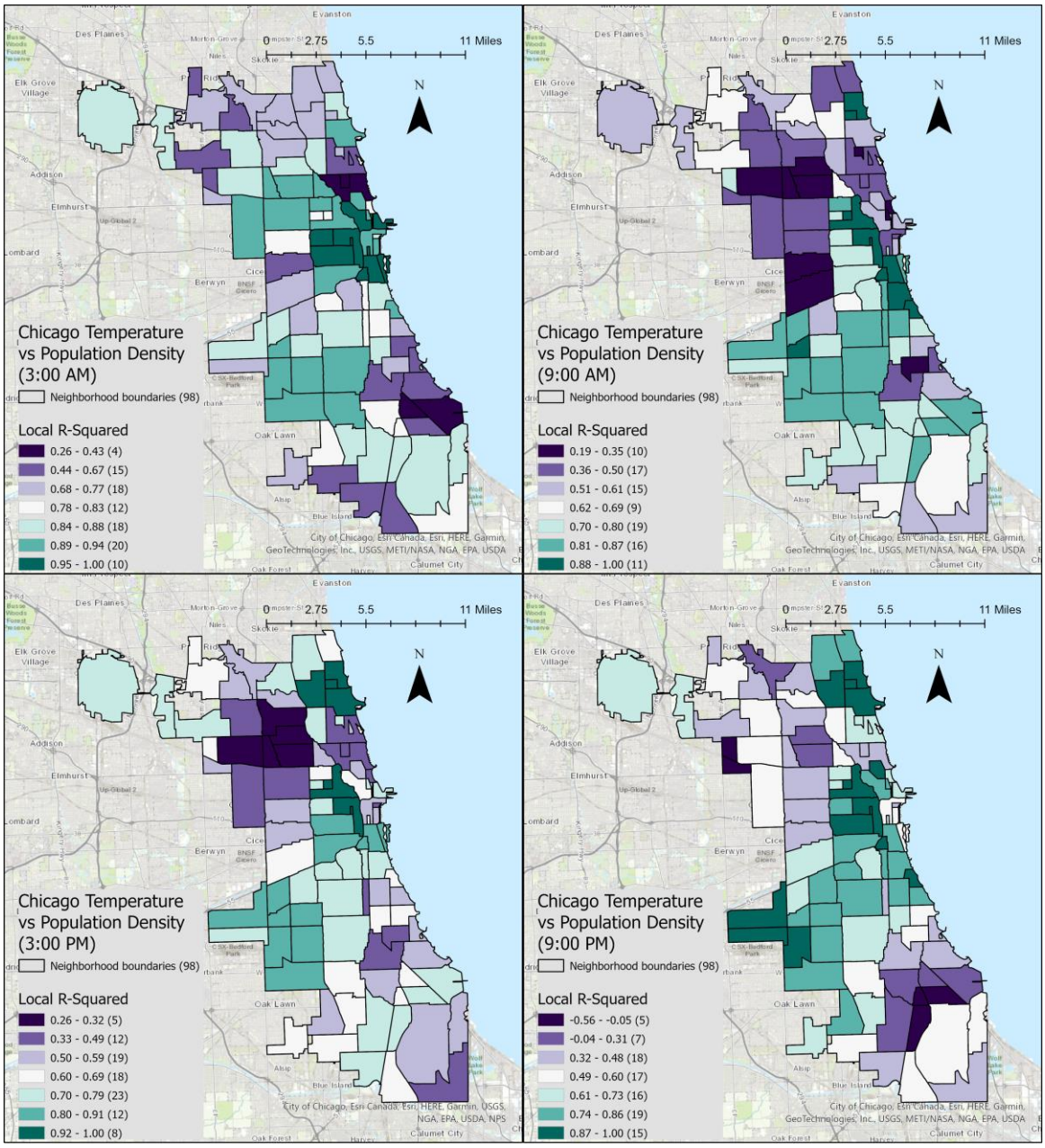


Figure 5-6: Geographically weighted regression of temperature vs. population density for Chicago

Figure 5-6 illustrates the GWR results for temperature values and population density. The average overall R-squared value for all four maps was .83, indicating a fairly strong goodness of fit. When comparing these mapped results to those in Figure 5-5, strong similarities are present, with results at 3:00 PM for both maps nearly identical. The same is true for 9:00 AM when considering the raw R-squared values rather than the classes used. At

3:00 AM, R-squared values for the near South side are slightly higher for Figure 5-6, while values in the northwest are slightly lower. At 9:00 PM, R-squared values for most neighborhoods are slightly higher in Figure 5-6, but the southeasternmost part of the city is a notable exception to this. The populations of each class in figure 5-6 tend to be semi-normal, but 3:00 AM and 9:00 AM exhibit a marked decrease in the central-most class compared to its adjacent, neighboring classes.

The shifts in R-squared values for Figure 5-6 are subtly different from those in Figure 5-5. The far northwest is particularly difficult to interpret with values of .84 to .88 abutting values of .44 to .67 at 3:00 AM, then both values shifting toward the middle at 9:00 AM before gradually increasing at 3:00 PM and 9:00 PM. Adjacent to them is a cluster in the center-north of the city that begins at moderately high R-squared values at 9:00 AM before plunging to values of .19 to .36 for 9:00 AM and 3:00 PM, and finally increasing to .36 to .60 by 9:00 PM. On the other hand, the far northern portion of the city shows a consistent increase in R-squared values across the day from 3:00 AM to 9:00 PM.

*5.1.3- GWR for the Netherlands*

GWR for the Netherlands begins with Figure 5-7, which compares average income with population density. The overall R-squared value was .52, indicating a mediocre goodness of fit. The distribution of classes here is markedly normal with the middle classes far more populous than the lower and higher end classes. The highest R-squared values are found in the distant south near Maastricht as well as along much of the North Sea coast except for the central section. Clusters of very low R-squared values appear across much of the central east-west band of the country, trending northward as one moves east. Gradations between these opposing trends are steady and gradual aside from an abrupt switch in the center-north portion of the country.

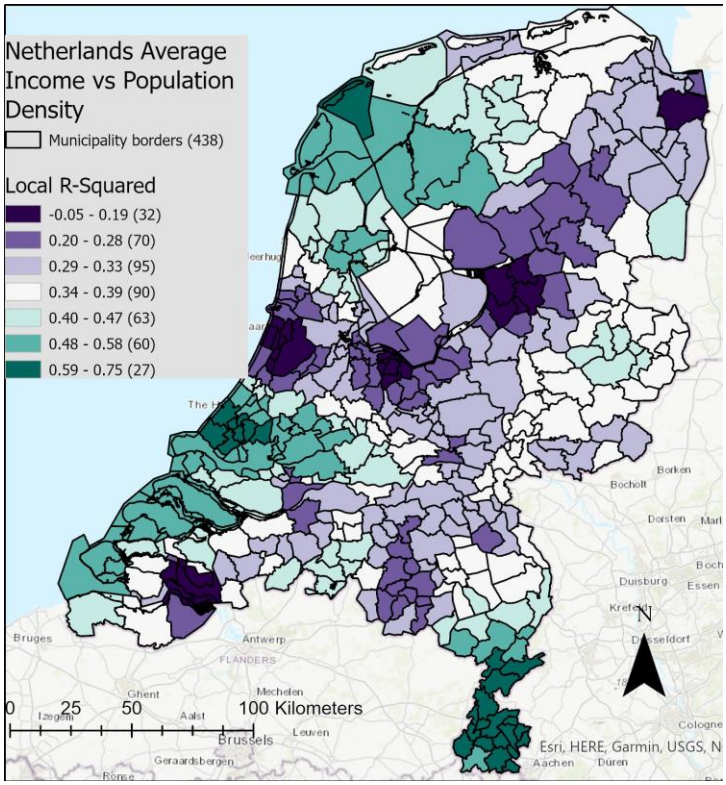


Figure 5-7: Geographically weighted regression of average income vs. population density for the Netherlands

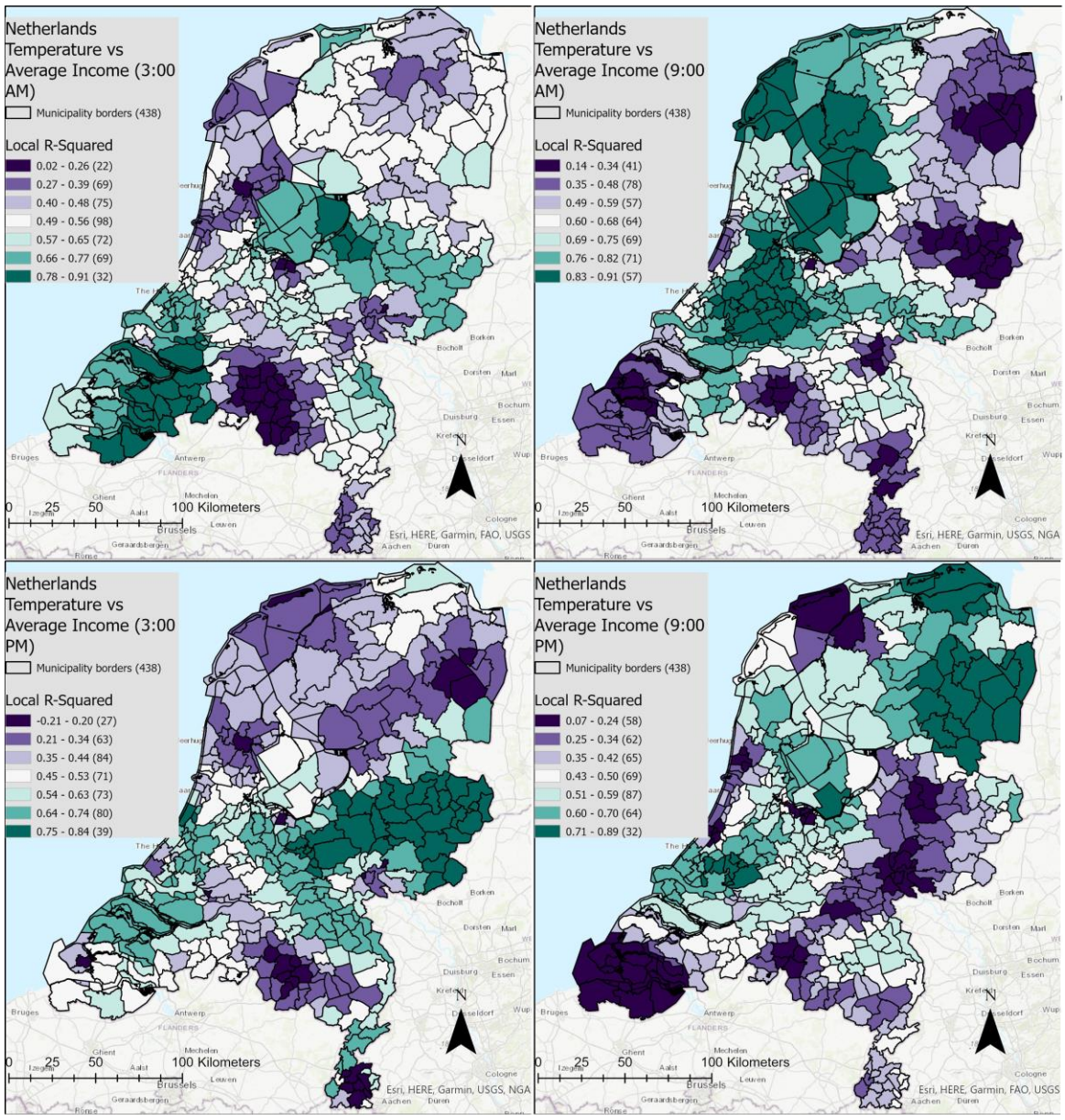


Figure 5-8: Geographically weighted regression of temperature vs. average income for the Netherlands

Figure 5-8 illustrates the GWR results for temperature values and average income across the four times chosen. The average R-squared value for all four maps was .83, indicating a strong goodness of fit. The mapped results show, via the feature count, that the class distribution is normal at 9:00 AM, although this curve/ trend flattens a bit as the day proceeds. Finding consistent trends for R-squared values regionally is difficult since the map shows clear and robust clusters that appear and disappear at each of the four times rather abruptly. The clustering here is more evident and larger than for any of the other four study areas with clear gradations around the highest and lowest R-squared values at the center of each cluster. One of the few consistent clusters can be seen in the Randstad, slightly

southwest of the center of the country, where municipalities exhibit R-squared values of .49 to .91 across the day. The cluster is largest and values highest at 9:00 AM. Another consistent cluster is found in the south-central portion of the country with R-squared values of .27 to .48. The size and shape of the cluster shift across the four times, but the values and their ranges do not noticeably change throughout the day.

The large bands and clusters change considerably across the day, establishing patterns that are seemingly abrupt and often inconsistent. For example, the far southern region near Maastricht exhibits R-squared values of .27 to .48 across the entire day except for a cluster at

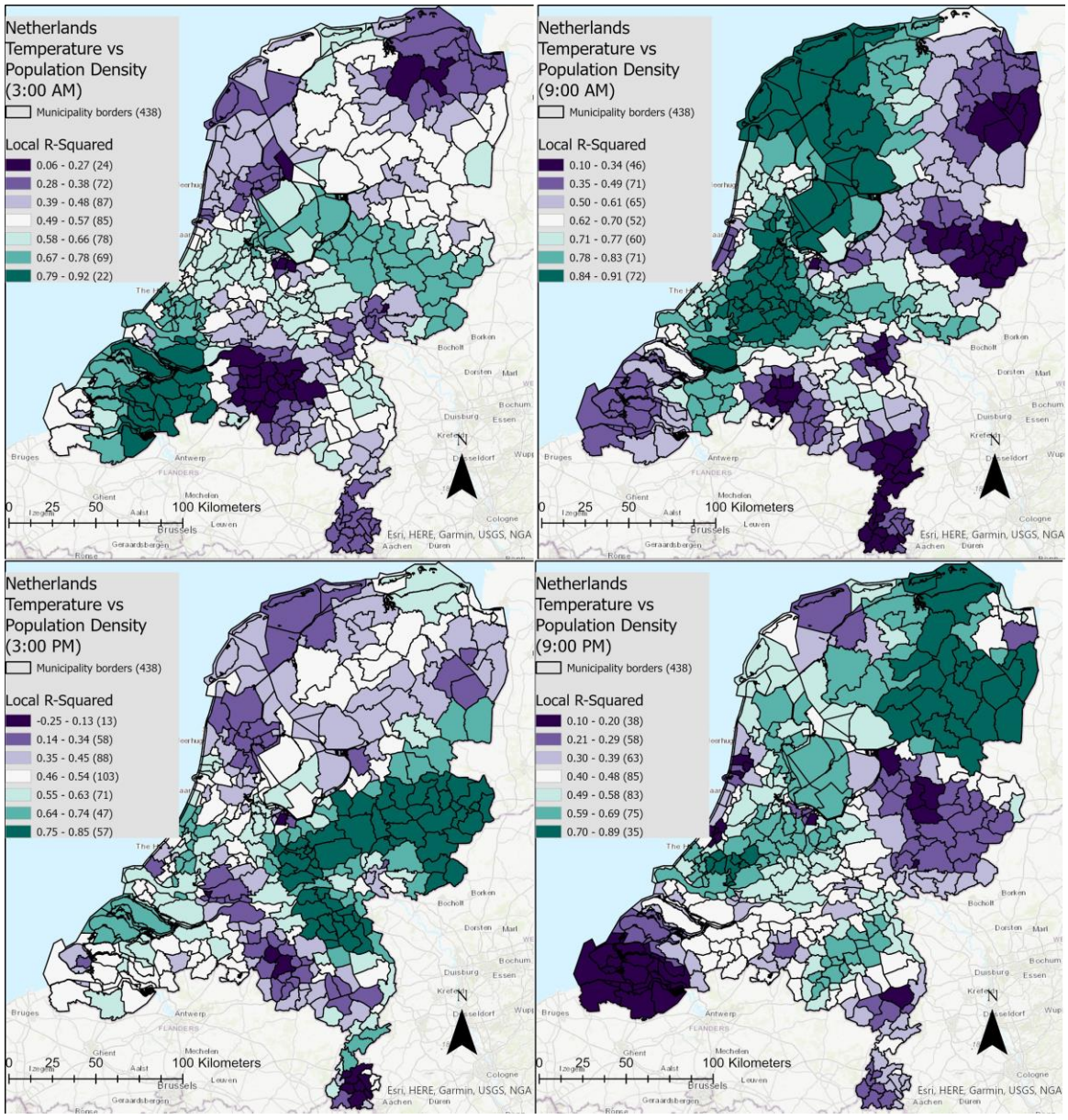


Figure 5-9: Geographically weighted regression of temperature vs. population density for the Netherlands

the northern end of the strip that has values of .64 to.74 at 3:00 PM. At 3:00 AM, a large strip with R-squared values of .66 to .91 is evident across much of the center-east portion of the country, but at 9:00 AM this band thins and moves south while the easternmost portion abruptly decreases to values of .14 to .48, forming a new cluster. By 3:00 PM, that cluster has expanded an encompassed the previous band while values have increased to a range of .64 to .84., but the trend reverses once again at 9:00 PM with values of .25 to .43. The far northeastern portion of the country exhibits moderate R-squared values of .40 to .65 at 9:00 AM, but then shifts to a large, low value cluster at 9:00 AM and 3:00 PM before transitioning to an even larger cluster at 9:00 PM with high values of .60 to .89. A final example of back-and-forth trends involves the one seen in the southwesternmost portion of the country. It exhibits R-squared values of .57 to .91 at 3:00 AM then shifts to  a low value cluster at 9:00 AM (range of .35 to .59) before trending back up to values of .45 to .74 at 3:00 PM, then ends the day at 9:00 PM with very low values of .25 to .42.

Figure 5-9 illustrates the GWR results for temperature values and population density. The average R-squared value for all four maps was .83, indicating a strong goodness of fit. When comparing the mapped results with those of Figure 5-8, it is striking how similar the two maps are. All of the large clusters with markedly high or low R-squared values are all replicated in Figure 5-9, but there are subtle differences. For example, at 3:00 AM, the values attached to the clusters in Figure 5-9 are slightly more pronounced in the far north and south-center, while being less pronounced in the east-central municipalities. At 9:00 AM, the cluster in the southwest shows slightly higher R-squared values while those in the far south show lower values than in Figure 5-8. At 3:00 PM, the band in the south that northwest-southeast has higher R-squared values, while the low value band that runs perpendicular to it in Figure 5-8 at 9:00 PM is almost non-existent in Figure 5-9. Like the previous figure, the mapped results for population density show a normal distribution of classes, though is less clear at 9:00 AM. Any trends or changes over time seen in this figure parallel those described in Figure 5-8.

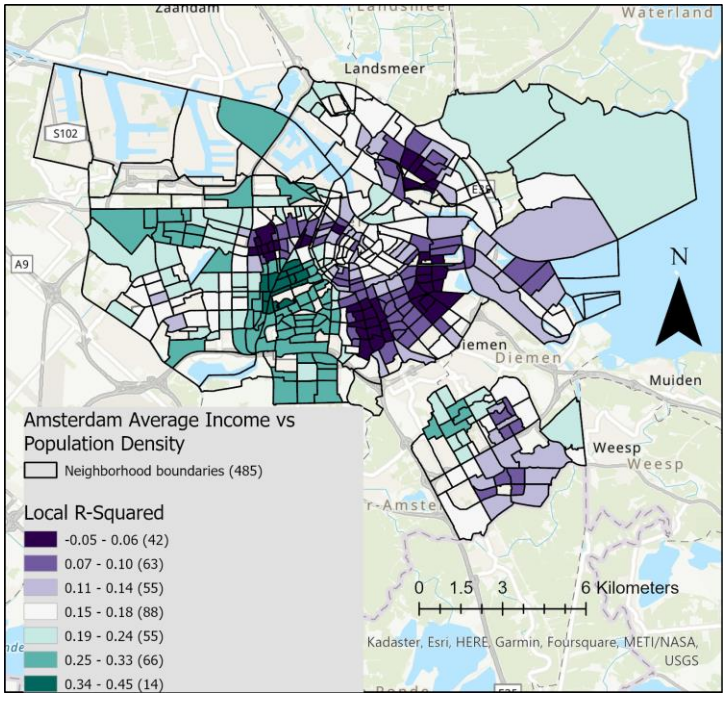


Figure 5-10: Geographically weighted regression of average income vs. population density for Amsterdam

*5.1.4- GWR for Amsterdam*

Figure 5-10 illustrates the GWR comparing average income with population density for Amsterdam. The overall R-squared value was .30, indicating a poor goodness of

fit. The feature count shows a fairly even distribution of the seven classes with a slightly larger population in the central class with values of .15 to .18. Clusters with R-squared values barely above zero appear in the Oost, West, and Noord districts. Neighborhoods with the highest R-squared values are seen in Zuidoost, much of Zuid, and the more distant portions of Nieuw-West. Gradations here are steady and few to no opposing trends or clusters abut each other. The R-squared values for this map are much lower than for any of the other GWR runs for this or the other study areas; the author is at a loss as to why this is the case.

Figure 5-11 illustrates the GWR results for temperature values and average income across the four times chosen. The average R-squared value for all four maps was .74, indicating a moderately strong goodness of fit. The feature counts indicate that the populations of each class are relatively even with some tendency toward a normal distribution. Some trends in the distribution of R-squared values across the city over the day are evident. For example, the eastern sections of the Noord district and much of the IJburg

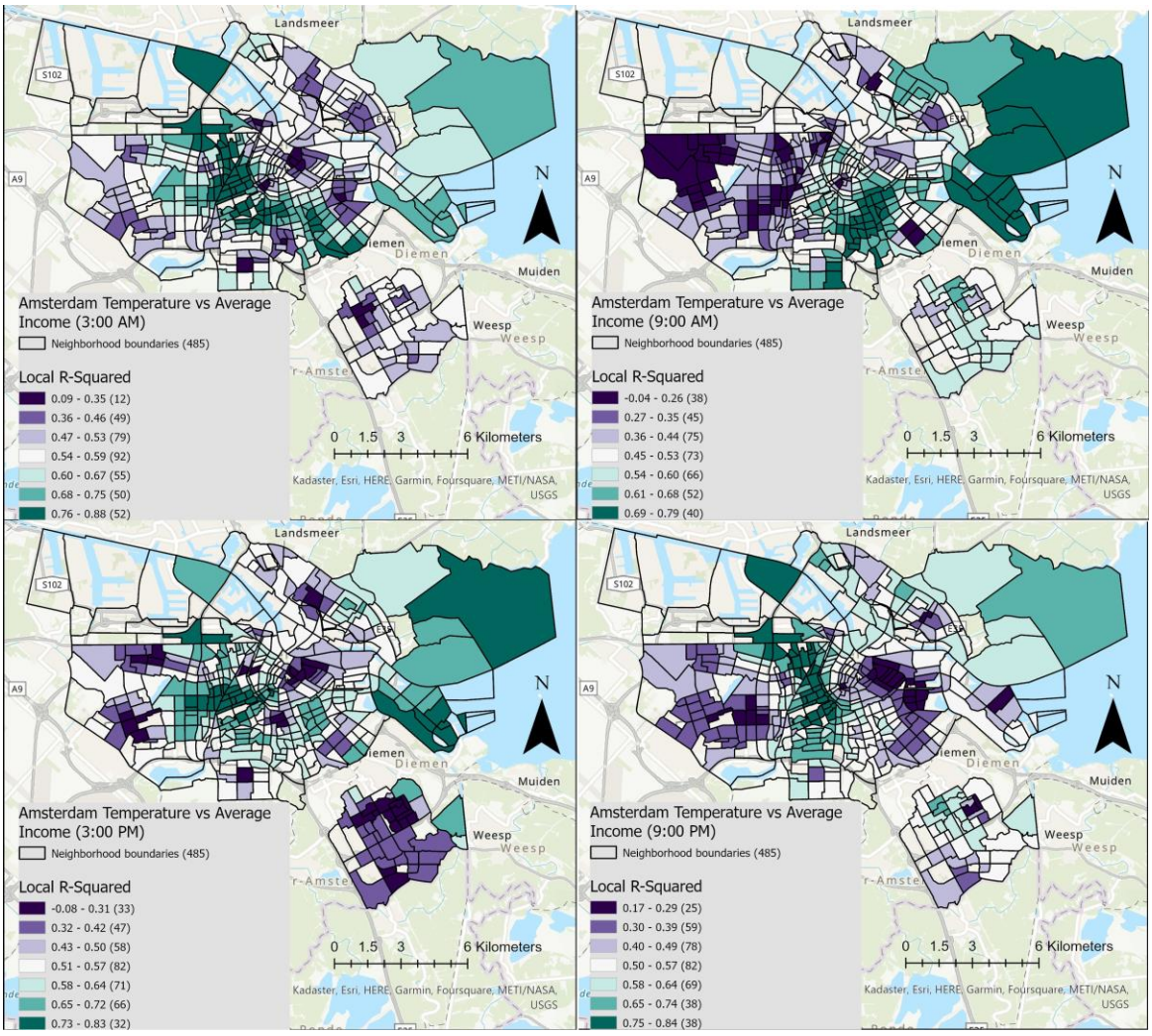


Figure 5-11: Geographically weighted regression of temperature vs. average income for Amsterdam

exhibit values of .60 to .83, while most of the Nieuw-West district shows clustering with R-squared values of 0 to .47 throughout the day. A large high value cluster that spreads across the border between the Zuid and West districts shows R-squared values of .68 to .84 for much of the day, but briefly dips to values as low as .45 at 9:00 AM.

Other clusters are less consistent and show more back-and-forth trends across the four times. The Zuidoost district's neighborhoods exhibit mostly middling R-squared values of .40 to .64 with some slight increases and decreases throughout the day, but a cluster forms at 3:00 PM that suddenly divides the district into very low and moderately high R-squared values (0 to .42 and .65 to .72, respectively). Although the Nieuw-West neighborhoods tend to show low R-squared values across the day, the extent shifts with values being markedly lower at 9:00 AM when compared to other times. The Oost neighborhoods also shift throughout the day and have some of the most abrupt changes in R-squared values between adjacent neighborhoods. For example, neighborhoods with values of.76 to .88 are only two neighborhoods away from those wit values of 0 to .35. This absence of gradations between opposing trends is otherwise less common in Figure 5-11 with most transitions between the classes more gradual and spatially well-distributed.

Figure 5-12 illustrates the GWR results for temperature values and population density. The average R-squared value for all four maps was .74, indicating a moderately strong goodness of fit. Some caution has to be used when comparing Figures 5-11 and 5-12 because some of the more industrial neighborhoods in Amsterdam are recorded as having very few residents and thus a tiny population density but no appreciable average income values. This results in these neighborhoods not being comparable between the two, which may affect trends and adjacent neighborhoods. Nonetheless, the two maps are very similar to each other, with the same general trends in terms of high and low value clusters with middling values between them appearing in many of the same districts and neighborhoods at the same times of the day. There are, however, some differences between the two. At 3:00 AM, for example, R-squared values in much of the Noord district and the southernmost portions of Zuid are slightly lower in Figure 5-12, but slightly higher in Zuidoost when compared to Figure 5-11. Conversely, at 9:00 AM, the low value clustering seen in the far west is less pronounced in figure 5-12, while the high value clustering seen along the border of the Zuid and Oost districts as well as in Zuidoost is much more pronounced in Figure 5-12. At 3:00 PM, the low value clustering in the southwesternmost parts of the city are more pronounced in Figure 5-12. R-squared values in central Noord district are also a bit lower in Figure 5-12. Finally, the distribution of classes in figure 5-12 is very similar to the previous figure.

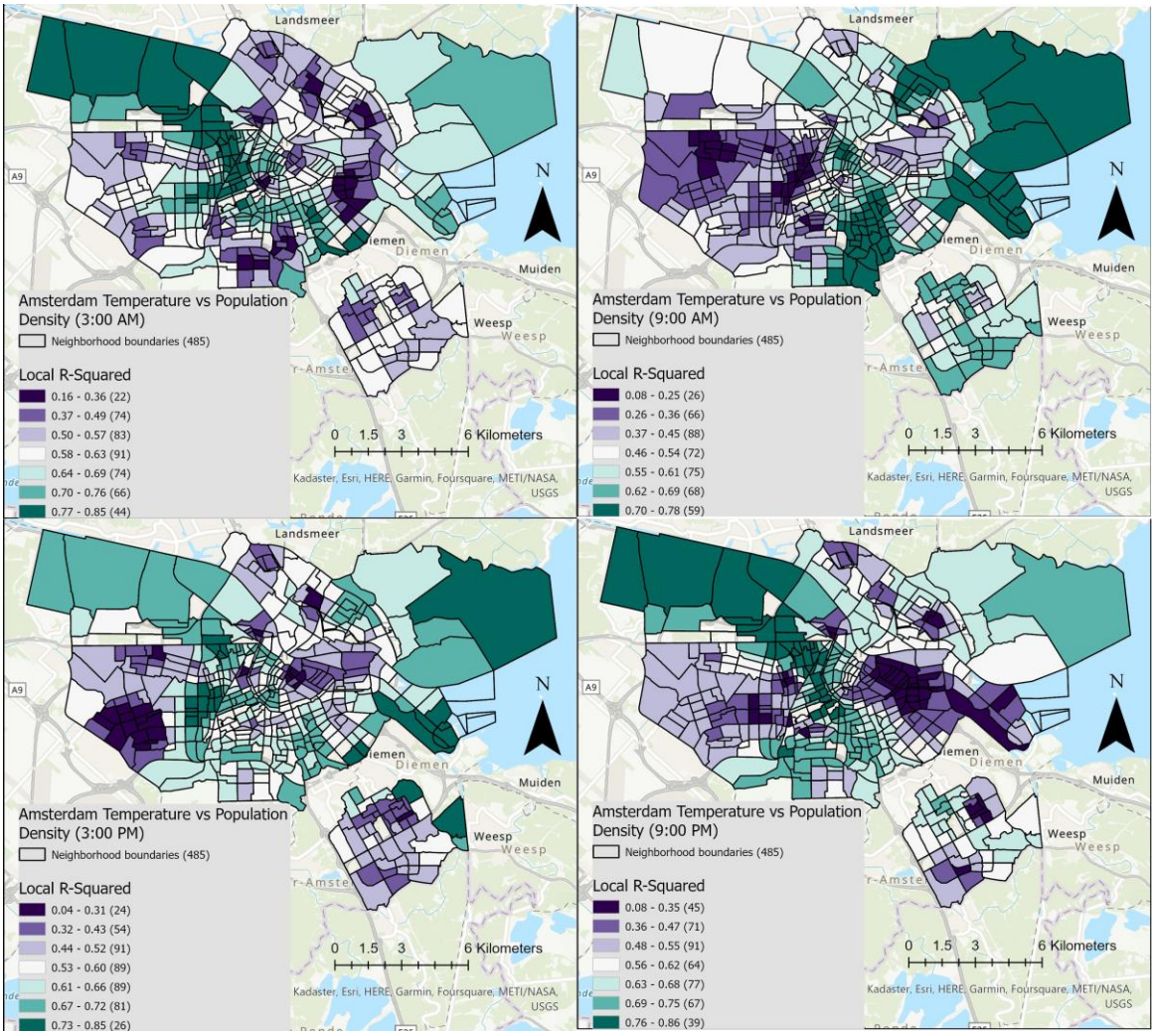


Figure 5-12: Geographically weighted regression of temperature vs. population distribution for Amsterdam

### *5.2- Bivariate analysis*

The BA used for this project compared the average surface air temperature for each administrative unit with that of both average income and population density for each administrative unit, similar to the GWR performed. This process created maps with each zone color coded into one of the six classes depending on the statistically significant relationship perceived by the tool. For more detailed information regarding this process, its set-up, and how to interpret the resulting classes, please see section ***3.5- Data analysis***.

*5.2.1-BA for Illinois and Chicago*

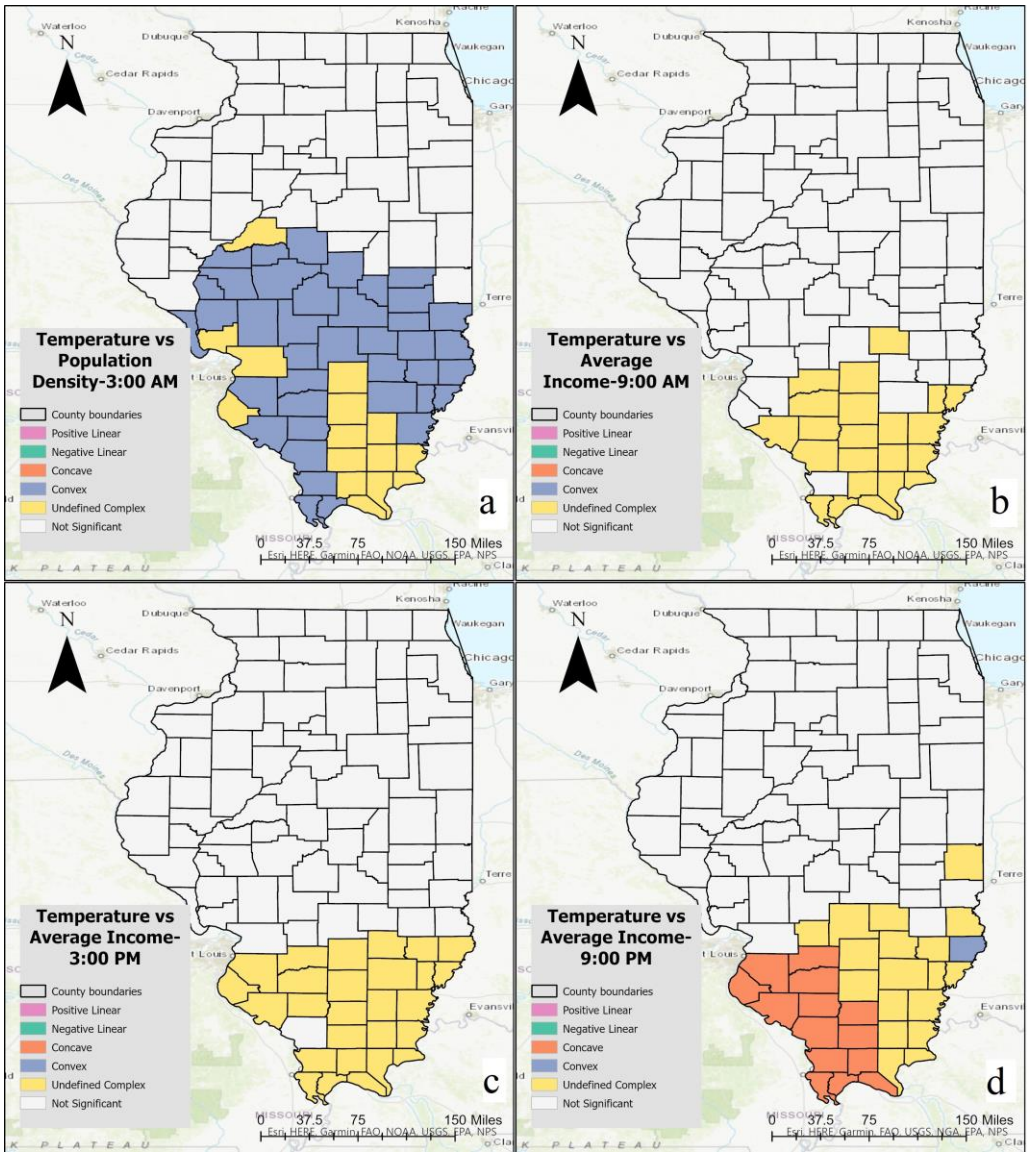


Figure 5-13: Bivariate analysis of Illinois (maps with no significant correlation are not pictured)

Bivariate analysis for Illinois gave few results and even these are ambiguous, as shown in Figure 5-13. 5-13a shows the only significant correlation between temperature and population density. Significance was only found in the central and southern portion of the state, where a convex relationship was found. This means that as population density increases, temperature changed along a convex curve. Testing for average income garnered more results but these are unclear. Figure 5-13b, 5-13c, and 5-13d illustrate how there seems to be a significant relationship between temperature and average income for the southern portion of the state, but it is not reliably described using this statistical method. In the case of 5-13d, a concave relationship can also be seen between these variables.

Figure 4-1 serves as a reminder that this part of the state tends to be less densely populated and tends to have lower average income per household. At the same time, traveling further south in Illinois generally results in higher temperatures than the north due to climate patterns. So it may be that fewer people and reduced urban fabric in this portion of the state results in reduced UHI regionally. Coupling this with the naturally higher temperatures expected may result in a correlation that is not based on UHI. Figure 6-1 also illustrates how site data for this portion of the state was not well spread and largely consists of a single thin band of sites in the northernmost portion of southern Illinois. This lack of data likely explains the paucity of results using bivariate analysis here.

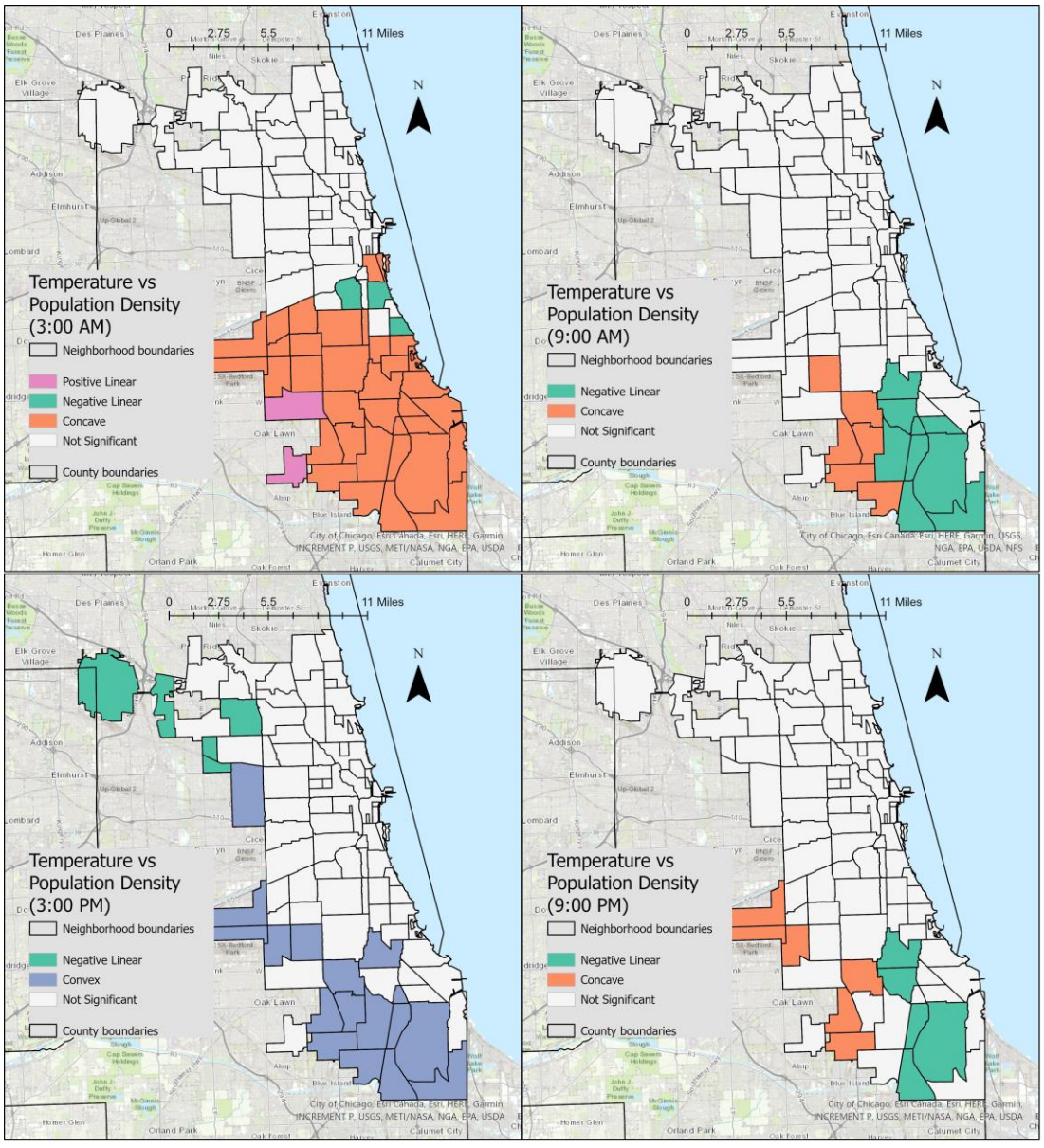


Figure 5-14: Bivariate analysis of temperature vs. population density for Chicago

Bivariate analysis for Chicago consistently showed a significant relationship between temperature and population density, although the nature and location of that relationship varied. The majority of the significance was relegated to the southern half of the city, with only 3:00 PM showing any significance for the northern half, as seen in Figure 5-14. However, the 3:00 PM map's indication of a negative linear relationship in the northwest is supported by the fact that the areas near O'Hare Airport are less heavily populated and may exhibit less UHI as a result. The situation in the southern portion of the city is very different, though. Whereas the relationship between these two variables begins as concave at 3:00 AM, this transitions to a negative linear relationship at 9:00 AM before flipping to a convex relationship at 3:00 PM, and finally returns to a concave or negative linear relationship at 9:00 PM. So the results for 9:00 AM and 9:00 PM parallel each other, though results are less complete for 9:00 PM. This may be explained by the fact that many of the southernmost neighborhoods of the city are less densely populated and have lower average income per household, as shown in Figure 4-3. These factors are linked since the large propensity of people with less income results in fewer tall buildings being constructed due to a lack of investment, which keeps the population density lower. The result is a subtle but semi-consistent indication of the relationship between the variables measured.

Significant relationships between temperature and average income were nearly entirely absent for Chicago and so are not represented visually here.

*5.2.2- BA for the Netherlands*

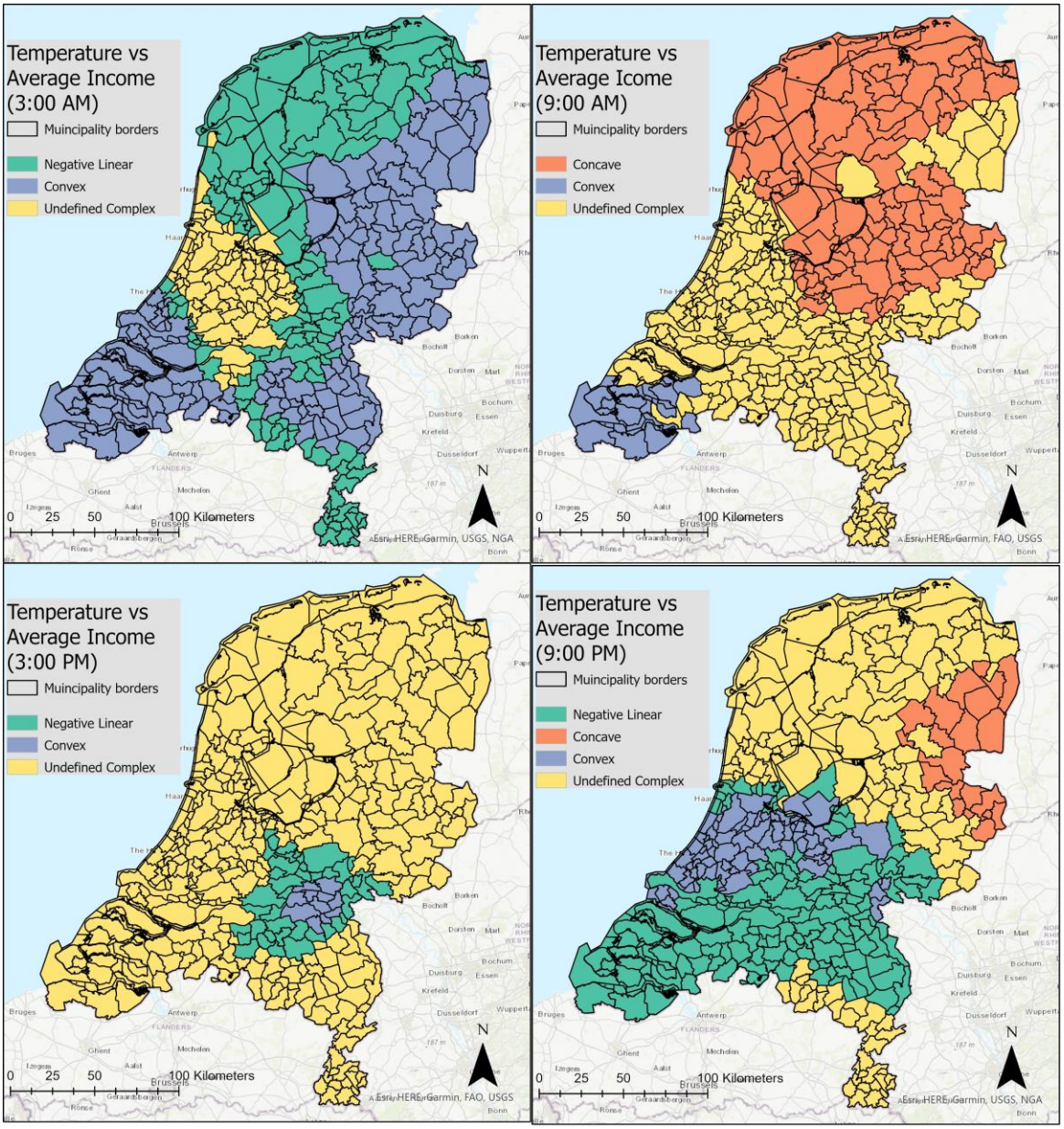


Figure 5-15: Bivariate analysis of temperature vs. average income for the Netherlands

Bivariate analysis of the Netherlands gave results far more consistent and robust than the other three study areas, as shown in Figure 5-15. Significant relationships between both pairs of variables were found for all four of the times analyzed. This is likely because of the superior coverage/ spread of the data points for the Netherlands, as shown in Figure 6-3. For temperature versus average income, the analysis for 3:00 AM shows a convex relationship for much of the easternmost and westernmost municipalities, but transitions to a negative linear relationship as it nears the heart of the country. This area is known as the Randstad and includes the four cities of Amsterdam, Utrecht, The Hague, and Rotterdam. This area is

characterized by a an undefined complex relationship between the variables, surrounded by a thin band of negative linear relationships. Because UHI should be most severe at 3:00 AM, this is a significant indication of how these variables relate to each other. The situation inside the Randstad area may show a stronger relationship than its surroundings but other factors complicate the data such that the program can not quite tease it out.

At 9:00 AM, the undefined complex area has grown to encompass more of the country while much of the northern municipalities now show a concave relationship. Only the southwesternmost areas still show a concave relationship. By 3:00 PM, when UHI should be lowest, much of the country has transitioned to an undefined complex relationship. However the central eastern municipalities near ‘s-Hertogenbosch and Nijmegan show a distinctive cluster of negative linear areas surrounding a core of convex relationships. Figure 4-5 illustrates how mixed these two clusters are in terms of average income and population density. Therefore it is hard to pin down what may be causing this, so perhaps regional climactic influences are playing a part.

By 9:00 PM, as UHI should be increasing, most of the southern half of the country has transitioned to a negative linear relationship with a smattering of convex municipalities in an east-west strip at the center of the nation. However, much of the northern half of the country shows an undefined complex relationship with a concave one in a band along the eastern border with Germany. Figure 4-5 shows how the average income of the municipalities drops off along a northeast-southwest running band that begins at the narrowest part of the nation and ends at the west coast. The pattern of negative linear and convex relationships seems to follow this band, although it strays a bit north of it. This and the 3:00 AM map illustrate that a semi-consistent negative correlation exists between average income per household and surface air temperature.

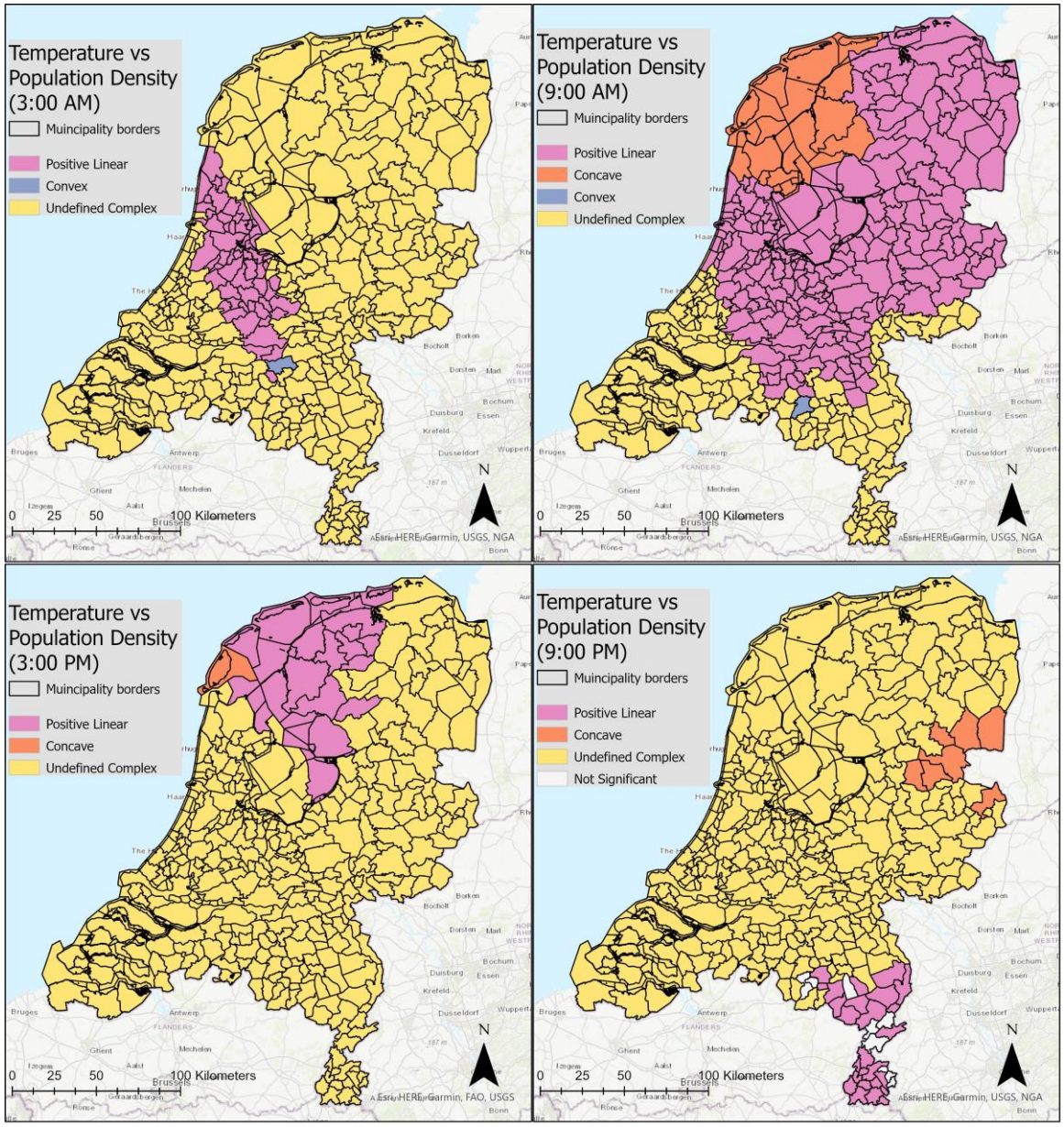


Figure 5-16: Bivariate analysis of temperature vs. population density for the Netherlands

The results of bivariate analysis for the Netherlands in relation to population density were less decisive than for average income, but still significant for all municipalities throughout the day. This is shown in Figure 5-16. At 3:00 AM, when UHI should be most severe, much of the country shows an undefined complex relationship. However, a northwest-southeast band of municipalities that include the cities of Amsterdam and Utrecht show a positive linear relationship. Figure 4-5 reveals that these same municipalities show the highest contiguity of those with medium to high population density second only to those along the west coast. This reinforces the significance of this finding, especially when considering the evidence (mentioned in the literature review) that suggests that contiguity of urban build-up may be a primary cause of UHI.

By 9:00 AM, the positive linear relationship has greatly expanded to include roughly two-thirds of the country. Meanwhile the southeastern and southwestern corners of the county show an undefined complex relationship while the northeastern corner shows a concave relationship. This is strong evidence for higher population density relating to higher temperature and UHI. The less clear effect along the northern coast may be due to regional climate patterns, such as strong cooling from the sea muddying the data. By 3:00 PM, as UHI should be at its lowest, most of the municipalities show an undefined complex relationship. Only the northeastern most municipalities, who previously showed a concave relationship, now show a positive linear relationship, buttressing the theory that a regional climactic effect may be at work here.

Finally, by 9:00 PM, when UHI should be increasing, much of the country still shows an undefined complex relationship. Only the southeastern "tail" of the country shows a positive linear relationship while a cluster of municipalities in the northeast show a concave relationship. It is worth noting, once again, that a result of "Undefined Complex" is not equivalent to a result of "Not Significant." It simply means that the program has determined that the two variables are indeed significantly related, but not in a way that can be reliably categorized using the existing classifications ("How Local Bivariate Relationships works—ArcGIS Pro | Documentation," n.d.). This fact strengthens the data and supports the hypothesis that these factors are strongly related. However, other factors not accounted for in this study may be obfuscating the nature of their relationship.

*5.2.3- BA for Amsterdam*

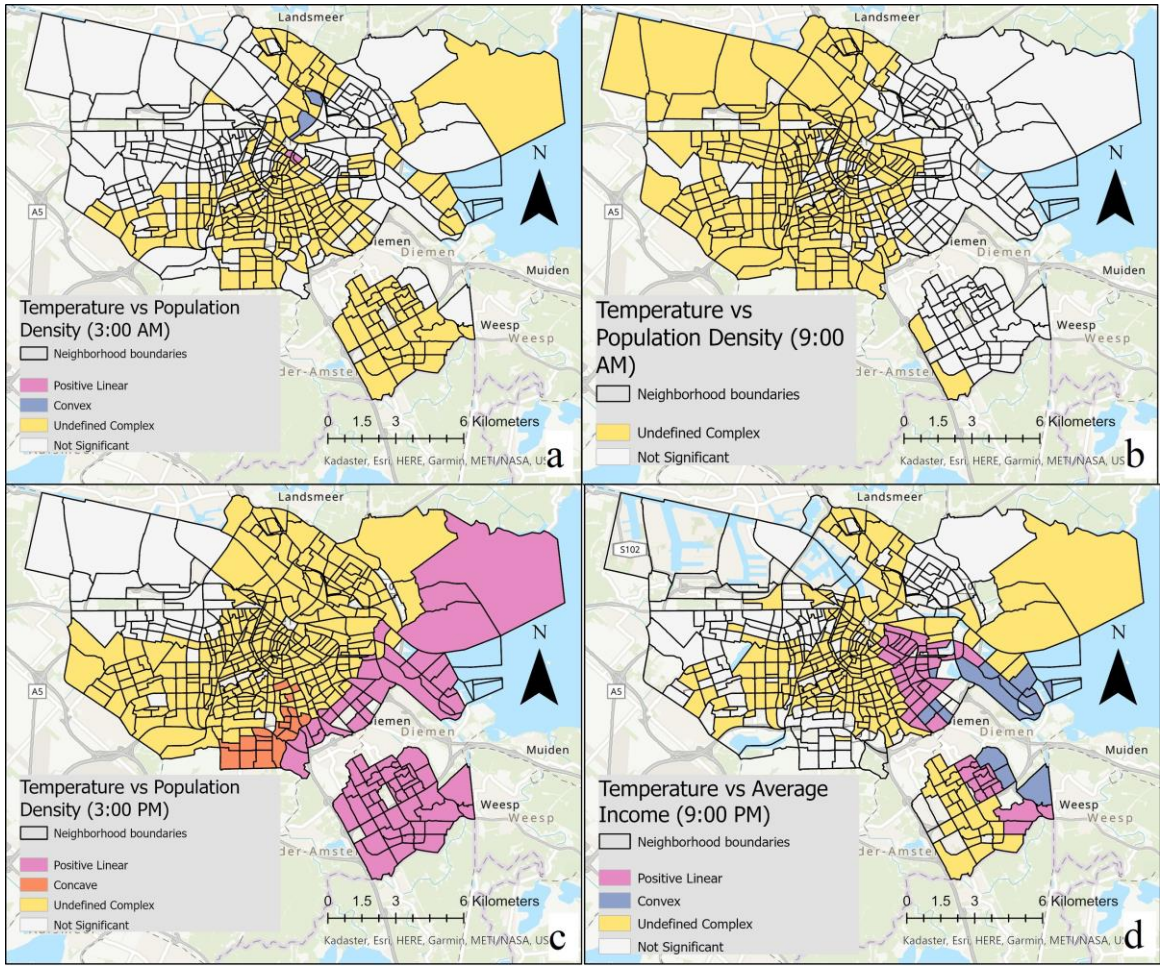


Figure 5-17: Bivariate analysis of Amsterdam (maps with no significant correlation are not pictured)

Bivariate analysis for Amsterdam was less conclusive than for the Netherlands as a whole and favored population density as being more significant than average income. Figure 5-17 shows the results of this analysis for both variables. Figure 5-17a shows that at 3:00 AM, when UHI should be most severe, much of the city shows an undefined complex relationship aside from the Westerpoort region and most of the other neighborhoods in the northwest. Scattered neighborhoods throughout the city also show no significant relationship but there are no consistent trends to be seen. The separated Zuidoost portion of the city in the southeast parallels the rest of the city in this regard. It is noteworthy that many of the neighborhoods which show no significant relationship are also those which have the lowest population density, as seen in Figure 4-7.

By 9:00 AM, the regions of undefined complex relationship have moved west, as shown in Figure 5-17b. The undefined complex relationship dominate the western half of the city's neighborhoods while the eastern half shows no significant relationship. This suggests

that a similar relationship is at work at both 3:00 AM and 9:00 AM but it shifts position as UHI falls and surface air temperature increases. By 3:00 PM, things become a bit more clear. The easternmost third of the city shows a positive linear relationship while much of the rest of the city shows an undefined complex relationship. Once again, Westpoort and the neighborhoods just south of it show no significant relationship. For the latter, many of these neighborhoods have moderate population density, as seen in Figure 4-7, so this is difficult to interpret. The south-central neighborhoods show a concave relationship as well. Figure 5-17c, at 3:00 PM shows most significant and spatially continuous trend for the analysis of Amsterdam. This is unexpected since UHI should be at its lowest at this time, but temperature should be nearing its highest point in the day. This is doubly curious since these neighborhoods show a wide range of population densities, as seen in Figure 4-7.

Figure 5-17d shows the only significant result for the analysis between temperature and average income. It occurs at 9:00 PM, when UHI should be increasing as temperature decreases. The neighborhoods just east of the city center show a positive linear relationship that runs in a northwest-southeast band. Just east of the band are clusters of neighborhoods showing a convex relationship. The rest of the city, however, shows an undefined complex relationship or no significant relationship. The neighborhoods with an undefined complex relationship are clustered near the center of the city with some outlying band extending to the north and northeast. Most of these neighborhoods have higher average income as seen in Figure 4-7. Only the well-to-do neighborhoods in the far west defy this trend. This suggests that the relationship between these two variables is indeed significant but that other factors not accounted for in the study are concealing its precise nature. As Figure 7-4 illustrates, the spread of site data for Amsterdam was less than ideal, so the lack of spread over the study area may help explain the unclear results.

# 6. Conclusions

## *6.1- Limitations of this study*

One of the greatest limitations to this study was the number of data points available for recording surface air temperature using NETATMO. This was not an issue for the Netherlands and was only an issue to a lesser extent in Amsterdam where the point data tended to be a bit clustered. For Illinois and Chicago, however, the lack of point data led to a noticeable lack of spread/ coverage in the data gathered. This led to clustering of data and large swaths of each map with no data points recorded. This is illustrated in Appendix A for each study area. The poor spread of this point data likely resulted in less accurate results when this data was used to interpolate the gaps between the points. Less accurate interpolated data then undermines the average temperatures derived for each zone, which then undermines the geographically weighted regression and bivariate analysis using these averaged values. It is also worth mentioning that GWR is known to give poor results for datasets with less than a few hundred features, so this further undermined the results for Illinois and Chicago. The paucity of temperature data in the U.S. and at higher resolution in the Netherlands was the single greatest limitation of the study.

Another consideration is the inverse distance weighting (IDW) used to interpolate the temperatures between the recorded data points. IDW is a reliable tool, but it is considered to be less accurate than a technique like Kriging. Because this interpolation was vital to acquiring the average surface temperatures for each zone, a more advanced and accurate technique may have provided better results, which would have led to more accurate results for the data analysis as well. A final limitation was the inability to better interpret the results of the bivariate analysis. The indication of a concave or convex relationship would have been more clear if that relationship could have been represented visually as a chart. Despite the author's best efforts, this did not seem to be possible.

As a final consideration, the average R-squared values derived from GWR comparing air surface temperature with either average income values or population density across all study areas ranged from .72 to .83. Because a value of 1 is considered a perfect fit, the resulting R-squared values indicate that other factors not accounted for in this study may be responsible for the disparity between the recorded and predicted values for the variables analyzed.

### *6.2- Conclusions reached*

The primary goal of this study was to determine "How are surface temperatures in urban areas tied to factors which may increase or decrease the intensity of UHI for urban residents?" The results indicate that heat is distributed unevenly across the four study areas, particularly the two cities analyzed at higher resolution. However determining the extent to which UHI is present in these temperature values proved elusive. Instead the greatest insights were gleaned regarding how temperatures change over the course of a day in each study area. Because these changes are complicated and uneven, sometimes even contradictory, tentative conclusions can be made as to where some of these changes are due to UHI rather than local or regional climate processes. Doing so, however, requires careful consideration of the built-up fabric of the area as well as the general urbanity of the area under consideration. This is, admittedly, a more speculative and less quantitative assessment than had been hoped for.

The sub-questions of this study were also answered to varying extents. (1) The in-situ surface air temperatures gathered from NETATMO appear to be reliable and accurate. When questionable values were encountered, the filtering tool instantly removed them. Some sites could not be used because they lacked data for the chosen day as well. (2) Surface air temperature on its own may suggest where UHI occurs, but this study was not able to derive UHI definitively from the temperature values recorded. Instead, temperature variations across time and space were the focus but did seem to indicate areas of higher temperature where UHI was suspected to be more intense due to the presence of controlling factors. (3) Average income per household seems to be a fair indicator of vulnerability to UHI, but only at relatively high spatial resolutions. For large areas with low spatial resolution and large administrative units such as Illinois and the Netherlands, the variable appeared to be less valid and the correlation more difficult to analyze/ isolate. (4) Population density was a fair indicator of urban build-up at lower spatial resolutions. For large areas like Illinois and Netherlands, it was indicative of where urbanization was most advanced. For small areas like

Chicago and Amsterdam, it was less adequate, especially when considering highly built-up areas with fewer permanent residents (like Chicago's financial district).

(5) The question of whether average income and population density have a statistically significant relationship with surface air temperature and/or each other is still uncertain. The GWR results suggest that temperature and population density have a murky correlation, as evidenced by R-squared values of .64 for Illinois, .89 for Chicago, .52 for the Netherlands, and .30 for Amsterdam. It was believed that this relationship would have a stronger correlation with a metropolitan area as opposed to the entirety of a state or small nation, but the results for Amsterdam cast doubt on this hypothesis. It should be remembered that many lower SES areas of metropolises outside the city center may have lower population density due to lack of housing development as well as the fact that population density may be relatively high in high-priced high-rise apartment buildings. This results in very inconsistent relationships between average income and population density. GWR results that compared each of these variables with surface air temperature values throughout the day on August 20, 2021 are more conclusive and show a clearer overall trend. The averaged local R-squared values for each GWR run in all four study areas ranged from .72 to .83. Considering that a value of 1 would indicate a perfect fit and the clearest correlation between the two variables analyzed, this means that a moderately strong correlation was found between temperature and both of the demographic variables across all four study areas. In spite of the radically different distances and scales studied in each area, these results fell into a fairly narrow and consistent range of values. This indicates that there is indeed a clear correlation between the variables analyzed as per the study's hypothesis. The BA results, although less clear, suggest this as well.

(6) The precise nature of the relationship between the studied variables is a bit more difficult to quantify, however. The GWR results don't indicate whether the correlation found is positive or negative. This is reinforced by the lack of consistency on the GWR maps in terms of what areas had higher or lower local R-squared values for each administrative unit. Because the range of local R-squared values was so wide (as low as 0 or as high as .86), it is very difficult to draw additional conclusions here. This ambiguity is mirrored by the frequency with which the BA results reported an "undetermined complex" relationship between the variables analyzed. The author continues to believe that surface air temperature should correlate positively with population density and negatively with average income values but the tools and processes used in this study failed to determine if that was true or not.

(7) Average incomes and population density patterns were quite different when comparing the Netherlands and Illinois as well as the metropolises that each holds. Average income ranges were similar in that the lowest values were about 30% of the highest values. However the distribution of the classes across that range was a bit more equitable in the Netherlands. The opposite is seen for Chicago and Amsterdam, however. In Chicago, the lowest income value is 20% of the maximum, while in Amsterdam, it is only 10%. It may be, however, that these values were gathered using very different methodologies. Population

density comparisons showed greater differences between the Netherlands and Chicago. Even after accounting for the difference in persons per square mile and persons per square kilometer, Illinois has much lower minimum and maximum values per county than Netherlands' values per municipality; Illinois values are 25-35% of those in Netherlands. The situation is similar for Chicago and Amsterdam, though less severe. Chicago's maximum values are about 70% of Amsterdam's but it's minimum values are drastically higher. This is likely due to the low population densities of Amsterdam's industrial sectors heavily skewing the numbers at the low end.

In terms of temperature, both Chicago and Amsterdam saw wider ranges of temperatures than the state or country in which they were found, likely due to UHI. Illinois and Chicago had much higher minimum and maximum temperatures than Netherlands and Amsterdam- 18.8 ℃ and 37.8 ℃ versus 13.3 ℃ and 28.7 ℃. Additionally, Illinois and Chicago exhibited slightly wider ranges of temperatures at each time recorded than Netherlands and Amsterdam. These are strong indicators of how different the two climates are for the North American and European study areas. Comparing the four study areas in terms of the data analysis is very difficult. The Netherlands was so much more data rich than the other areas that is effectively stands in its own separate class. When comparing Chicago and Amsterdam, the spatial pattern of the BA results clearly indicate data gaps for large sections of Chicago. Because of the large differences in the number and spread of data points available, this likely weakened the otherwise promising results of GWR.

### *6.3- Summary of the study*

This study set out to answer several questions and was unable to conclusively answer several of them. The goal was to use crowdsourced surface air temperature data to identify temperature variations over time in Illinois and the Netherlands at both the regional and local scale. This data was used to create interpolated temperature maps for all study areas at four different times on a single day. That data was then compared with the demographic data in each administrative unit for the residents' average income per household and population density. Geographically weighted regression and bivariate analysis were both used to probe for statistically significant relationships between these variables. Many of the results of these processes are represented visually as maps in the previous chapters, while foundational data can be found in the Appendices.

This study found that in-situ air surface temperature data collected was consistent across each study area, showed reasonable levels of variance, and that data derived from it appears to be fairly reliable. In addition, this temperature data did indicate where and when UHI was more or less severe without having to specifically derive a value for UHI. Evidence for this was most strongly seen in the interpolated temperature maps for Illinois, Chicago, and Amsterdam. Based on the study's results as a whole, average income per household seemed to act as a fair indicator for the heat vulnerability of residents in a given administrative unit, although the range of incomes in some units makes this less ideal. Similarly, population density often acted as a good indicator for urban build-up, although this

was less true in the skyscraper-filled business districts at the heart of Chicago and Amsterdam.

The results of this study also suggest that average income values and population density values do consistently affect surface air temperature values, though the precise nature of this is uncertain. The geographically weighted regression maps for each variable show support for this unspecified relationship across each study area. The bivariate analysis maps also tentatively suggest a statistically significant relationship between surface air temperature and the other two variables. For average income per household, the relationship tends to be negatively correlated. This means that as average income per household decreases in a given administrative unit, surface air temperature tends to increase. Evidence for this was most strongly present in the BA maps of the Netherlands, but the map for Chicago also hinted at a similar relationship. For population density, however, the opposite holds true since it seems to be positively correlated. So as population density increases in a given administrative unit, so does UHI. Evidence for this was most strongly present in the bivariate analysis maps of the Netherlands, but the maps for Chicago and Amsterdam also suggest a similar, though less clear, relationship. Although the results for Chicago and Illinois were not nearly as conclusive as those found for the Netherlands, results from study areas on both sides of the Atlantic seem to offer some support for this study's hypothesis while also showing significant regional differences in terms of how heat was distributed and changed throughout the day of August 20, 2021.

### *6.4- Future research*

One of the biggest concerns for this study was the lack of coverage/ spread for the temperature data in Illinois, Chicago, and Amsterdam. To ameliorate this issue, different crowdsourcing avenues for the data could be explored. Alternatively, in-situ data from weather stations or fieldwork could be used to fill in the gaps and improve the overall coverage and contiguity of the point data gathered. This would lead to more robust, more reliable data upon which interpolation and tests for statistical significance could be performed with more confidence. Other indicators of vulnerability and contributing factors to UHI could also be explored beyond average income per household and population density. The role of ethnicity, ownership versus tenancy, or average building height are just a few examples of other factors that could be analyzed for each administrative unit, then compared with surface temperature to find a significant relationship. Finally, a future study could compare cities within the same country or region in order to minimize the number of differences and climactic factors between them, which could lead to clearer data and more straightforward relationships between the variables studied.

## References

Amsterdam Climate and Weather | Amsterdam.info. (n.d.). Retrieved July 25, 2022, from https://www.amsterdam.info/weather/

Amsterdam Districts and Neighborhoods. (n.d.). Retrieved January 22, 2022, from https://www.amsterdamsights.com/about/neighborhoods.html

Azevedo, J. A., Chapman, L., & Muller, C. L. (2016). Quantifying the daytime and night-time urban heat Island in Birmingham, UK: A comparison of satellite derived land surface temperature and high resolution air temperature observations. *Remote Sensing*, *8*(2). https://doi.org/10.3390/rs8020153

Bechtel, B., Pesaresi, M., See, L., Mills, G., Ching, J., Alexander, P. J., et al. (2016). Towards consistent mapping of urban structures - Global human settlement layer and local climate zones. *International Archives of the Photogrammetry, Remote Sensing and Spatial Information Sciences - ISPRS Archives*, *41*(July), 1371–1378. https://doi.org/10.5194/isprsarchives-XLI-B8-1371-2016

Bechtel, Benjamin, Zakšek, K., Oßenbrügge, J., Kaveckis, G., & Böhner, J. (2017). Towards a satellite based monitoring of urban air temperatures. *Sustainable Cities and Society*, *34*(May), 22–31. https://doi.org/10.1016/j.scs.2017.05.018

CBS Open data StatLine. (n.d.). Retrieved January 16, 2022, from https://opendata.cbs.nl/statline/portal.html?_la=en&_catalog=CBS

Chapman, L., Azevedo, J. A., & Prieto-Lopez, T. (2013). Urban heat & critical infrastructure networks: A viewpoint. *Urban Climate*, *3*, 7–12. https://doi.org/10.1016/j.uclim.2013.04.001

Chen, X. L., Zhao, H. M., Li, P. X., & Yin, Z. Y. (2006). Remote sensing image-based analysis of the relationship between urban heat island and land use/cover changes. *Remote Sensing of Environment*, *104*(2), 133–146. https://doi.org/10.1016/j.rse.2005.11.016

Cheval, S., & Dumitrescu, A. (2015). The summer surface urban heat island of Bucharest (Romania) retrieved from MODIS images. *Theoretical and Applied Climatology*, *121*(3–4), 631–640. https://doi.org/10.1007/s00704-014-1250-8

Chicago, IL Neighborhood Map - Income, House Prices, Occupations - list of neighborhoods. (n.d.). Retrieved January 16, 2022, from https://www.city-data.com/nbmaps/neigh-Chicago-Illinois.html#

City of Chicago :: Weather Extremes - Extreme Temperatures. (n.d.). Retrieved July 25, 2022, from https://www.chicago.gov/city/en/depts/oem/supp_info/alertrespond/extremetemps.html

Climate of Illinois - Narrative, Illinois State Climatologist Office, Illinois State Water Survey, U of I. (n.d.). Retrieved December 27, 2021, from https://www.isws.illinois.edu/statecli/General/illinois-climate-narrative.htm

Debbage, N., & Shepherd, J. M. (2015). The urban heat island effect and city contiguity. *Computers, Environment and Urban Systems*, *54*, 181–194. https://doi.org/10.1016/j.compenvurbsys.2015.08.002

Doick, K. J., Peace, A., & Hutchings, T. R. (2014). The role of one large greenspace in mitigating London's nocturnal urban heat island. *Science of the Total Environment*, *493*, 662–671. https://doi.org/10.1016/j.scitotenv.2014.06.048

File:Chicago community areas map.svg - Wikipedia. (n.d.). Retrieved January 22, 2022, from

https://en.wikipedia.org/wiki/File:Chicago_community_areas_map.svg

Flores R., J. L., Pereira Filho, A. J., & Karam, H. A. (2016). Estimation of long term low resolution surface urban heat island intensities for tropical cities using MODIS remote sensing data. *Urban Climate*, *17*, 32–66. https://doi.org/10.1016/j.uclim.2016.04.002

Guéritée, J., & Tipton, M. J. (2015). The relationship between radiant heat, air temperature and thermal comfort at rest and exercise. *Physiology and Behavior*, *139*(2015), 378–385. https://doi.org/10.1016/j.physbeh.2014.11.064

Hart, M. A., & Sailor, D. J. (2009). Quantifying the influence of land-use and surface characteristics on spatial variability in the urban heat island. *Theoretical and Applied Climatology*, *95*(3–4), 397–406. https://doi.org/10.1007/s00704-008-0017-5

Hidalgo, J., Dumas, G., Masson, V., Petit, G., Bechtel, B., Bocher, E., et al. (2019). Comparison between local climate zones maps derived from administrative datasets and satellite observations. *Urban Climate*, *27*(August 2018), 64–89. https://doi.org/10.1016/j.uclim.2018.10.004

Hondula, D. M., Kuras, E. R., Betzel, S., Drake, L., Eneboe, J., Kaml, M., et al. (2021). Novel metrics for relating personal heat exposure to social risk factors and outdoor ambient temperature. *Environment International*, *146*, 106271. https://doi.org/10.1016/j.envint.2020.106271

How Geographically Weighted Regression (GWR) works—ArcGIS Pro | Documentation. (n.d.). Retrieved June 1, 2022, from https://pro.arcgis.com/en/pro-app/2.8/tool-reference/spatial-statistics/how-geographicallyweightedregression-works.htm

How Local Bivariate Relationships works—ArcGIS Pro | Documentation. (n.d.). Retrieved January 30, 2022, from https://pro.arcgis.com/en/pro-app/2.8/tool-reference/spatial-statistics/learnmore-localbivariaterelationships.htm

Hu, L., & Brunsell, N. A. (2015). A new perspective to assess the urban heat island through remotely sensed atmospheric profiles. *Remote Sensing of Environment*, *158*, 393–406. https://doi.org/10.1016/j.rse.2014.10.022

Huang, G., Zhou, W., & Cadenasso, M. L. (2011). Is everyone hot in the city? Spatial pattern of land surface temperatures, land cover and neighborhood socioeconomic characteristics in Baltimore, MD. *Journal of Environmental Management*, *92*(7), 1753–1759. https://doi.org/10.1016/j.jenvman.2011.02.006

Illinois Maps & Facts - World Atlas. (n.d.). Retrieved January 22, 2022, from https://www.worldatlas.com/maps/united-states/illinois

Illinois Median household income (in 2018 dollars), 2014-2018 by County. (n.d.). Retrieved January 16, 2022, from https://www.indexmundi.com/facts/united-states/quick-facts/illinois/median-household-income#map

Jaganmohan, M., Knapp, S., Buchmann, C. M., & Schwarz, N. (2016). The Bigger, the Better? The Influence of Urban Green Space Design on Cooling Effects for Residential Areas. *Journal of Environmental Quality*, *45*(1), 134–145. https://doi.org/10.2134/jeq2015.01.0062

Jeganathan, A., Andimuthu, R., Prasannavenkatesh, R., & Kumar, D. S. (2016). Spatial variation of temperature and indicative of the urban heat island in Chennai Metropolitan Area, India. *Theoretical and Applied Climatology*, *123*(1–2), 83–95. https://doi.org/10.1007/s00704-014-1331-8

Jenerette, G. D. (2018). Ecological contributions to human health in cities. *Landscape Ecology*, *33*(10), 1655–1668. https://doi.org/10.1007/s10980-018-0708-y

Jenerette, G. D., Harlan, S. L., Brazel, A., Jones, N., Larsen, L., & Stefanov, W. L. (2007). Regional relationships between surface temperature, vegetation, and human settlement in a rapidly urbanizing ecosystem. *Landscape Ecology*, *22*(3), 353–365. https://doi.org/10.1007/s10980-006-9032-z

Kamruzzaman, M., Deilami, K., & Yigitcanlar, T. (2018). Investigating the urban heat island effect of transit oriented development in Brisbane. *Journal of Transport Geography*, *66*(May 2017), 116–124. https://doi.org/10.1016/j.jtrangeo.2017.11.016

Ketterer, C., & Matzarakis, A. (2015). Comparison of different methods for the assessment of the urban heat island in Stuttgart, Germany. *International Journal of Biometeorology*, *59*(9), 1299–1309. https://doi.org/10.1007/s00484-014-0940-3

Kim, H., Gu, D., & Kim, H. Y. (2018). Effects of Urban Heat Island mitigation in various climate zones in the United States. *Sustainable Cities and Society*, *41*(June), 841–852. https://doi.org/10.1016/j.scs.2018.06.021

Kim, Y. H., & Baik, J. J. (2002). Maximum urban heat island intensity in Seoul. *Journal of Applied Meteorology*, *41*(6), 651–659. https://doi.org/10.1175/1520-0450(2002)041<0651:MUHIII>2.0.CO;2

Krüger, E. L. (2015). Urban heat island and indoor comfort effects in social housing dwellings. *Landscape and Urban Planning*, *134*, 147–156. https://doi.org/10.1016/j.landurbplan.2014.10.017

Lai, J., Zhan, W., Huang, F., Voogt, J., Bechtel, B., Allen, M., et al. (2018). Identification of typical diurnal patterns for clear-sky climatology of surface urban heat islands. *Remote Sensing of Environment*, *217*(February), 203–220. https://doi.org/10.1016/j.rse.2018.08.021

Lai, J., Zhan, W., Voogt, J., Quan, J., Huang, F., Zhou, J., et al. (2021). Meteorological controls on daily variations of nighttime surface urban heat islands. *Remote Sensing of Environment*, *253*(163), 112198. https://doi.org/10.1016/j.rse.2020.112198

Levermore, G., Parkinson, J., Lee, K., Laycock, P., & Lindley, S. (2018). The increasing trend of the urban heat island intensity. *Urban Climate*, *24*, 360–368. https://doi.org/10.1016/j.uclim.2017.02.004

Li, H., Zhou, Y., Li, X., Meng, L., Wang, X., Wu, S., & Sodoudi, S. (2018). A new method to quantify surface urban heat island intensity. *Science of the Total Environment*, *624*, 262–272. https://doi.org/10.1016/j.scitotenv.2017.11.360

Li, W., Cao, Q., Lang, K., & Wu, J. (2017). Linking potential heat source and sink to urban heat island: Heterogeneous effects of landscape pattern on land surface temperature.

*Science of the Total Environment*, *586*, 457–465. https://doi.org/10.1016/j.scitotenv.2017.01.191

Liang, Z., Wu, S., Wang, Y., Wei, F., Huang, J., Shen, J., & Li, S. (2020). The relationship between urban form and heat island intensity along the urban development gradients. *Science of the Total Environment*, *708*, 135011. https://doi.org/10.1016/j.scitotenv.2019.135011

Loughnan, M., Nicholls, N., & Tapper, N. J. (2012). Mapping Heat Health Risks in Urban Areas. *International Journal of Population Research*, *2012*, 1–12. https://doi.org/10.1155/2012/518687

Lowe, S. A. (2016). An energy and mortality impact assessment of the urban heat island in the US. *Environmental Impact Assessment Review*, *56*, 139–144. https://doi.org/10.1016/j.eiar.2015.10.004

Madrigano, J., Jack, D., Anderson, G. B., Bell, M. L., & Kinney, P. L. (2015). Temperature, ozone, and mortality in urban and non-urban counties in the northeastern United States - No section-. *Environmental Health: A Global Access Science Source*, *14*(1), 1–11. https://doi.org/10.1186/1476-069X-14-3

Mallen, E., Stone, B., & Lanza, K. (2019). A methodological assessment of extreme heat mortality modeling and heat vulnerability mapping in Dallas, Texas. *Urban Climate*, *30*(May), 100528. https://doi.org/10.1016/j.uclim.2019.100528

Mathew, A., Khandelwal, S., & Kaul, N. (2018). Analysis of diurnal surface temperature variations for the assessment of surface urban heat island effect over Indian cities. *Energy and Buildings*, *159*, 271–295. https://doi.org/10.1016/j.enbuild.2017.10.062

Memon, R. A., Leung, D. Y. C., & Liu, C. H. (2009). An investigation of urban heat island intensity (UHII) as an indicator of urban heating. *Atmospheric Research*, *94*(3), 491–500. https://doi.org/10.1016/j.atmosres.2009.07.006

Méndez-Lázaro, P., Muller-Karger, F. E., Otis, D., McCarthy, M. J., & Rodríguez, E. (2018). A heat vulnerability index to improve urban public health management in San Juan, Puerto Rico. *International Journal of Biometeorology*, *62*(5), 709–722. https://doi.org/10.1007/s00484-017-1319-z

Mirzaei, P. A., & Haghighat, F. (2010). Approaches to study Urban Heat Island - Abilities and limitations. *Building and Environment*, *45*(10), 2192–2201. https://doi.org/10.1016/j.buildenv.2010.04.001

Mohajerani, A., Bakaric, J., & Jeffrey-Bailey, T. (2017). The urban heat island effect, its causes, and mitigation, with reference to the thermal properties of asphalt concrete. *Journal of Environmental Management*, *197*, 522–538. https://doi.org/10.1016/j.jenvman.2017.03.095

Netatmo Weathermap. (n.d.). Retrieved January 16, 2022, from https://weathermap.netatmo.com/

Netherlands - Climate data and average monthly weather | Weather Atlas. (n.d.). Retrieved January 4, 2022, from https://www.weather-atlas.com/en/netherlands-climate

Netherlands Maps | Maps of Netherlands. (n.d.). Retrieved January 22, 2022, from https://ontheworldmap.com/netherlands/

Netherlands Population 2021 (Demographics, Maps, Graphs). (n.d.). Retrieved December 27, 2021, from https://worldpopulationreview.com/countries/netherlands-population

Ngie, A., Abutaleb, K., Ahmed, F., Darwish, A., & Ahmed, M. (2014). Assessment of urban heat island using satellite remotely sensed imagery: A review. *South African Geographical Journal*, *96*(2), 198–214. https://doi.org/10.1080/03736245.2014.924864

Oke, T. R. (1982). The energetic basis of the urban heat island. *Quarterly Journal of the Royal Meteorological Society*, *108*(455), 1–24. https://doi.org/10.1002/qj.49710845502

Pakarnseree, R., Chunkao, K., & Bualert, S. (2018). Physical characteristics of Bangkok and its urban heat island phenomenon. *Building and Environment*, *143*(February), 561–569. https://doi.org/10.1016/j.buildenv.2018.07.042

Per Capita Income | City of Chicago | Data Portal. (n.d.). Retrieved January 16, 2022, from https://data.cityofchicago.org/Health-Human-Services/Per-Capita-Income/r6ad-wvtk

Rafiee, A., Dias, E., & Koomen, E. (2016). Local impact of tree volume on nocturnal urban heat island: A case study in Amsterdam. *Urban Forestry and Urban Greening*, *16*, 50–61. https://doi.org/10.1016/j.ufug.2016.01.008

Sabrin, S., Karimi, M., Fahad, M. G. R., & Nazari, R. (2020). Quantifying environmental and social vulnerability: Role of urban Heat Island and air quality, a case study of Camden, NJ. *Urban Climate*, *34*(August), 100699. https://doi.org/10.1016/j.uclim.2020.100699

Schwarz, N., Schlink, U., Franck, U., & Großmann, K. (2012). Relationship of land surface and air temperatures and its implications for quantifying urban heat island indicators - An application for the city of Leipzig (Germany). *Ecological Indicators*, *18*, 693–704. https://doi.org/10.1016/j.ecolind.2012.01.001

Sheng, L., Tang, X., You, H., Gu, Q., & Hu, H. (2017). Comparison of the urban heat island intensity quantified by using air temperature and Landsat land surface temperature in Hangzhou, China. *Ecological Indicators*, *72*, 738–746. https://doi.org/10.1016/j.ecolind.2016.09.009

Siu, L. W., & Hart, M. A. (2013). Quantifying urban heat island intensity in Hong Kong SAR, China. *Environmental Monitoring and Assessment*, *185*(5), 4383–4398. https://doi.org/10.1007/s10661-012-2876-6

Smart Weather Station Indoor Outdoor | Netatmo. (n.d.). Retrieved July 25, 2022, from https://www.netatmo.com/en-gb/weather/weatherstation

Soux, A., Voogt, J. A., & Oke, T. R. (2004). A model to calculate what a remote sensor "sees" of an urban surface. *Boundary-Layer Meteorology*, *112*(2), 109–132. https://doi.org/10.1023/B:BOUN.0000010995.62115.46

Steeneveld, G. J., Koopmans, S., Heusinkveld, B. G., Van Hove, L. W. A., & Holtslag, A. A. M. (2011). Quantifying urban heat island effects and human comfort for cities of variable size and urban morphology in the Netherlands. *Journal of Geophysical*

*Research Atmospheres*, *116*(20), 1–14. https://doi.org/10.1029/2011JD015988

Stewart, I. D. (2011). Redefining the Urban Heat Island. *October*, (October), 1–352. Retrieved from https://circle.ubc.ca/handle/2429/38069

Streutker, D. R. (2002). A remote sensing study of the urban heat island of Houston, Texas. *International Journal of Remote Sensing*, *23*(13), 2595–2608. https://doi.org/10.1080/01431160110115023

Streutker, David R. (2003). Satellite-measured growth of the urban heat island of Houston, Texas. *Remote Sensing of Environment*, *85*(3), 282–289. https://doi.org/10.1016/S0034-4257(03)00007-5

Susca, T., Gaffin, S. R., & Dell'Osso, G. R. (2011). Positive effects of vegetation: Urban heat island and green roofs. *Environmental Pollution*, *159*(8–9), 2119–2126. https://doi.org/10.1016/j.envpol.2011.03.007

Tomlinson, C. J., Prieto-Lopez, T., Bassett, R., Chapman, L., Cai, X. M., Thornes, J. E., & Baker, C. J. (2013). Showcasing urban heat island work in Birmingham - Measuring, monitoring, modelling and more. *Weather*, *68*(2), 44–49. https://doi.org/10.1002/wea.1998

Tomlinson, Charlie J., Chapman, L., Thornes, J. E., & Baker, C. (2011). Remote sensing land surface temperature for meteorology and climatology: A review. *Meteorological Applications*, *18*(3), 296–306. https://doi.org/10.1002/met.287

U.S. Census Bureau QuickFacts: Chicago city, Illinois; Illinois. (n.d.). Retrieved December 27, 2021, from https://www.census.gov/quickfacts/fact/table/chicagocityillinois,IL/PST045219

U.S. Census Bureau QuickFacts: Illinois. (n.d.). Retrieved December 27, 2021, from https://www.census.gov/quickfacts/IL

Voogt, J. A., & Oke, T. R. (1997). Complete urban surface temperatures. *Journal of Applied Meteorology*, *36*(9), 1117–1132. https://doi.org/10.1175/1520-0450(1997)036<1117:CUST>2.0.CO;2

Voogt, J. A., & Oke, T. R. (2003). Thermal remote sensing of urban climates. *Remote Sensing of Environment*, *86*(3), 370–384. https://doi.org/10.1016/S0034-4257(03)00079-8

Yadav, N., & Sharma, C. (2018). Spatial variations of intra-city urban heat island in megacity Delhi. *Sustainable Cities and Society*, *37*(October 2017), 298–306. https://doi.org/10.1016/j.scs.2017.11.026

Yadav, N., Sharma, C., Peshin, S. K., & Masiwal, R. (2017). Study of intra-city urban heat island intensity and its influence on atmospheric chemistry and energy consumption in Delhi. *Sustainable Cities and Society*, *32*(April), 202–211. https://doi.org/10.1016/j.scs.2017.04.003

Yang, J., Wang, Y., Xiu, C., Xiao, X., Xia, J., & Jin, C. (2020). Optimizing local climate zones to mitigate urban heat island effect in human settlements. *Journal of Cleaner*

*Production*, *275*, 123767. https://doi.org/10.1016/j.jclepro.2020.123767

Yuan, F., & Bauer, M. E. (2007). Comparison of impervious surface area and normalized difference vegetation index as indicators of surface urban heat island effects in Landsat imagery. *Remote Sensing of Environment*, *106*(3), 375–386. https://doi.org/10.1016/j.rse.2006.09.003

Zhao, S., Zhou, D., & Liu, S. (2016). Data concurrency is required for estimating urban heat island intensity. *Environmental Pollution*, *208*, 118–124. https://doi.org/10.1016/j.envpol.2015.07.037

Zinzi, M., Agnoli, S., Burattini, C., & Mattoni, B. (2020). On the thermal response of buildings under the synergic effect of heat waves and urban heat island. *Solar Energy*, *211*(November), 1270–1282. https://doi.org/10.1016/j.solener.2020.10.050

# Appendices

***Appendix A- NETATMO site maps***

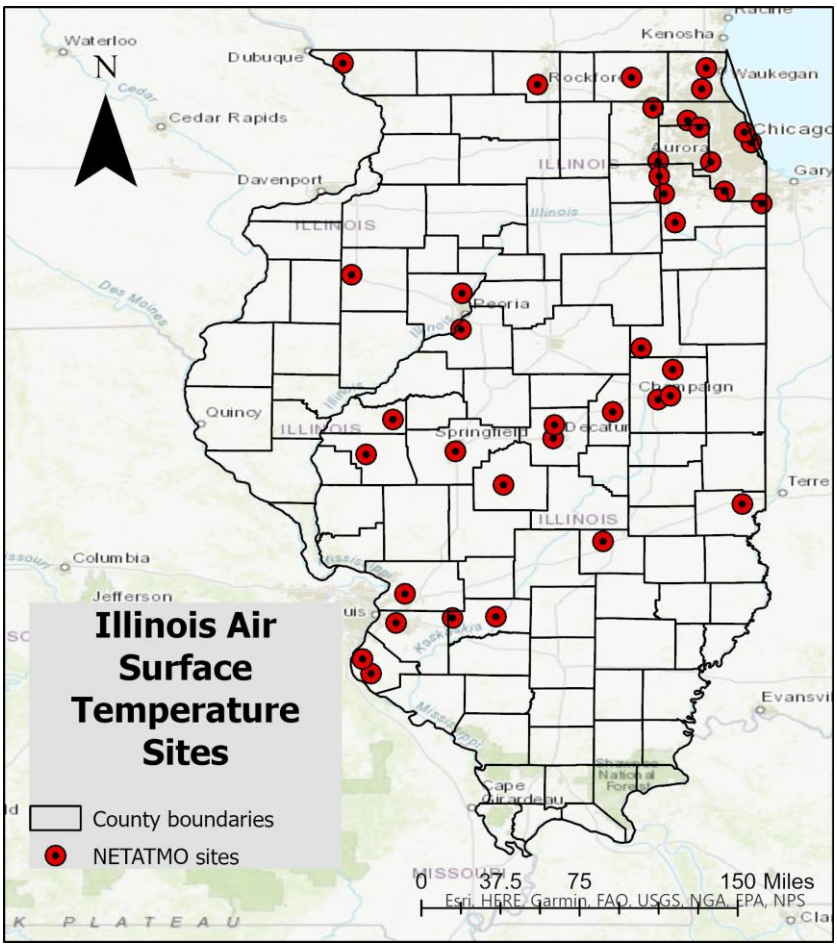


Figure 6-1: Illinois sites for which surface air temperature values were gathered

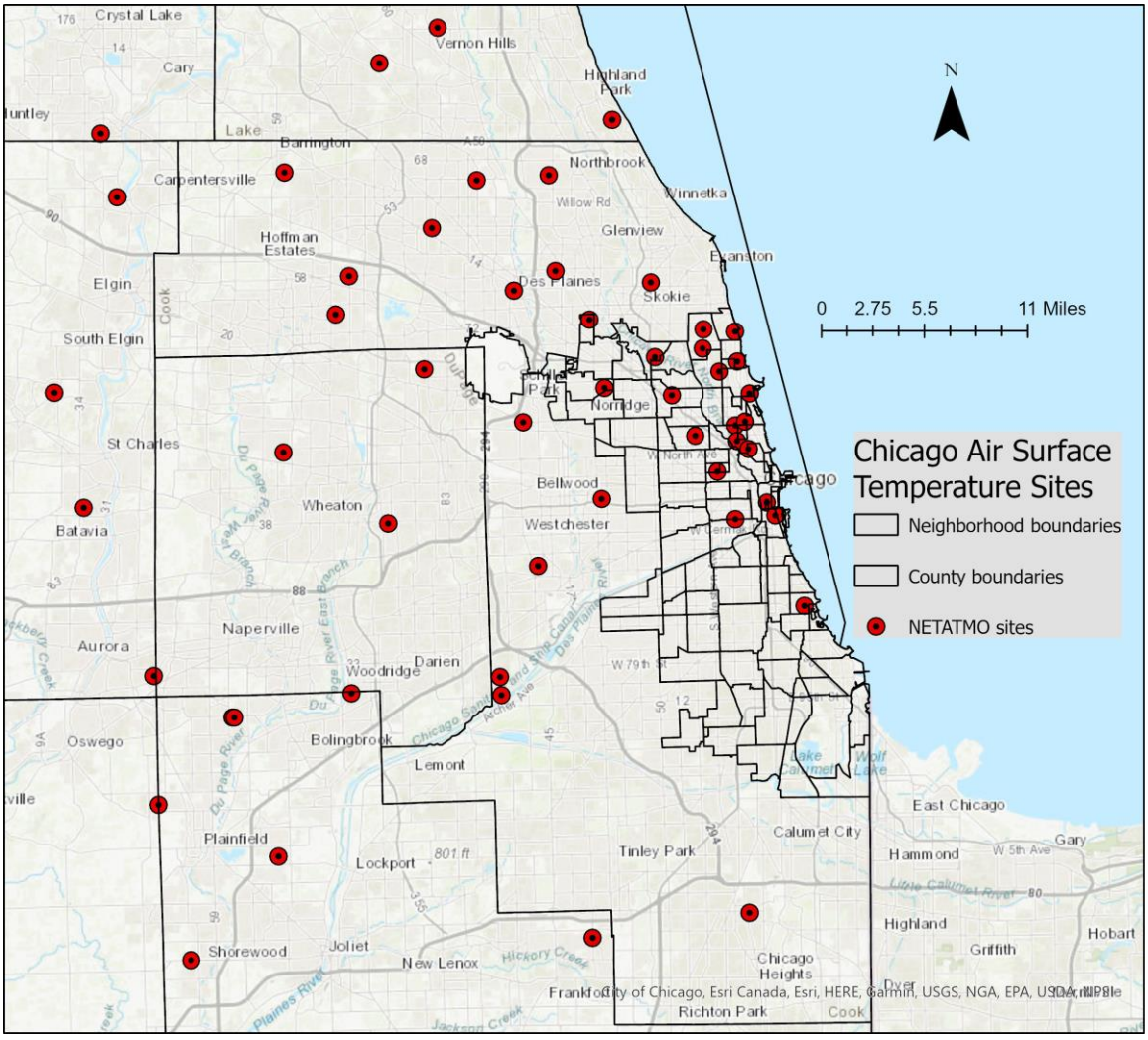


Figure 6-2: Chicago sites for which surface air temperature values were gathered; this includes sites in the counties surrounding the city

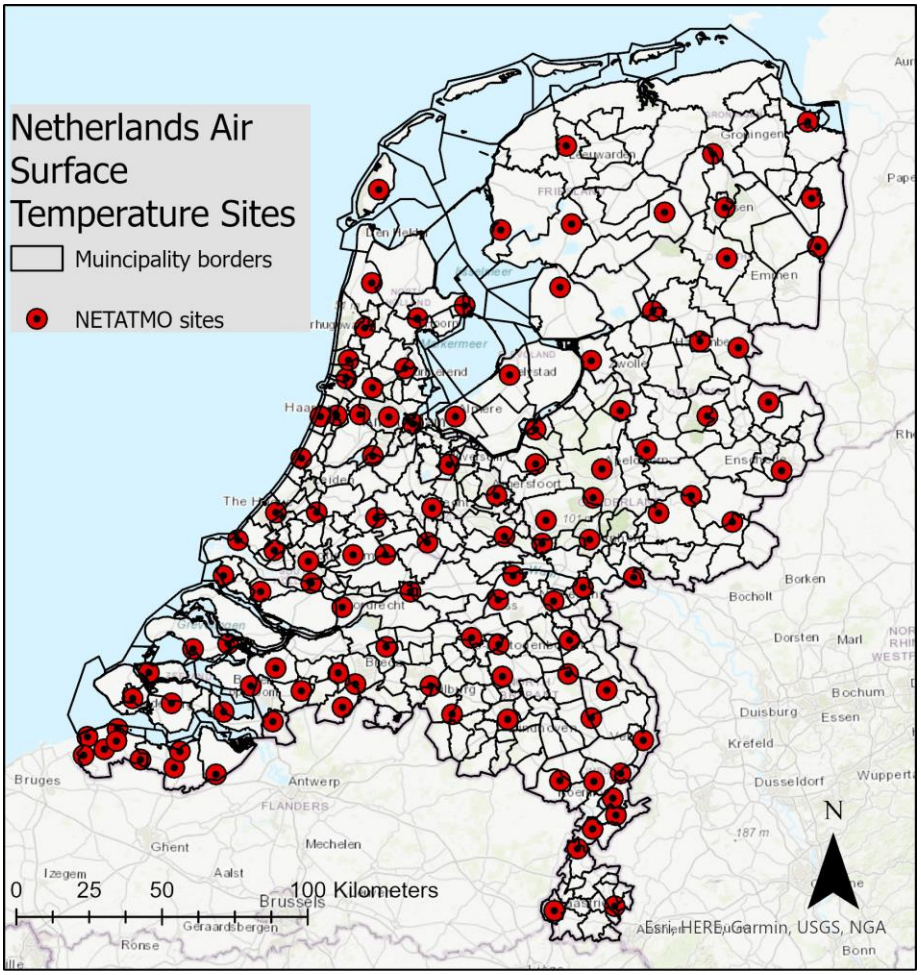


Figure 6-3: Netherlands sites for which surface air temperature values were gathered

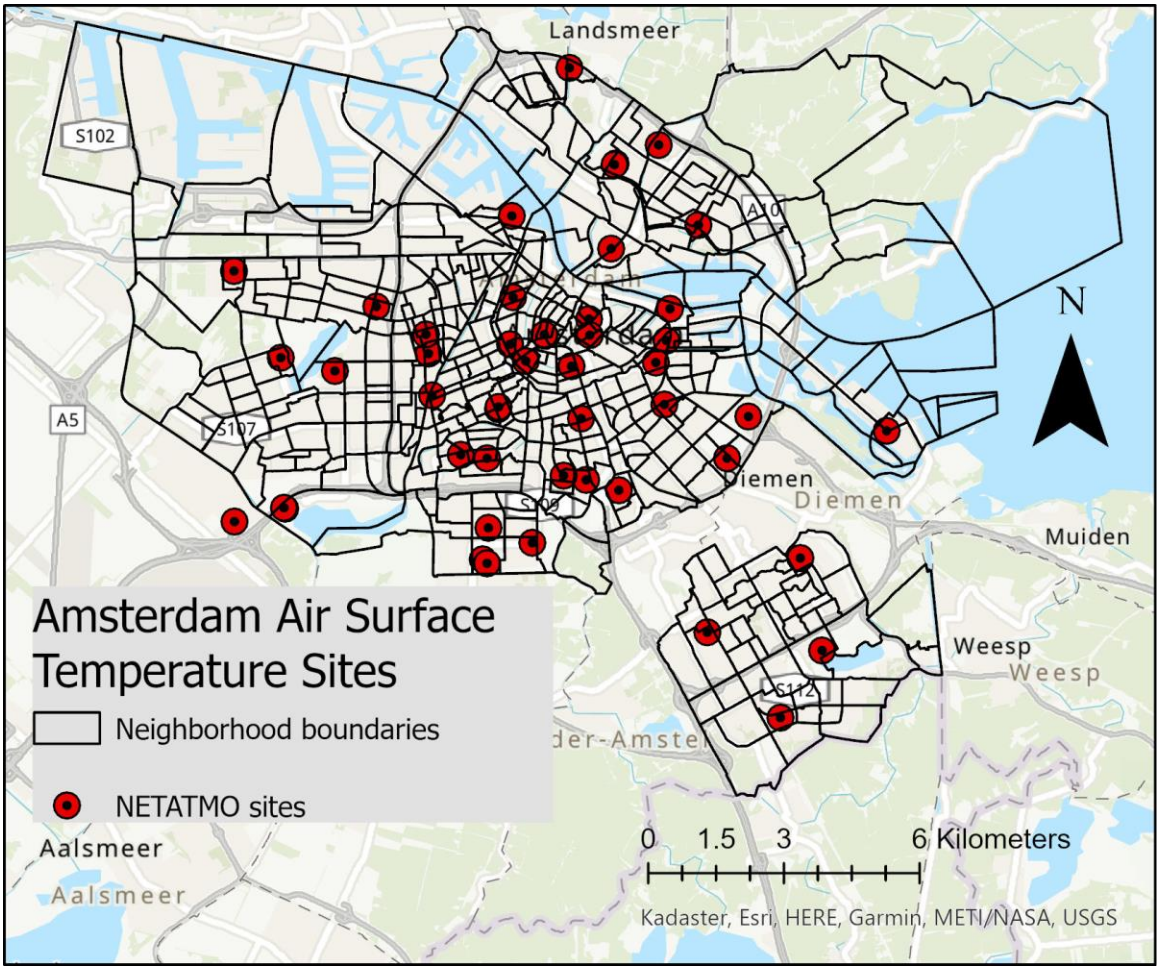


Figure 6-4: Amsterdam sites for which surface air temperature values were gathered

***Appendix B- NETATMO in-situ temperature data***

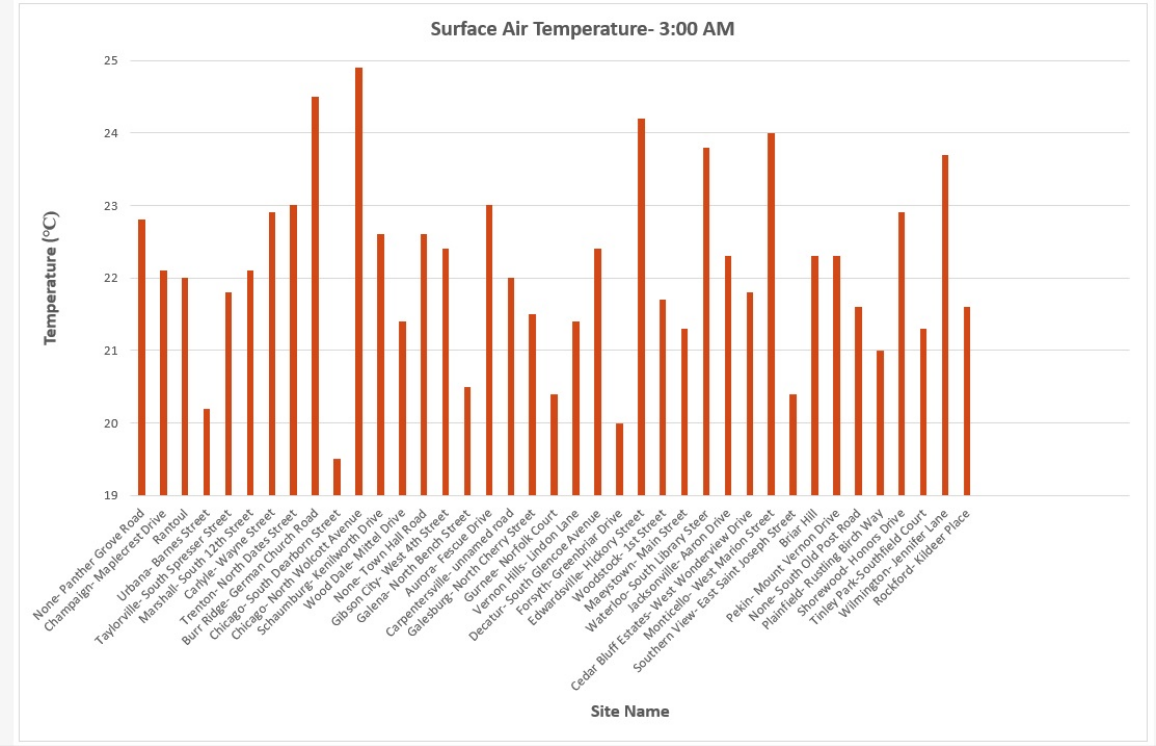


Figure 6-5: Illinois in-situ surface air temperatures for 3:00 AM

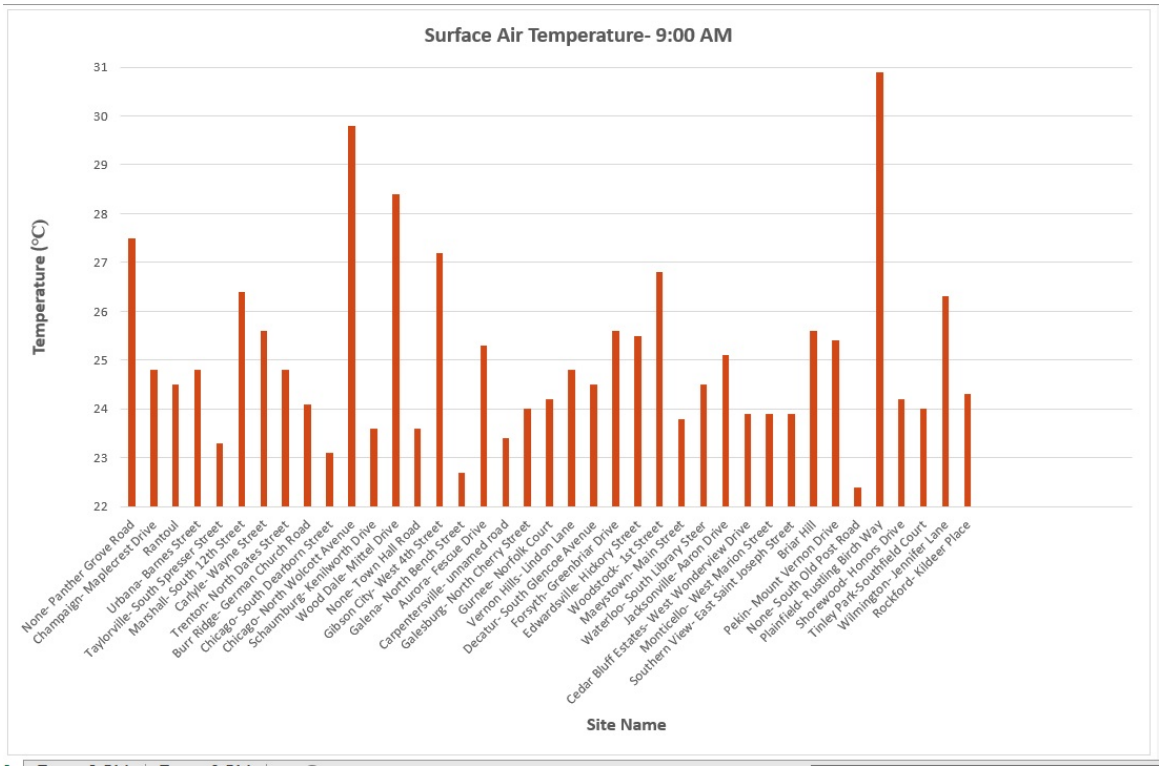


Figure 6-6: Illinois in-situ surface air temperatures for 9:00 AM

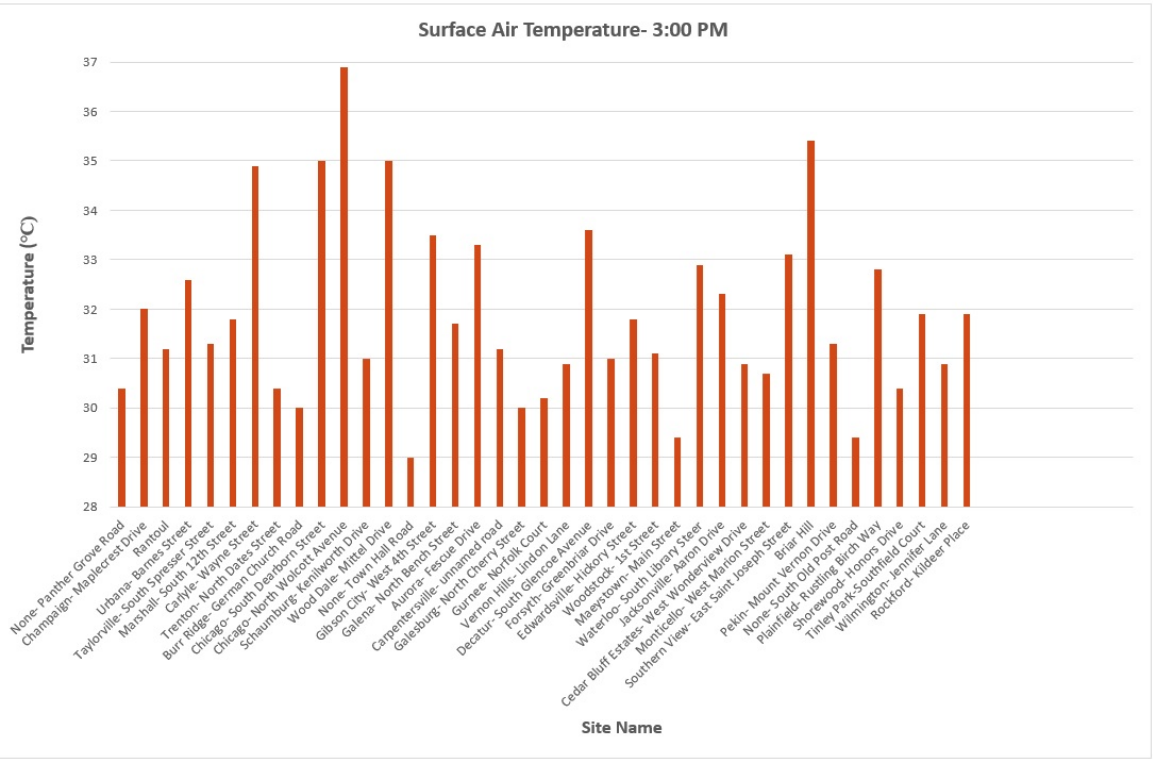


Figure 6-7: Illinois in-situ surface air temperatures for 3:00 PM

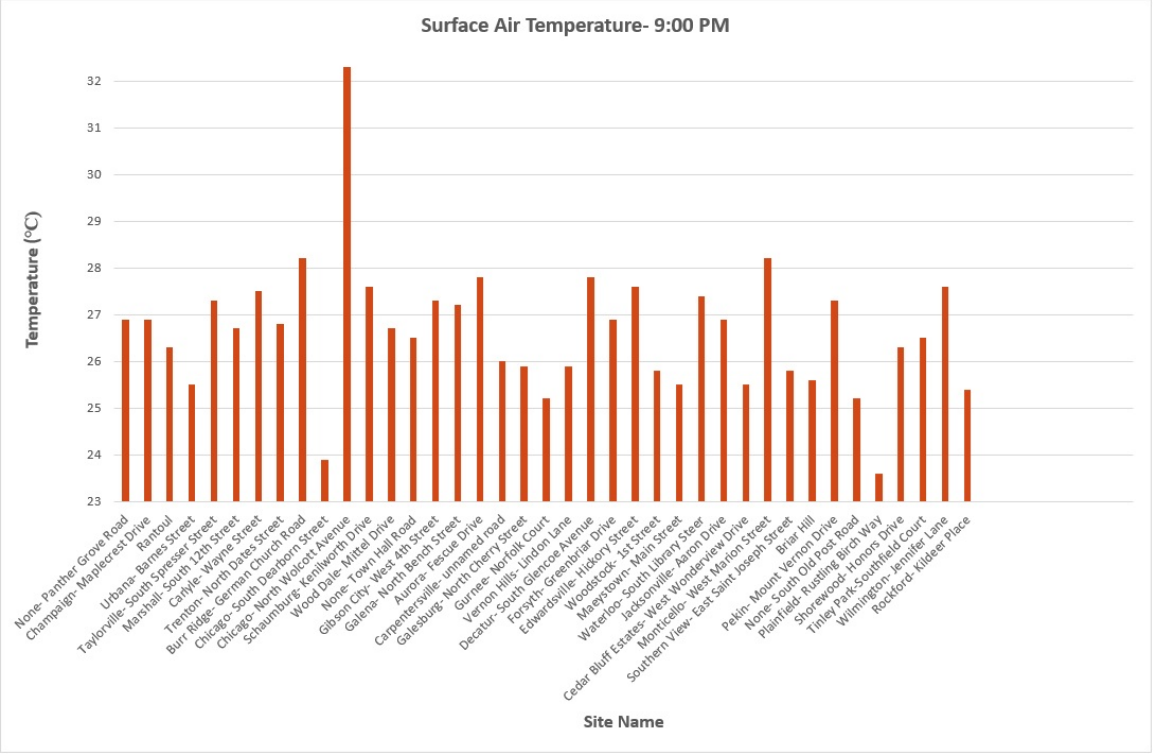


Figure 6-8: Illinois in-situ surface air temperatures for 9:00 PM

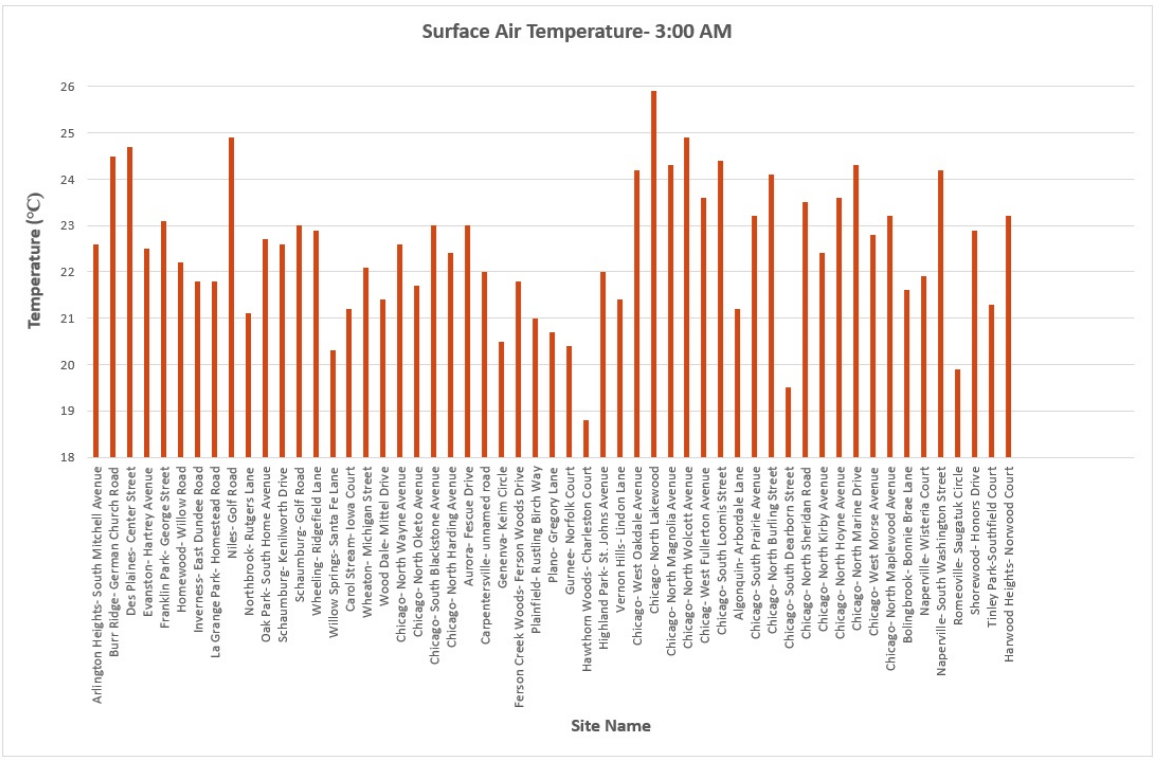


Figure 6-9: Chicago in-situ surface air temperatures for 3:00 AM

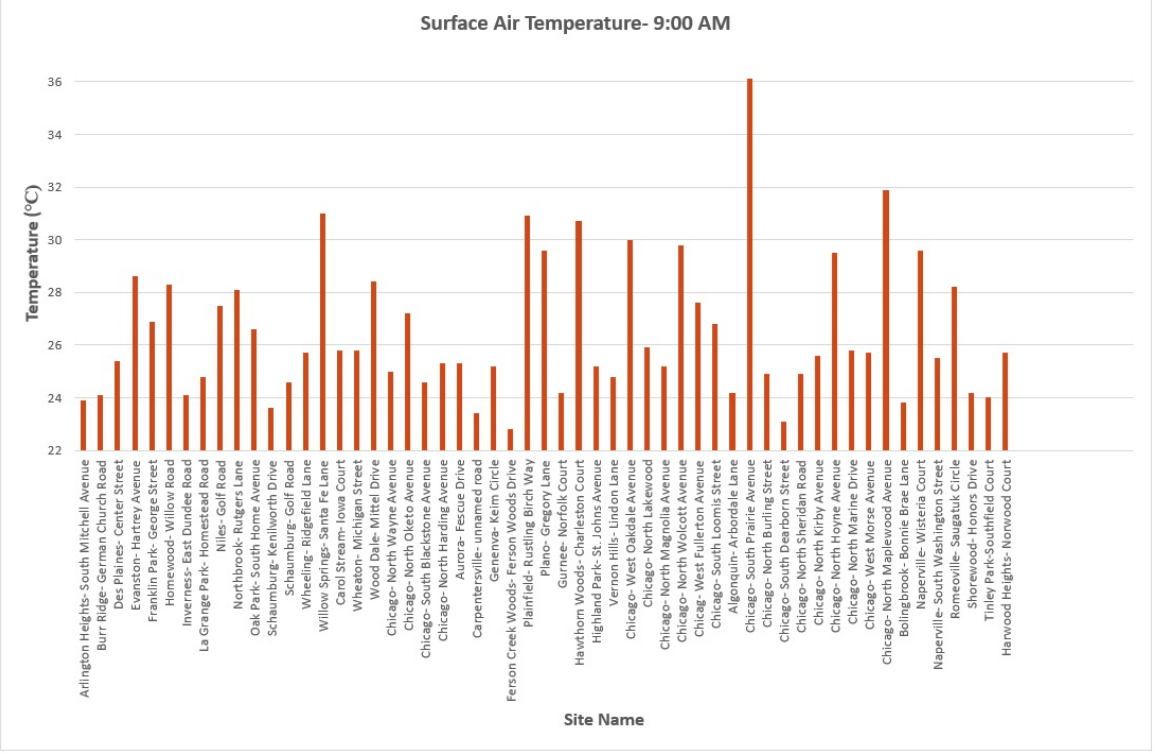


Figure 6-10: Chicago in-situ surface air temperatures for 9:00 AM

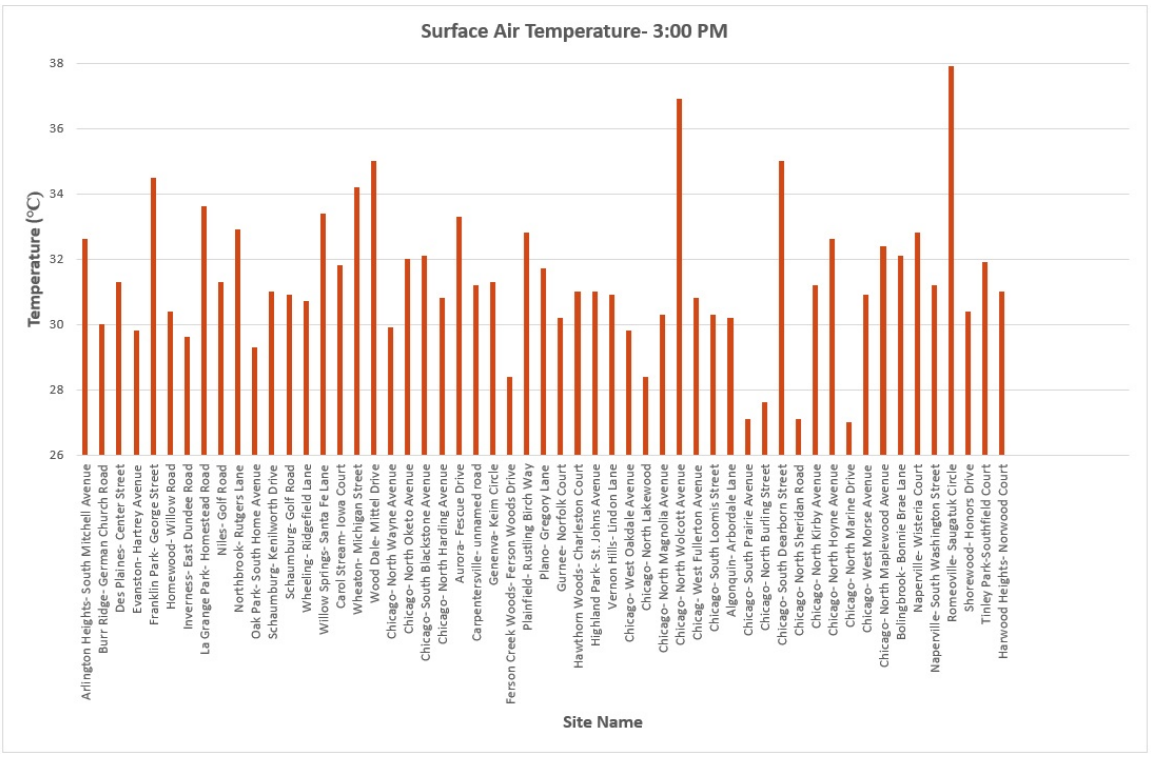


Figure 6-11: Chicago in-situ surface air temperatures for 3:00 PM

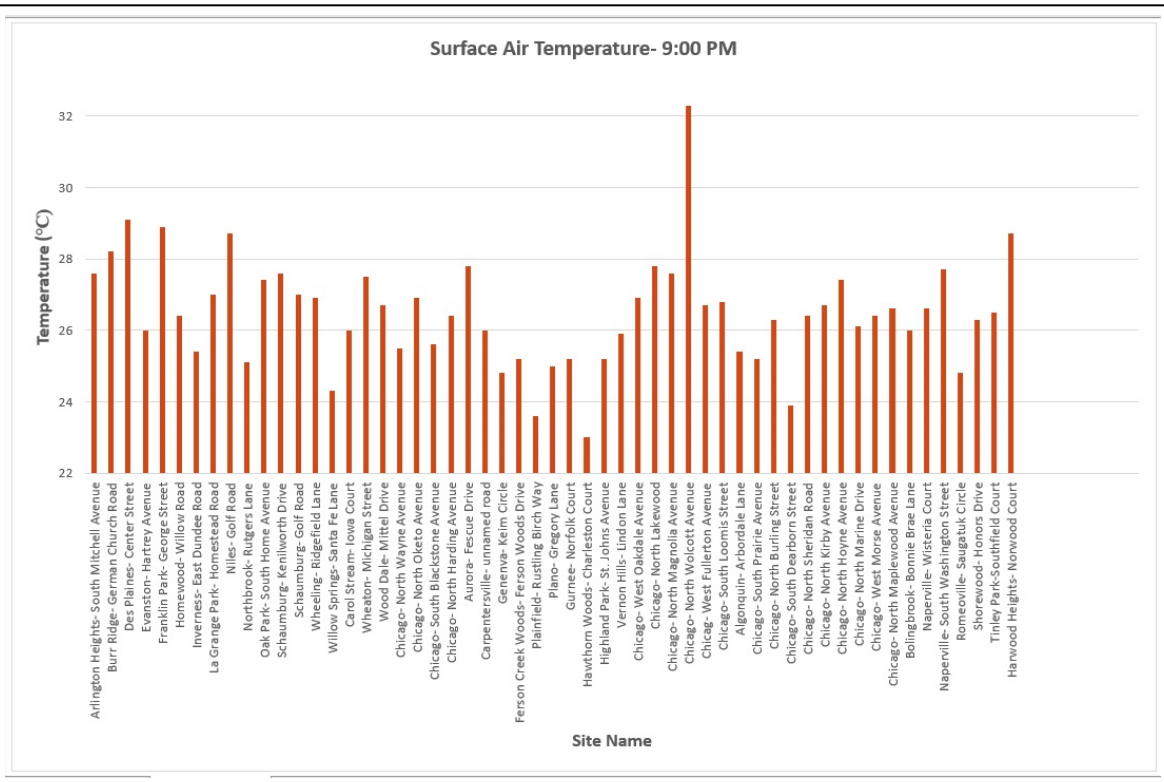


Figure 6-12: Chicago in-situ surface air temperatures for 9:00 PM

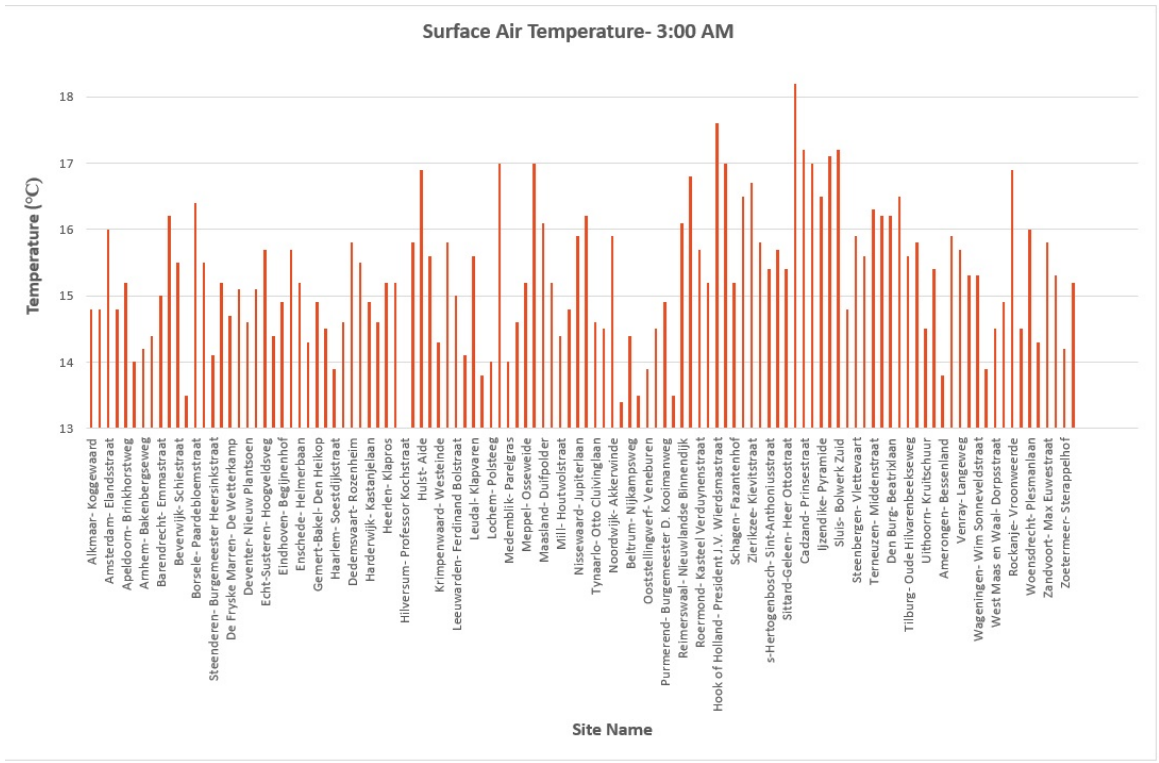


Figure 6-13: Netherlands in-situ surface air temperatures for 3:00 AM

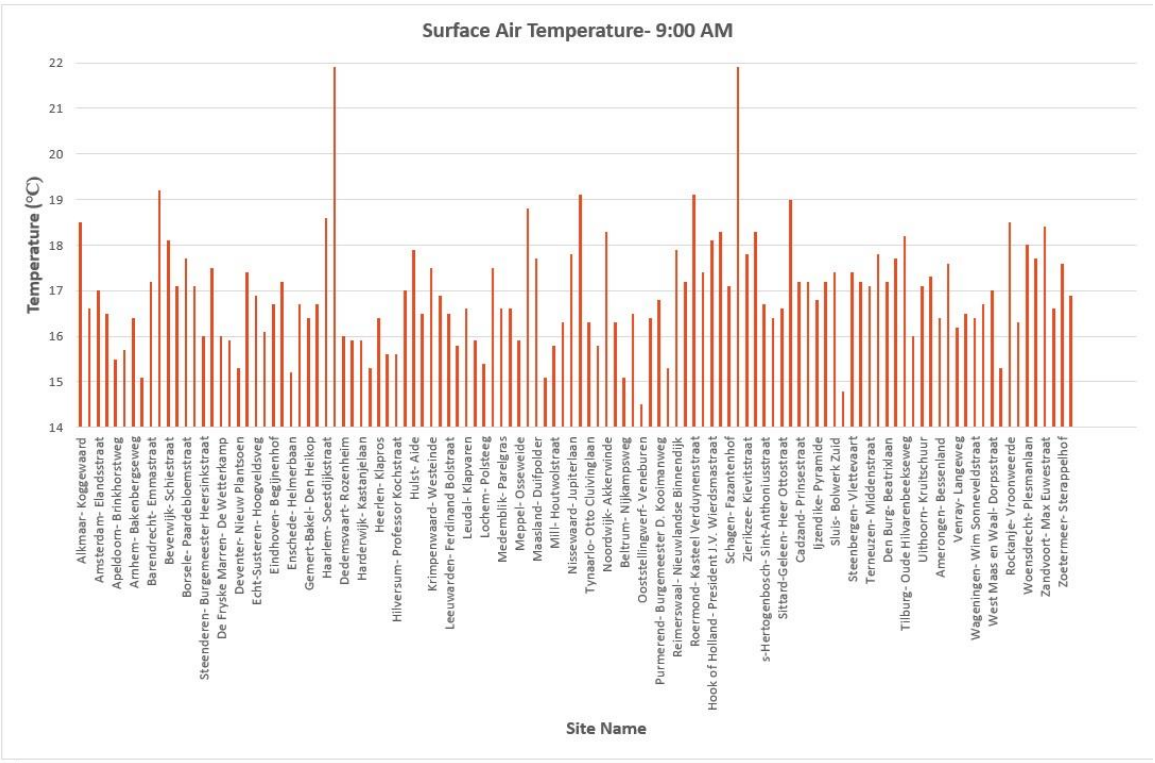


Figure 6-14: Netherlands in-situ surface air temperatures for 9:00 AM

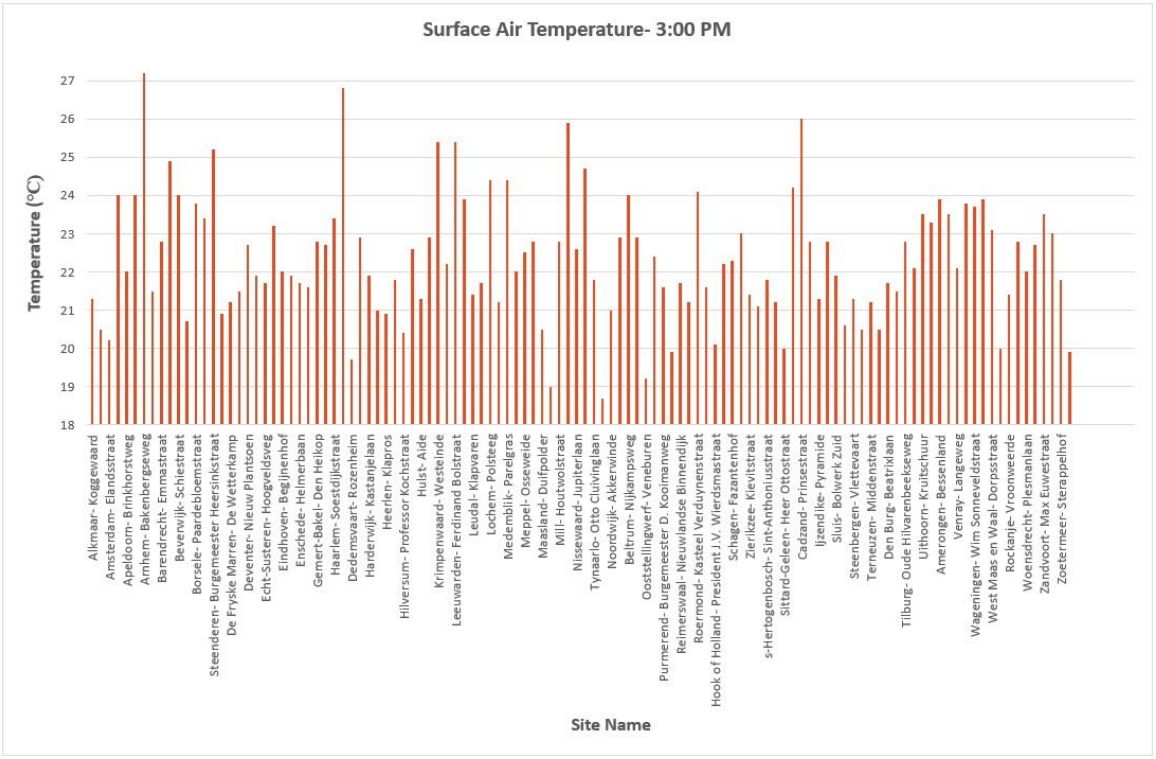


Figure 6-15: Netherlands in-situ surface air temperatures for 3:00 PM

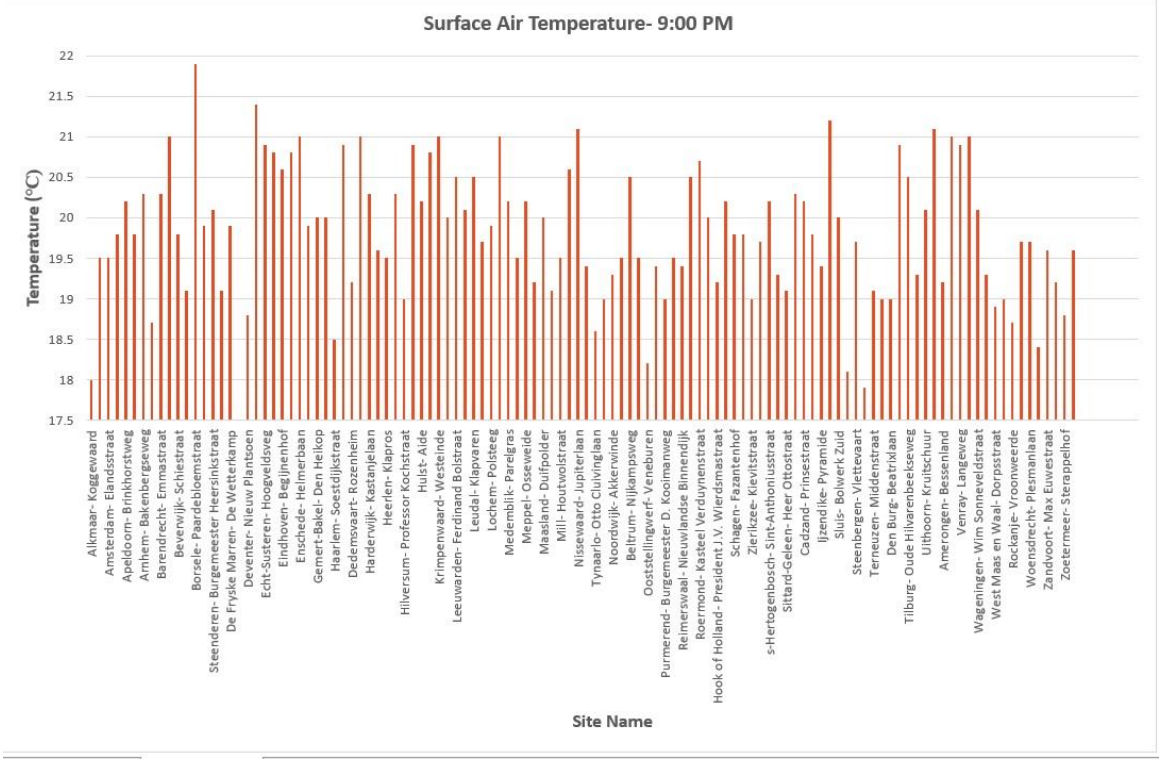


Figure 6-16: Netherlands in-situ surface air temperatures for 9:00 PM

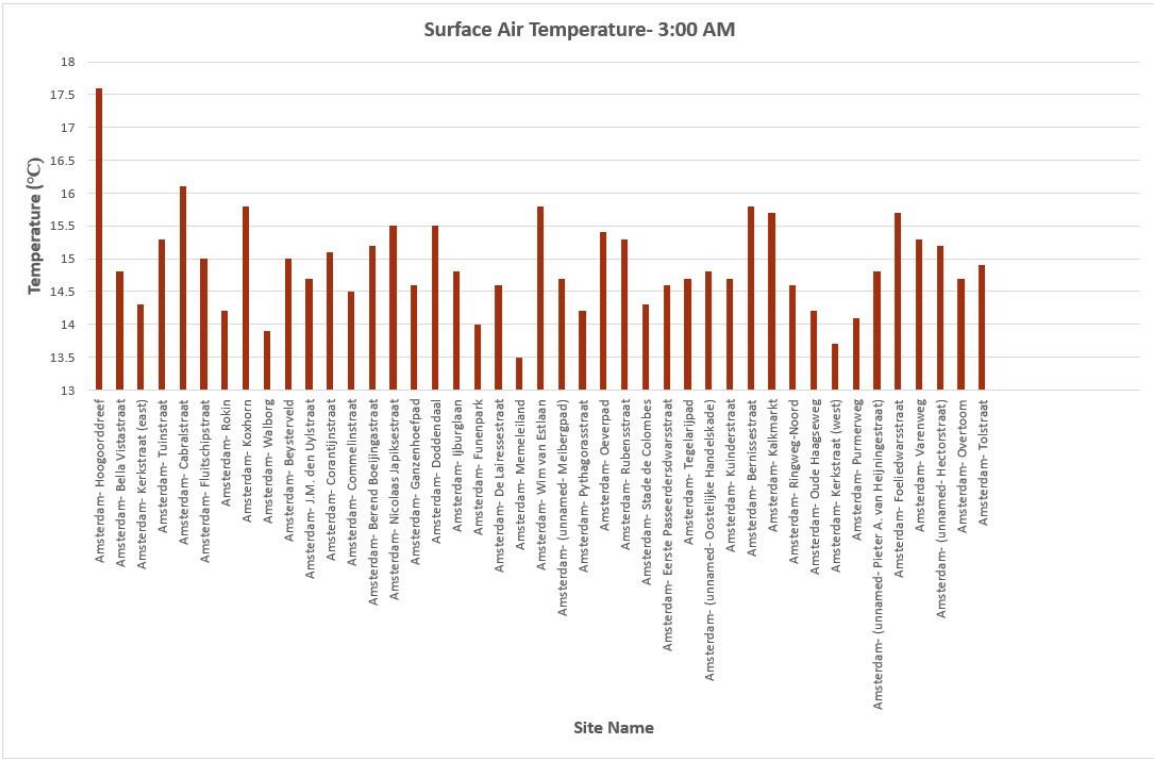


Figure 6-17: Amsterdam in-situ surface air temperatures for 3:00 AM

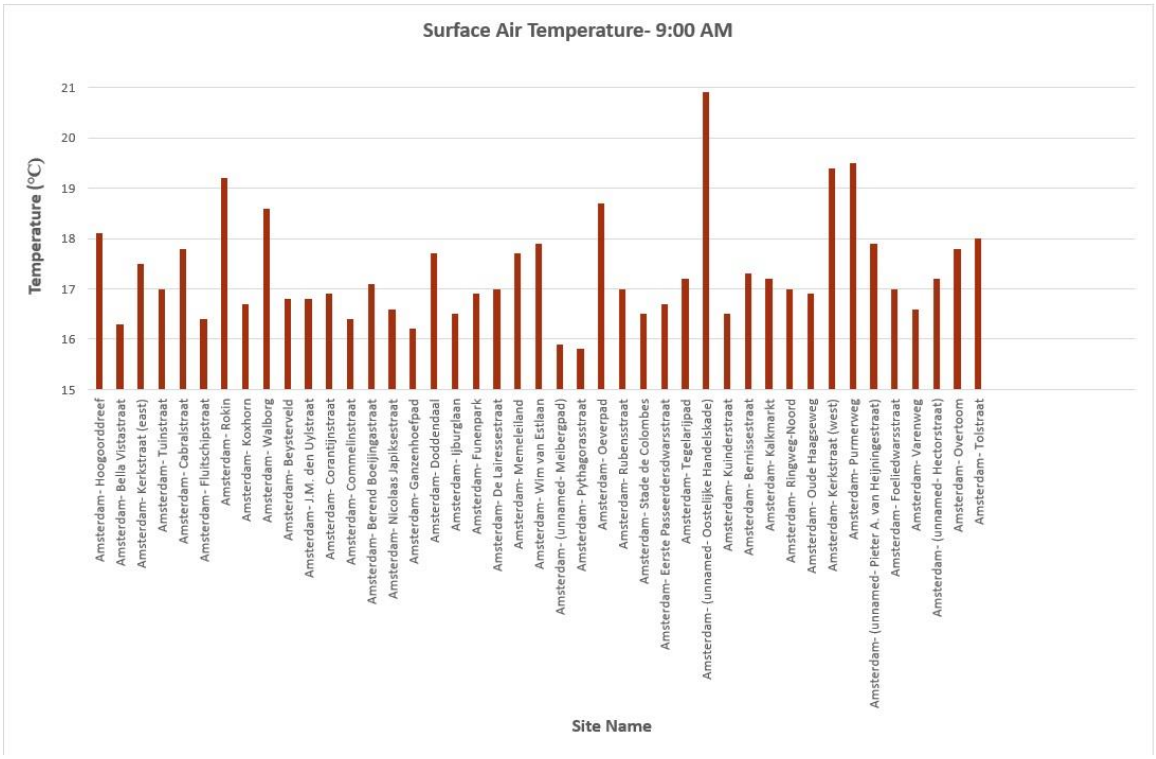


Figure 6-18: Amsterdam in-situ surface air temperatures for 9:00 AM

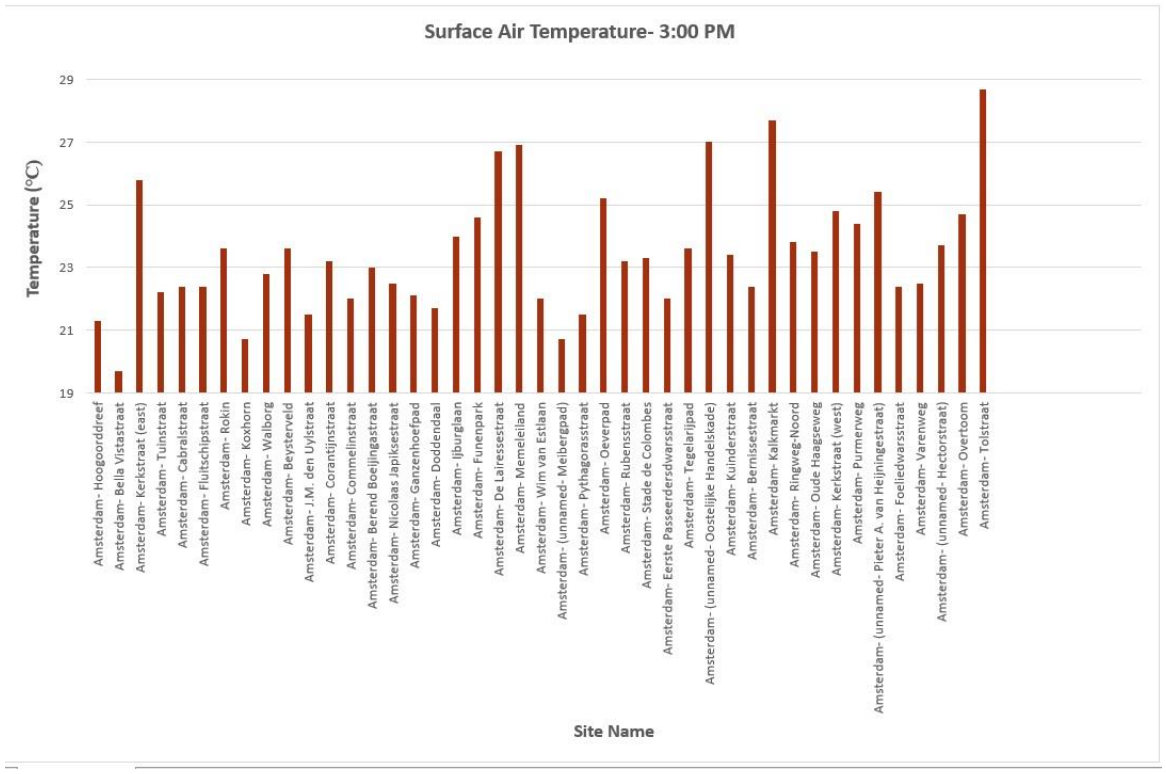


Figure 6-19: Amsterdam in-situ surface air temperatures for 3:00 PM

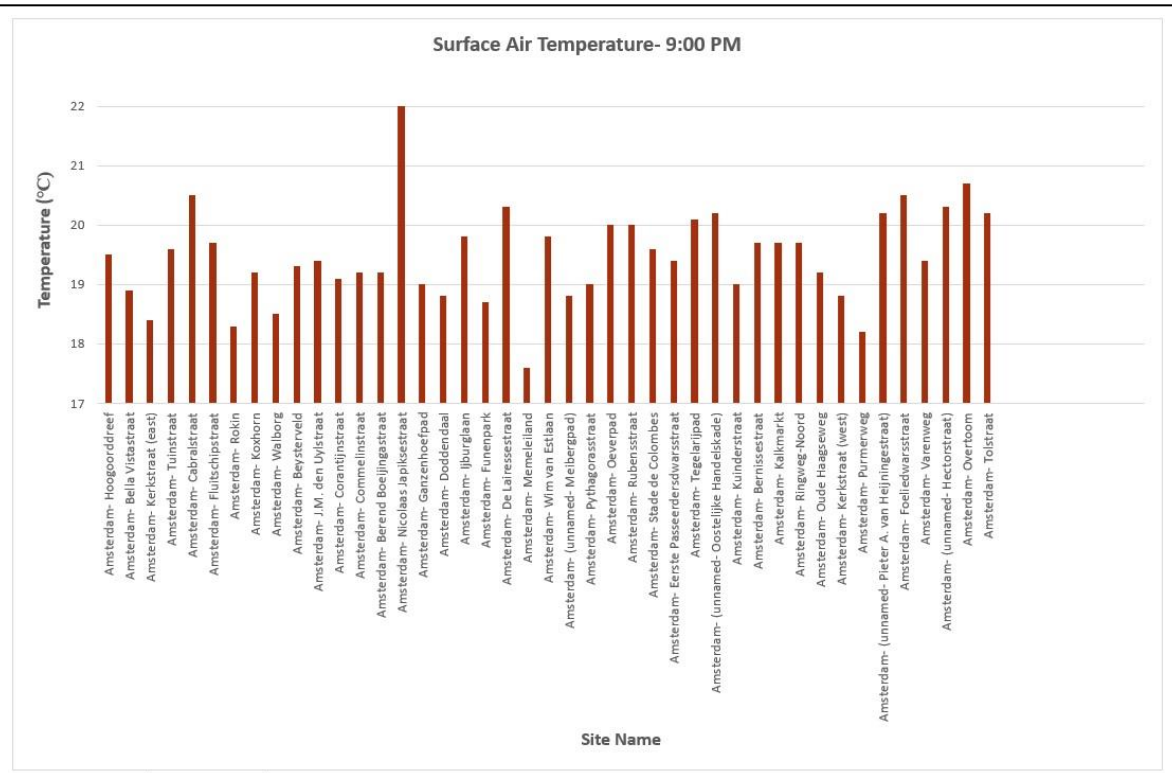


Figure 6-20: Amsterdam in-situ surface air temperatures for 9:00 PM

***Appendix C- ArcGIS Pro tools used***

| **Tool Used** | **Function** | **Use in this study** |
|---|---|---|
| Add Join | Joins layer data onto a different layer's attribute table | Adding average income, population density, and air surface temperature data to the shapefile with administrative unit borders |
| Clip Raster | Cuts out a portion of a raster dataset | Trimming down interpolated surface air temperature maps to only include the bounds of the study area |
| Geographically Weighted Regression | A local form of linear regression used to model spatially varying relationships between variables | Finding correlation between temperature data and possible explanatory variables |
| Inverse Distance Weighting | Interpolates from point data to create a continuous field as a raster | Filling in gaps in temperature data between NETATMO sites |
| Local Bivariate Relationships | Analyzes two variables for statistically significant relationships based on their values and the locality | Finding correlation between temperature data and possible exacerbating factors |
| Table to Excel | Converts a table to an MS Excel file | Consolidating and re-organizing data as a precursor to data analysis |
| Zonal Statistics as Table | Calculates the values of a raster within the zones of another dataset, then reports these as a table | Finding the average surface air temperature for each administrative unit at all four times at each study area |